Universität Zürich[UZH]

Geographisches Institut

The effects of 10 years of soil warming on the weathering degree of deep mineral soil profiles and the role of spatial heterogeneity

GEO 511 Master's Thesis

Author: Julia van Leeuwen, 19-754-241

Supervised by: PD Dr. Guido Lars Bruno Wiesenberg, Binyan Sun

Faculty representative: PD Dr. Guido Lars Bruno Wiesenberg

30.09.2025

Abstract

Soil warming has the potential to accelerate mineral soil weathering. Higher soil temperatures influence geochemical processes such as mineral dissolution and transformation, which can impact nutrient cycles, soil fertility and carbon storage. While most studies have focused on short-term warming effects in surface soils, the effects of soil warming on the soil weathering degree in whole soil profiles have not been analysed before and have become more relevant with climate change. This study analysed the effects of 10 years of +4°C soil warming on the weathering degree of 1 m deep mineral soil profiles of granitic origin in the Blodgett Forest in California. The analysis included how warming influenced pH, the elemental composition, oxalate- and dithionite-extracted aluminium, iron and manganese and the soil organic matter composition. Additionally, weathering indices such as the CIA, PIA were calculated. Furthermore, the role of spatial heterogeneity has been assessed by comparing replicate control soil profiles, which were initially assumed to be equivalent. The results showed that soil warming accelerated subsoil primary weathering which may alter nutrient redistribution and long-term ecosystem processes, but soil warming had no significant impact in the topsoil. Significantly higher iron, potassium, magnesium, sulphur and oxalate-extracted iron concentrations were found in the subsoil whereas the CIA showed lower values with soil warming. Significant spatial heterogeneity was found and was most prominent in the subsoil. It was also found that the soil profiles furthest apart from each other showed the most differences. Several variables including CIA, potassium, magnesium, sulphur and iron, which showed differences with soil warming in the subsoil were also the variables that exhibited high spatial variation in the subsoil. These findings highlight that soil warming can accelerate subsoil weathering and that it is essential to include subsoils in soil warming studies. The results also point out the need to consider spatial heterogeneity when assessing long-term ecosystem responses to climate change.

Table of Contents

List of Figures

List of Tables

List of Abbreviations

AAS	Atomic Absorption Spectroscopy
AIC	Akaike information criterion
Al	Aluminium
Al_2O_3	Aluminium oxide
Al_d	Dithionite-extracted aluminium
Al_o	Oxalate-extracted aluminium
Al_t	Total aluminium
ANOVA	Analysis of variance
Aromatic C-C	Aromatic carbon-carbon bonds
Aromatic C-H	Aromatic carbon-hydrogen bonds
a.s.l.	Above sea level
AUC	Area under curve
C	Carbon
Ca	Calcium
$CaCl_2$	Calcium chloride
CIA	Chemical index of alteration
C/N	Carbon nitrogen ratio
DRIFT	Diffuse Reflectance Infrared Fourier Transform
DSI	Drifts stability index
Fe	Iron
Fe_d	Dithionite-extracted iron
Fe_o	Oxalate-extracted iron
Fe_t	Total iron
H_2O	Water
IPCC	Intergovernmental Panel on Climate Change
K	Potassium
K2O	Potassium oxide
MAOM	Mineral-associated organic matter
Mg	Magnesium
Mn	Manganese
Mn_d	Dithionite-extracted manganese
Mn_o	Oxalate-extracted manganese
Mn_t	Total manganese
N	Nitrogen
Na	Sodium
P	Phosphorus
PIA	Plagioclase index of alteration
rpm	Revolutions per minute
S	Sulphur
Si	Silicon
SNV	Standard normal variate
SOC	Soil organic carbon
SOM	Soil organic matter
XRF	X-Ray Fluorescence

1. Introduction

Soils are essential for ecosystem functioning, are involved in the cycling of carbon and other elements and provide nutrients and water for plants (Goebes et al., 2019). Soils are also the largest terrestrial carbon sink, which has the potential to help mitigate climate change or become a source of carbon in the atmosphere through warming (Angst et al., 2021). Temperate forest soils contain 10 % of total soil carbon and 70 % of the carbon within the temperate forest ecosystem, making them a significant carbon sink (van den Enden et al., 2021; Rasmussen et al., 2005). Climate change increases air and soil temperatures and alters precipitation patterns, which impacts soils globally (Pareek, 2017). According to the IPCC, soils are expected to warm by 4.5°C by 2100 under the RCP 8.5 scenario (Ofiti et al., 2021). While carbon dynamics under climate change have received increasing attention in the last decades and it has been shown that warming increases soil organic matter decomposition and can lead to carbon losses from the soil (Ofiti et al., 2021; Hicks Pries et al., 2017; van den Enden et al., 2021), less attention has been given to how warming influences soil weathering. Higher temperatures are expected to accelerate soil weathering (Belyazid et al., 2022), as warming impacts various geochemical processes and can enhance the dissolution of silicate minerals, change soil processes and mineral formation and transformation, which are central to pedogenesis (Goddéris et al., 2013; Kronnäs et al., 2023; Egli et al., 2008). This includes providing long-term nutrient supply to enter plant nutrient cycles, impacting soil fertility, and affecting the surface characteristics of minerals which influence carbon storage in soils (Zhang et al., 2024; Belyazid et al., 2022; Goebes et al., 2019; Fang et al., 2023). This highlights the need for long-term, in-situ experiments to understand how warming influences weathering throughout soil profiles.

Temperate forest soils are often more acidic due to higher plant productivity and the release of organic acids from roots and litter (Oliva et al., 2003). Acidic parent material, such as nutrient-poor granite, can further add to the acidity (Belyazid et al., 2022). Granitic soils predominantly consist of quartz, feldspar and mica, which are minerals that weather slowly and provide limited nutrient input (Belyazid et al., 2022). The mineral composition of soils and their weathering influences carbon dynamics through the formation of organo-mineral associations and controlling aggregate stability and formation (Rasmussen et al., 2005). Thus, ecosystem functioning in temperate forests depends on the balance between organic matter turnover and the rates of mineral weathering.

Different weathering processes occur at different depths throughout the soil profile (Goebes et al., 2019), therefore it is important to include the subsoil in weathering studies. Unfortunately, the subsoil is often overlooked, due to an increased complexity during sampling (Johnson & Turner, 2019; Fang et al., 2023).

1.1 Soil weathering

Soil mineral weathering is an integral part of soil development (pedogenesis) (Heidari & Raheb, 2020; Abbaslou & Baghernejad, 2013). Mineral weathering can be defined as the alteration of soil, parent rock and secondary minerals through physical, biological and chemical processes into other soil components and secondary minerals (Belyazid et al., 2022; Alsalam et al., 2020; Heidari & Raheb, 2020). Soil weathering is driven by parent material, climate, organisms such as vegetation and microbial community, topography and time (Guimarães et al., 2022; Huang et al., 2021). Temperature, next to precipitation, is the strongest climatic factor influencing soil weathering, since it increases the chemical alteration of minerals and biological activity (Oliva et al., 2003; Kronnäs et al., 2023). Root exudates and microorganisms release organic acids, which further increase mineral transformation (Huang et al., 2014; Ren et al., 2024). Additionally,

microbial activity can influence redox conditions and affect the mobility of elements such as of iron and manganese (Kleber et al., 2015). Increased biological activity can acidify the soil, accelerating weathering rates, as acidic conditions promote weathering processes (Kleber et al., 2015; Ren et al., 2024). Chemical weathering also depends on soil moisture, the reactivity and supply of minerals, altitude and seasonal patterns, which can offset the accelerating effect of temperature on weathering (Egli et al., 2008; Kronnäs et al., 2023; Belyazid et al., 2022).

Weathering processes include solution, hydrolysis, carbonization, oxidation, reduction and clay formation (Abbaslou & Baghernejad, 2013), which entails the dissolution of minerals releasing elements and leading to the loss of mobile elements through leaching and plant uptake and the relative enrichment of immobile elements (Alsalam et al., 2020), resulting in more stable mineral phases, like clay (Egli et al., 2008). This can be described as an acid-base reaction, where acids, for example from root exudations, are neutralized by bases from feldspar and transformed into secondary minerals (Middelburg et al., 1988).

Elements in the soil can be grouped into mobile and immobile elements during soil weathering (Middelburg et al., 1988). Ca, Na, Mg and K are considered mobile elements and more susceptible to leaching. Al and Fe are more immobile during weathering. Elements such as Fe and Mn are influenced by redox conditions in the soil, since they can be soluble under reducing conditions and insoluble under oxidizing conditions (Middelburg et al., 1988). Chemical weathering processes lead to the depletion of these mobile elements (Middelburg et al., 1988). The chemical composition of the soil in the beginning of pedogenesis is regulated by the composition of the parent material. In later soil development stages, the elemental distribution is increasingly influenced by climate and pedogenic processes (Abbaslou & Baghernejad, 2013).

Poorly crystalline minerals are reactive weathering products of primary minerals that can stabilize organic matter by making it less accessible to decomposition via organo-mineral associations and by contributing to the formation of aggregates which physically protect SOM from decomposition (Slessarev et al., 2022; Wei et al., 2016). These short-range ordered phases include oxalate-extractable Al, Fe and Mn (poorly crystalline and organically complexed oxides and aluminosilicates) which are products of active weathering during initial weathering stages (Ashida et al., 2021; Ren et al., 2024; Dahms et al., 2012). Due to their large and reactive surface area, they can increase the recalcitrance of carbon in the soil by forming organo-mineral associations and thereby increasing the SOM residence time in the soil (Kleber et al., 2015). However, over time through weathering the poorly crystalline minerals transform into less reactive crystalline minerals, which are less effective in stabilizing organic matter and can therefore reduce carbon stability (Slessarev et al., 2022). Dithionite extracted Al, Fe and Mn are short-range-ordered (hydr)oxides including the crystalline and poorly crystalline forms and non-silicate bound Al (Ren et al., 2024). Since the weathering and transformation of poorly crystalline Al and Fe (hydr)oxides influences SOM stability, and both processes are influenced by warming (Slessarev et al., 2022; Ren et al., 2024; Ofiti et al., 2021), it is important to analyse how warming alters these minerals to understand implications for SOM stabilization. The changes in SOM with warming are depth dependent, where the SOM in the subsoil is more strongly influenced than in the topsoil. The decomposition in deeper soil horizons is accelerated with warming and decomposes the pre-existing SOM (Ofiti et al., 2021). Warming can shift the SOM composition towards more microbially transformed material, leaving the more stable compounds and decomposing the less stable ones (Ofiti et al., 2021). The balance between soil weathering, mineral transformation and SOM decomposition is one factor determining carbon loss or persistence in the soil, which is influenced by soil warming.

1.2 Spatial heterogeneity

Spatial heterogeneity is inherent in soils and refers to differences within soil properties across different scales, space (horizontally) and depth (vertically) within the soil, and is controlled by the interaction of biological, chemical and physical characteristics and processes (Saleh, 2018; Durán et al., 2018). These include intrinsic structural characteristics like parent material and mineralogy, and external factors like climate, topography, vegetation, litter input and microbial activity, and soil management practices (Saleh, 2018; Pan et al., 2024; Stoyan et al., 2000; Lucas, 2001; Kautz et al., 2013). Climatic variables like temperature and humidity influence soil and vegetation properties which directly affect the spatial heterogeneity of soils, making it relevant in the context of climate change (Durán et al., 2018). Soil processes, such as weathering and nutrient cycling, change soil properties on various spatial scales resulting in different interconnected soil property gradients leading to variability throughout the soil with depth (Saleh, 2018). These processes result in heterogeneous water dynamics, weathering rates, element mobility and distribution, leading to variability in the soil (Durán et al., 2018). Small-scale spatial heterogeneity encompasses non-uniformly distributed microbial communities, which concentrate in spots of favourable moisture and nutrient conditions, so-called hot spots, creating local variability through changed redox and pH conditions, especially in the topsoil and rhizosphere (Lucas, 2001; Huang et al., 2014; Kleber et al., 2015). Further heterogeneity results from nutrient cycling and redistribution by plants which is dependent on the root density and distribution (Kautz et al., 2013).

Spatial heterogeneity within the soil can enhance ecosystem resilience and balance ecosystem processes like nutrient cycling, plant performance, competitiveness and productivity and can increase the diversity within the soil ecosystem (Durán et al., 2018). Studying the variability of soils can help to understand dynamic changes of soils within an ecosystem and can build the basis for effective land management and restoration of degraded soils and ecosystems (Pan et al., 2024). It can also help in interpreting the effects of other factors, such as soil warming. Analysing spatial heterogeneity provides an overview of the scale at which natural differences occur within soils in close proximity, allowing these to be set into the context of differences caused by warming.

1.3 Research gaps

Research about weathering has been conducted in the context of geological time scales in terms of chronosequences and with the approach of using space as a substitute for time, but short-term shifts in weathering dynamics especially under soil warming are not well studied (Johnson & Turner, 2019; Doetterl et al., 2018; Lucas, 2001; Gewirtzman et al., 2019). Research on short-term changes under climate change is mostly conducted using weathering models as has been done or reviewed by Belyazid et al. (2022), Johnson & Turner (2019), Akselsson et al. (2016) and Kronnäs et al. (2023). However, models often cannot contain all relevant processes and cannot account for local heterogeneities and unexpected external influences (Johnson & Turner, 2019; Ren et al., 2024). Ren et al. (2024) have noted that Al and Fe (hydr)oxides are often not included within ecosystem models even though they are essential in predicting SOC storage and for connecting SOM to soil weathering. Furthermore, the modelling data are dependent on the quality of the input data, which shows the importance for in-situ field measurements (Belyazid et al., 2022). Many long-term in-situ field experiments focussing on the effect of warming have analysed SOM, carbon and microbial responses (Ofiti et al., 2021; Soong et al., 2021; Hanson et al., 2020; Cheng et al., 2017). But the effect of warming on the soil weathering degree has not been assessed in such an experiment. Such long-term in-situ experiments can show short-term (compared to

geological scales) dynamics and changes in soil weathering, pH and mineral and (hydr)oxide composition. The duration of the experiment must at least span several years of warming treatment to make sure changes in soil weathering can be detected, as soil dynamics are extremely complex and soil processes all work on different time scales (van den Enden et al., 2021; Ofiti et al., 2021).

Subsoil and deep soil are often neglected in studies, in which the focus usually lies on the top 20-30 cm (Kautz et al., 2013; Angst et al., 2021; Ofiti et al., 2021). Subsoil processes and characteristics often remain untested even though they are depth dependent and the subsoil contains a large carbon and nutrient reservoir (Kautz et al., 2013; Ofiti et al., 2021; Goebes et al., 2019). Spatial heterogeneity is a key limiting factor in in-situ experiments, where local variability cannot be captured well with sampling (Riley et al., 2025), thus taking soil spatial heterogeneity into account is helpful to reduce overestimations and underestimations within soil properties.

The aim of this study is to analyse the effect of long-term soil warming on soil weathering, including several weathering indicators and their linkage to SOM stability throughout 1 m deep mineral soil profiles. This fills the research gaps of using in-situ long-term experimental data to analyse soil weathering in the context of soil warming while including the dimension of soil depth. Analysing spatial heterogeneity separately from warming can place the weathering results with warming into the context of natural local variability.

1.4 Research questions and hypotheses

This thesis analyses the effect of 10 years of soil warming on the degree of soil weathering in deep granitic mineral soils in a mediterranean climate. The analysis is based on an in-situ soil warming experiment which has been running for ten years, and it uses several soil weathering indicators and parameters, including pH, oxalate and dithionite extractable Al, Fe and Mn, bulk elemental composition (Ca, Na, K, Mg, P, S, C, N, Al, Fe, Mn, Si) and soil organic matter composition (aliphatics, aromatics, carboxylics, lignin and polysaccharides) data. The weathering degree will be assessed based on these data, as well as on the weathering indices CIA and PIA and several ratios. Furthermore, spatial heterogeneity of the soil profiles without warming treatment will be assessed to understand site-specific differences in weathering and its parameters.

Therefore, the research questions are the following:

1. **What is the effect of 10 years of soil warming on the soil weathering degree of in-situ deep mineral soil profiles of granitic origin in a temperate forest under mediterranean climate?**

It is hypothesized that soil weathering increases with 10 years of soil warming, since higher temperatures accelerate soil weathering processes such as mineral dissolution, microbial activity and SOM decomposition, which produces organic acids that enhance mineral dissolution (Belyazid et al., 2022; Oliva et al., 2003). Due to increased plant and microbial activity, more organic acids enter the soil, which is expected to reduce pH (Lucas, 2001). Mobile element concentrations are expected to be lower due to increasing leaching from the soil, whereas immobile elements such as Fe and Al will be relatively higher (Middelburg et al., 1988). It is hypothesized that the abundance of poorly crystalline and crystalline (hydr)oxides increases with warming since warming increases mineral dissolution and crystallization (Slessarev et al., 2022). Soil organic carbon is expected to be lower under soil warming, due to increased microbial activity, and the SOM composition will shift towards more transformed and stable compounds (Ofiti et al., 2021; Soong et al., 2021; Hicks Pries et al., 2017). However, since mineral soil weathering progresses over long timescales, the acceleration of weathering through warming is expected to be small (Doetterl et al., 2018). It is expected that there will be differences with soil

depth, since different weathering processes dominate at different depths, where weathering processes are more influenced by biological processes in the topsoil and geogenic processes in the subsoil (Guimarães et al., 2022; Lucas, 2001).

2. **What is the role of spatial heterogeneity in in-situ deep mineral soil profiles in a temperate forest based on mineral weathering indicators?**

It is expected that spatial heterogeneity in the soil plays a significant role within a temperate forest environment because of the interaction of biological, chemical and physical processes operating on different spatial and temporal scales (Durán et al., 2018). It is hypothesized that the soil profiles that are spatially furthest apart show the greatest differences within weathering indicators, while soil profiles closer to each other show less differences (Stoyan et al., 2000). Even though the soil profiles all have the same parent material, other parameters on a larger scale, such as vegetation, can differ. Between the profiles furthest apart, more factors at different scales can vary. It is also expected that not all variables exhibit the same spatial heterogeneity, as they are governed by different soil processes (Garten et al., 2007).

2. Materials and Methods

2.1 Sample site

To determine the effect of 10 years of soil warming on the weathering of deep mineral soil profiles, soil samples from an in-situ deep soil warming experiment at the Blodgett experimental forest in California (120°39'40'' W; 38°54'43'' N; 1370 m a.s.l.) were analysed (Ofiti et al., 2021). The site lies within a coniferous temperate forest in mediterranean climate with an annual mean air temperature of 12.5°C, with approximately 1700 mm precipitation and a soil classified as an Alfisol (Ofiti et al. 2021, Soong et al. 2021).

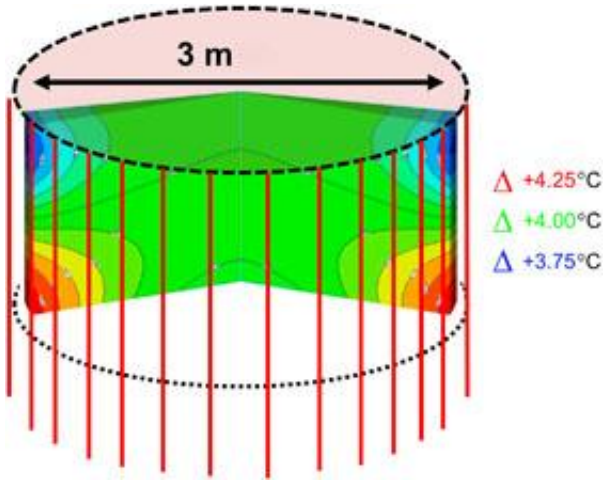

Figure 1: Schematic overview of the soil warming plot setup, showing the temperature gradient throughout the soil profile (Hanson et al., 2011).

The experimental setup consists of three different soil plot pairs, each including a control plot and a warmed plot. The individual plots are three meters in diameter and warmed down to one meter soil depth. The heating rods are set up as seen in Figure 1 for each plot and warmed to increase soil temperature consistently by +4°C compared to the control plots as described in Hanson et al. (2011). The experiment has been running since November 2013 and is still ongoing (Hicks Pries et al., 2017). Soil samples were taken after 4.5 years and after 10 years of soil warming in the three plot pairs. Three further soil plot pairs were set up in 2022 and warmed with the same method for 2 years. However, to answer the research question regarding how 10 years of soil warming has affected soil weathering, the samples taken after 10 years were analysed.

To determine the role of spatial heterogeneity within deep mineral soil profiles, the control samples after 10 years of warming and after 2 years of warming were analysed. The six control plots, which were not treated with warming, were assumed to be the same. So, differences in the

soil are due to natural spatial heterogeneity within the forest ecosystem. Figure 2 shows a map of the location of all soil plots in the Blodgett Forest experimental site.

Figure 2: Map of the experimental site in the Blodgett Forest. Control soil plots are shown in blue, warmed soil plots in red (Map created by Steve Kwatcho Kengdo).

The soil samples were taken in 10 cm depth increments from 0 – 90 cm depth and consisted of two soil cores from each soil plot, which were mixed for each depth increment. The samples were sieved to <2 mm and stored in sealed plastic bags until further analysis (Ofiti et al., 2021).

2.2 pH analysis

Soil pH was measured in $CaCl_2$, based on the method of Pansu & Gautheyrou (2006). 15 mL of 0.01 mol/L $CaCl_2$ solution was added to 3 g of soil (<2 mm), which was shaken on a shaker for 30 minutes at 150 rpm and subsequently filtered, resulting in a $CaCl_2$ soil extract. The pH was measured with a pH meter (Metrohm 914 pH/Conductometer) until the value showed no more fluctuations.

2.3 Elemental composition (XRF analysis)

The elemental composition was determined using X-Ray Fluorescence (XRF) analysis, which is commonly applied in weathering analyses. (Guimarães et al., 2022). Milled, air-dried soil was evenly filled into XRF sample cups with polyethylene film and measured in the XRF spectrometer (AMETEK SPEKTRO XEPOS). Quality control was ensured using internal reference materials, and elemental concentrations rather than oxides were used for XRF data analysis.

2.4 Fe, Al and Mn extractions and Atomic Absorption Spectroscopy (AAS)

To determine the amorphous and poorly crystalline bound Fe, Al and Mn (hydr)oxides, the elements were extracted with ammonium oxalate solution at pH 3 ± 0.1 and then measured with Atomic Absorption Spectroscopy (AAS) (Slessarev et al., 2022; Pansu & Gautheyrou, 2006). The procedure was performed twice for each sample to have technical replicate measurements. The solution was made with 16.1 g (0.11 mol/L) of ammonium oxalate monohydrate [$(NH_4)_2C_2O_4 * H_2O$]

and 10.9 g (0.087 mol/L) oxalic acid dihydrate [$H_2C_2O_4$ * $2H_2O$] and filled with deionized water resulting in a 1 L solution. 100 mL oxalate solution was added to 2.0–2.2 g of air-dried and sieved soil (<2 mm), then wrapped in aluminium foil for UV protection and subsequently placed on shakers for 120 minutes at 150 rpm for the extraction. After the extraction the samples were filtered to obtain the extracts.

Dithionite extraction can extract crystalline and non-crystalline Fe, Al and Mn oxides and hydroxides (Pansu & Gautheyrou, 2006). A 0.3 mol/L sodium citrate solution [$C_6H_5O_7Na_3 \cdot 2H_2O$] using 88.0 g, a 1 mol/L sodium bicarbonate solution [$NaHCO_3$] using 84.0 g, and a 0.1 mol/L magnesium sulphate solution [$MgSO_4$ * $7H_2O$] using 24.6 g were prepared. 8 mL of the sodium citrate solution and 2 mL of the sodium bicarbonate solution were added to 1 g of air-dried and sieved soil (<2 mm). After a hot water bath and 5 minutes of centrifuging at 4000 rpm, the supernatant solution was collected, and the process was repeated. Then 20 mL of the magnesium sulphate solution was added, centrifuged, collected, and diluted with deionized water (Pansu & Gautheyrou, 2006).

AAS was used to measure the poorly crystalline and crystalline Fe, Al and Mn concentrations from the oxalate and dithionite extraction. For the AAS measurements, the oxalate and dithionite extracts were diluted by a factor 5 to reduce clogging on the burner head from salt residues. An acetylene flame is used for Fe and Mn, which were measured at wavelengths of 348.3 nm and 279.5 nm, respectively. The acetylene was combined with nitrous oxide for the flame to measure Al, which was detected at 396.2 nm (Pansu & Gautheyrou, 2006). Standard solutions were used as quality control.

2.5 Organic matter composition (DRIFT analysis)

The organic matter composition was determined using Diffuse Reflectance Infrared Fourier Transform (DRIFT) spectroscopy (BRUKER INVENIO R). The samples were H_2O-corrected and subsequently imported into a R script (by Dr. Mike C. Rowley, unpublished; Stevens & Ramirez-Lopez, 2024) using the Savitzky-Golay filter to smooth the data, SNV (standard normal variate) normalization, and baseline correction. For the analysis the relative percentage of the area under curve (AUC) was used to analyse the relative abundance of the organic matter functional groups including aliphatic (2800- 3020 cm^{-1}), aromatic C-C (1380-1430 cm^{-1}, 1600-1670 cm^{-1}), aromatic C-H (725-775 cm^{-1}, 775-825 cm^{-1}), carboxylic (1680-1735 cm^{-1}), lignin (1500-1540 cm^{-1}), and polysaccharide (1040-1080 cm^{-1}) (Ofiti et al., 2021).

2.6 Carbon and nitrogen

Carbon and nitrogen data were provided for this thesis. C and N data were measured by dry combustion with an elemental analyser after the method described in Pansu & Gautheyrou (2006).

2.7 Weathering indices and ratios

2.7.1 Chemical index of alteration (CIA)

To assess the weathering degree of soil, the use of weathering indices can be helpful for the quantification. The chemical index of alteration (CIA) uses the elemental oxide forms to determine the ratio between the immobile Al and the mobile elements Ca, Na and K. The analytical results from the XRF analysis were used for the calculation. Values close to 100 represent soils with increased weathering and values under 50 indicate little to non-weathered soils (Wani et al., 2016, Price & Velbel, 2003).

$$CIA = \frac{Al_2O_3}{Al_2O_3 + Na_2O + K_2O + CaO} \times 100$$

The CaO only includes silicate minerals and must be corrected in case of carbonates. However, the soil samples did not contain any carbonates, which makes this weathering index well-suited to assess this soil.

2.7.2 Plagioclase index of alteration (PIA)

Another useful weathering index is the plagioclase index of alteration, which was proposed by Fedo et al. (1995). The major elements are expressed in molecular proportions, where the oxide weight in percent of the element was divided by the molecular weight (Heidari & Raheb, 2020). This weathering index assumes that Al_2O_3 remains immobile, and it accounts for the release of K_2O during weathering of mica and K-feldspars. The PIA ranges from 50 to 100, where a low value corresponds to fresh rocks and a high value to highly weathered material (Heidari & Raheb, 2020).

$$PIA = \frac{Al_2O_3 - K_2O}{Al_2O_3 + Na_2O + CaO - K_2O} \times 100$$

The PIA was also calculated from the analytical results of the XRF analysis.

2.7.3 (Hydr)oxide crystallinity ratio

To assess the crystallinity of the (hydr)oxides the following ratio, also called activity ratio, has been used for Fe, Al and Mn, respectively (Jaworska et al., 2016):

$$\frac{Fe_o}{Fe_d}$$

Where Fe_o corresponds to the oxalate extracted (hydr)oxides and Fe_d includes the dithionite extracted (hydr)oxides. The ratio gives insight into the proportion of poorly crystalline iron oxides relative to the total free iron oxides in a range usually from 0-1 (Ashida et al. 2021; Guimarães et al., 2022). The higher the ratio, the more (hydr)oxides are in poorly and non-crystalline forms and thus, less weathered (Guimarães et al., 2022). The ratio usually decreases with soil age (Jaworska et al., 2016).

2.7.4 Free oxides vs. total element content

The ratio between dithionite extracted (hydr)oxides and the total element content quantifies the proportion of pedogenic (free) oxides relative to the total element concentration in the soil and is especially used for iron. The ratio is used as a weathering index as it is controlled by pedogenic weathering and can be used to measure how much of the element is released from minerals during weathering (Huang et al., 2021; Jaworska et al., 2016).

$$\frac{Fe_d}{Fe_t}$$

A low ratio corresponds to a low degree of weathering (Jaworska et al., 2016). To calculate this ratio, the elemental concentration from the XRF data had to be transformed into mg/kg from the relative concentration in percent.

2.7.5 C/N ratio

The carbon to nitrogen ratio is an indicator of organic matter stability and quality (Amorim et al., 2023) and is often used for measuring nitrogen availability (Johnson & Turner, 2019). A low ratio corresponds to well-decomposed and microbially processed organic matter (Jones & Singh, 2014). High C/N ratios indicate inputs of fresh plant material which is only partially decomposed

and has a slower turnover due to lower nitrogen availability (Rasmussen et al., 2005; Amorim et al., 2023). The ratio was used to assess SOM stability and quality.

$$\frac{C}{N}$$

2.7.6 Drifts stability index (DSI)

The drifts stability index (DSI) is another ratio measuring the quality and stability of SOM (Laub et al., 2020). It shows the ratio between fast-cycling and slow-cycling SOM through the aliphatic and aromatic C-C functional groups (Laub et al., 2020). A higher ratio corresponds to a higher proportion of aliphatic compounds and a lower proportion of aromatic compounds, showing SOM with simpler structures and more easily decomposable carbon (Zheng et al., 2021). The ratio decreases with an increasing degree of decomposition (Margenot et al., 2015).

$$\frac{Aliphatic\ (2930\ cm^{-1})}{Aromatic\ (1620\ cm^{-1})}$$

In this thesis, the band limits for aliphatics are at 3020-2800 cm^{-1} and for aromatics at 1670-1600 cm^{-1}. For this ratio Laub et al. (2020) suggested that the band limits for aliphatic are at 3010-2800 cm^{-1} and for aromatic at 1660-1580 cm^{-1}, which shows a slight discrepancy.

2.8 Statistical analyses

The statistical analyses were performed per soil plot and per treatment and depth, which were afterwards averaged. This method resulted in three replicas per depth and treatment. The results were considered statistically significant with $p < 0.05$ and marginally significant with $p < 0.1$. The limited number of replicates reduces the statistical power of the analyses but still provides meaningful insights into the effect of soil warming throughout the soil profile.

2.8.1 Relative change [%]

The relative change [%] between the warmed and the control plots was calculated per depth and per soil plot individually with the following formula:

$$\frac{Warmed - Control}{Control} \times 100$$

Thereafter, the mean and the standard error of the relative change per treatment was calculated based on the three plot replicates. This was repeated for each variable with the original data and for the SOM composition with the AUC data (Ofiti et al., 2021).

2.8.2 Linear Mixed Effects Model

The effect of warming was additionally analysed with the help of a linear mixed effects model per variable. For the model, the fixed effects treatment and depth were used, since it was of direct interest how warming has changed the variable at each depth, and the changes were assumed to be consistent and reproducible. The factor plot was used as a random effect, since there was no direct interest individually, but the plots were a source of variability in the data (Oberg & Mahoney, 2007). The model was carried out with the *lme* function from the *nlme* package in R, accounting for autocorrelation with the *corAR1* function for depth (R Core Team, 2023; Pinheiro et al., 2025). The model assumptions included homoscedasticity and normality of residuals, which were tested visually in a residual plot and a Q-Q plot, and with a Shapiro-Wilk test on the residuals. Due to the small sample size, normality could not always be guaranteed and was improved with a log transformation of the variable. The performance of the model was assessed with ANOVA and the Akaike information criterion (AIC). The model structure and results of the ANOVA can be found in

the appendix in Table 2 and Table 3 for each variable. When significance was found, the *emmeans* post hoc test was used to get a pairwise result of the treatment effect at each soil depth, for which the significant results are found in the appendix in Table 4 (Lenth, 2025).

2.8.3 Correlation analysis

Correlation analysis was carried out in R to test the relationship of C with Fe_o and Al_o, and the DSI with Fe_o and Al_o (R Core Team, 2023). These correlations were carried out since the Fe and Al (hydr)oxides are critical for the formation of stable organo-mineral interactions and were found to explain the variation of carbon in the soil (Ren et al., 2024; Ashida et al., 2021). Normality was tested with Shapiro-Wilk tests and linearity between variables was checked with scatterplots. Spearman rank correlation was used for the correlation analysis since the data were not normally distributed and linearity was not always given (De Winter et al., 2016). Then Fisher's z transformation from the *cocor* package in R was used to see whether the correlations differed between the warmed and control plots (Diedenhofen & Musch, 2015). In a second correlation analysis depth was accounted for by using partial correlation with the *ppcor* package (Kim, 2015).

2.8.4 Spatial heterogeneity

Spatial heterogeneity was assessed by pairwise comparisons between the control plots 1-6 for each soil variable, using data from both the 10-year and 2-year soil warming experiment. The control plots in both experiments were not subjected to any treatment, thus, they were assumed to be equal, differing only through spatial differences. Due to a lack of true replicates and to enable the use of paired t-tests, pseudo-replicates were used by grouping soil depths into three categories, which included topsoil (0–10, 10–20, and 20–30 cm), subsoil (30–40, 40–50, and 50–60 cm), and deepsoil (60-70, 70-80, 80-90 and 90-100 cm). Thus, the depth group from 0-30 cm, and the group from 30-60 cm had 3 pseudo-replicates and the depth group from 60-100 cm had 4 pseudo-replicates.

Normality and homogeneity of variance for each depth group and for every variable were tested with a Shapiro-Wilk and a variance test in R. Depending on the outcome a t-test with equal or unequal variances, or a Wilcoxon test was performed to determine significant differences in concentrations of the variable between the six soil plots for each depth (Fay & Proschan, 2010). Since a large number of t-tests was carried out the results were accounted for multiple pairwise testing with the Benjamini–Hochberg procedure. The significant results can be found in the appendix in Table 5.

2.8.5 PCA analysis

Principal component analysis was carried out on the control plot data to analyse spatial heterogeneity. It is a statistical method which can reduce a large number of variables into principal components, which explain the variance of all included variables (Greenacre et al., 2022). 29 variables were included in the analysis and explained by the two major components. The analysis was carried out in RStudio with the packages *factoextra* with colour schemes used from *RColorBrewer* (R Core Team, 2023; Neuwirth, 2022; Kassambara & Mundt, 2020). The variables all were standardized to fit the same scale. The results were visualized in a two-dimensional biplot, showing the relationship between the variables through arrows, points and ellipses (Greenacre et al., 2022).

3. Results

In this section the results regarding the warming effect of 10 years of soil warming on the weathering degree and the effect of spatial heterogeneity between the six control plots are presented. The results include pH, elemental composition including the elements Al, Fe, Mn, Si,

Ca, K, Mg, Na, P, S, N and C, oxalate and dithionite extracted Al, Fe and Mn, and the relative abundance of soil organic matter functional groups including aliphatic, aromatic C-C, aromatic C-H, carboxylic, lignin and polysaccharide. Additionally, the results of the weathering indices and ratios are presented.

3.1 pH

The pH value showed no clear trend with depth and stayed consistent between 4.0-4.4 throughout the soil profile as seen in Figure 3. Treatment and depth did not have significant effects on pH (p = 0.41 and p = 0.28, respectively), and the relative change remained below ±10 %.

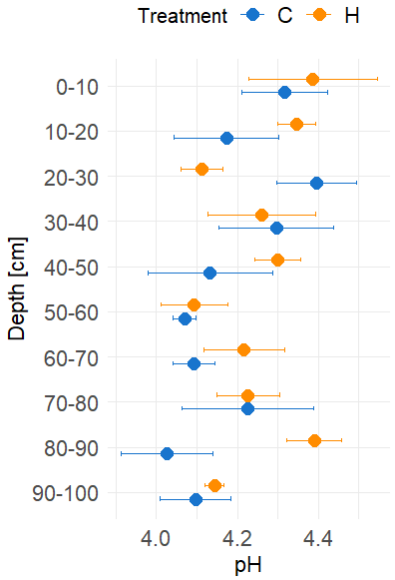

Figure 3: pH value per depth for control (blue) and warmed (orange) soil plots (mean ± SE, n = 3).

3.2 Elemental composition

For Fe the control plots showed no clear trend with depth whereas the warmed plots showed a positive trend with depth until 60-70 cm, then the values decreased with depth. Depth had a significant effect on Fe (p = 0.001), while treatment alone did not (p = 0.224). The interaction between depth and treatment showed a significant increase in the warmed plots at 60-70 cm depth (+22 %; p = 0.034), and a marginal increase at 70-80 cm (+16 %; p = 0.079) compared to the control plots. The overall relative change between treatments ranged between -4 % and +22 %.

Depth had no effect on Al (p = 0.828), but the control plots showed a small positive trend with depth throughout the soil profile, whereas the warmed plots showed an increase until 70-80 cm and then decreased with depth. Treatment had a marginal effect (p = 0.089), and the interaction between depth and treatment was marginal at 80-90 cm depth (-12 %; p = 0.050) but overall had no significant effect (p = 0.597). The concentration in the warmed plots was generally lower throughout the profile ranging from -12 % to +1 %.

Both warmed and control plots followed a clear negative trend for Mn concentrations with depth until 50-60 cm, after which the decrease strongly slowed. In the upper half of the soil profile Mn concentrations were lower in the warmed plots, whereas in the lower half they were higher compared to the control plots. Depth had a significant effect on Mn (p < 0.001), while treatment did not (p = 0.730). The relative change between treatments ranged from -26 % to +44 %.

Ca followed a significant negative trend with depth (p < 0.001). Although treatment had no significant effect (p = 0.426), the warmed plots showed higher concentrations in the topsoil and lower concentrations in the subsoil compared to the control plots with the relative change ranging from –38 % to +23 %.

Depth had a significant impact on K concentrations (p = 0.003). In the control plots K slightly increased with depth, while in the warmed plots the concentration followed a clear increase down to 60-70 cm depth, after which it remained stable downwards. Although treatment alone did not have a significant effect on K (p = 0.113), the interaction between depth and treatment was significant (p = 0.012), showing marginal to significant increases in K concentrations with warming. Increases were observed at 60-70 cm (+36 %; p = 0.050), at 70-80 cm (+42 %; p = 0.036), at 80-90 cm (+41 %; p = 0.061), and at 90-100 cm (+38 %; p = 0.087). Across the soil profile, the relative change with warming ranged from -4 % to +42 %.

Mg in the control plots showed stable concentration down to 30-40 cm depth, followed by a decrease with depth. In contrast, the warmed plots had stable but lower concentrations than control plots down to 40-50 cm depth, after which Mg concentrations increased with depth. Depth and treatment alone had no significant effect on Mg concentrations (p = 0.900 and p = 0.347, respectively). However, their interaction was significant (p < 0.001), specifically, Mg showed a marginal increase at 80-90 cm depth (+59 %; p = 0.090) and a significant increase at 90-100 cm depth (+102 %; p = 0.020) with warming. The relative change between treatments was between -15 % to +102 %.

Na followed a negative trend with depth for both treatments, where depth showed a significant impact (p < 0.001). The concentrations for the warmed plots were lower in the topsoil and higher throughout the rest of the soil profile compared to the control plots, even though treatment had no significant effect on Na (p = 0.324). The relative changes between warmed and control plots ranged from -9 % to +55 % throughout the soil profile.

Depth had a significant effect on S and P concentrations (p < 0.001), where both treatments showed a negative trend down to 50-60 cm depth, then the concentrations stayed consistent with depth. Depth showed a significant effect on S concentrations (p < 0.001), treatment alone had a marginal effect (p = 0.065), and the interaction of both fixed effects was significant (p = 0.006). The S concentrations increased significantly at 60-70 cm depth (+95 %; 0.023) and 90-100 cm (+93 %; p = 0.013), and the increase was marginal at 80-90 cm (+44 %; p = 0.074). Across the soil profile, the relative change with warming ranged from -3 % to + 95 % for S and from -4 % to +25 % for P, where concentrations generally were higher with warming, but the treatment effect was not significant (p = 0.411).

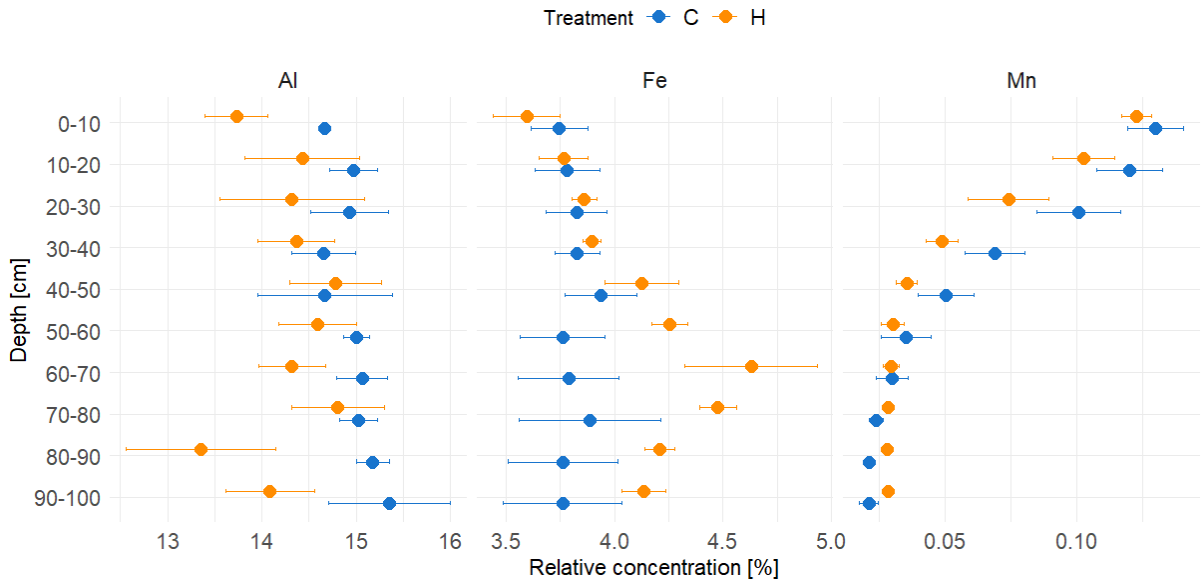

Figure 4: Al, Fe and Mn relative concentration [%] per depth for the control (blue) and warmed (orange) soil plots (mean ± SE, n = 3).

Si showed a positive trend with depth for both treatments (p < 0.001). Treatment alone had no significant effect on Si concentration (p = 0.774), whereas the interaction of treatment with depth showed marginal differences (p = 0.066), but not at specific depths. The relative difference with warming was low, ranging from -6 % to + 8%.

C and N both showed a significant negative trend with depth for both treatments (p < 0.001), with a strong decline until 40-50 cm depth, thereafter the decline was minimal with depth. Treatment

alone had no effect on either C or N (p = 0.487; p = 0.171). But the interaction of depth and treatment for C was significant (p = 0.002) and showed marginal differences at 60-70 cm (-49 %; p = 0.099) and at 80-90 cm (-45 %; p = 0.086). The range of change for C was between -49 % and +69 %, and for N between -39 % and +27 %.

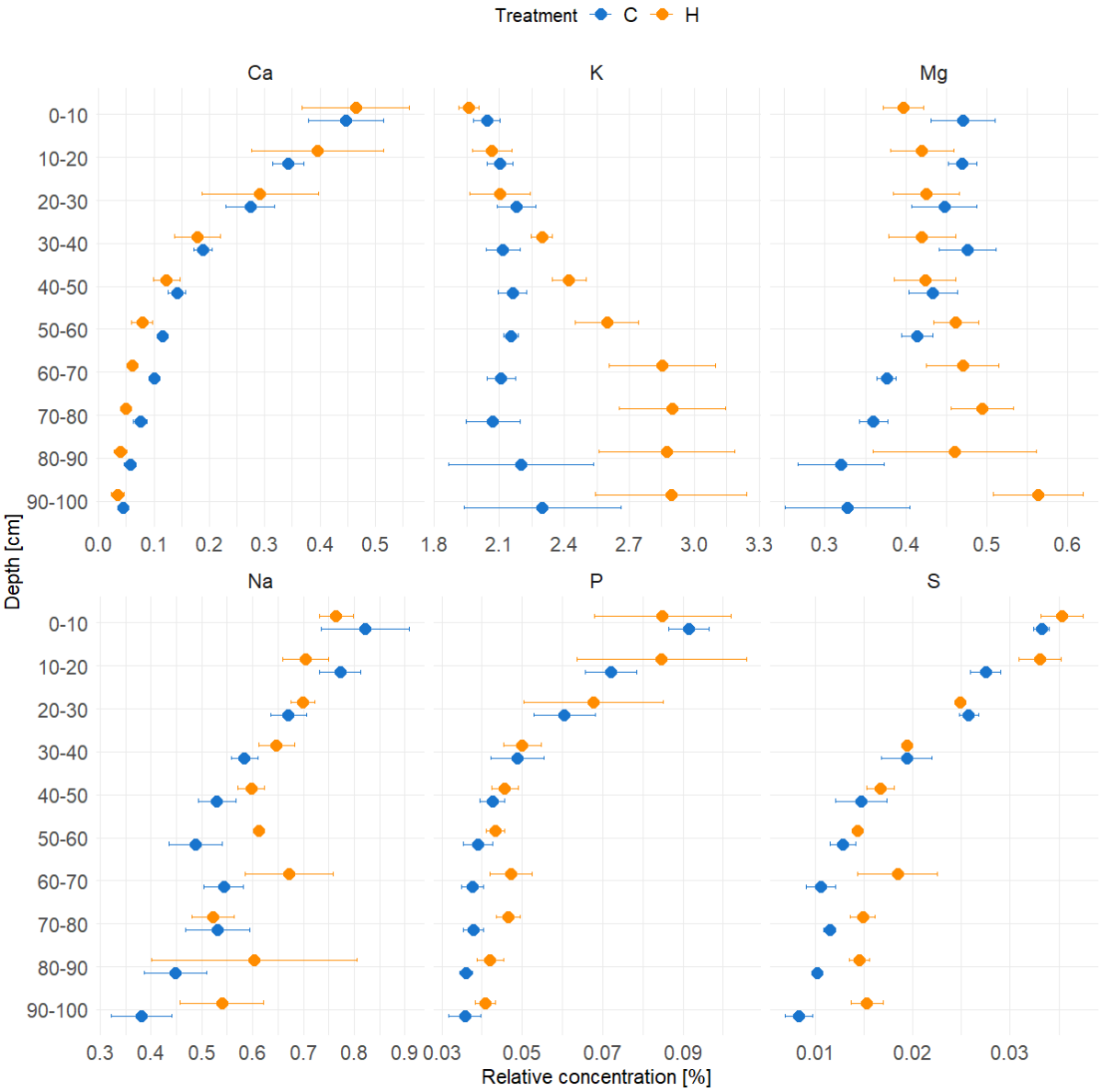

Figure 5: Relative Ca, K, Mg, Na, P and S concentration per depth for the control (blue) and warmed (orange) soil plots (mean ± SE, n = 3).

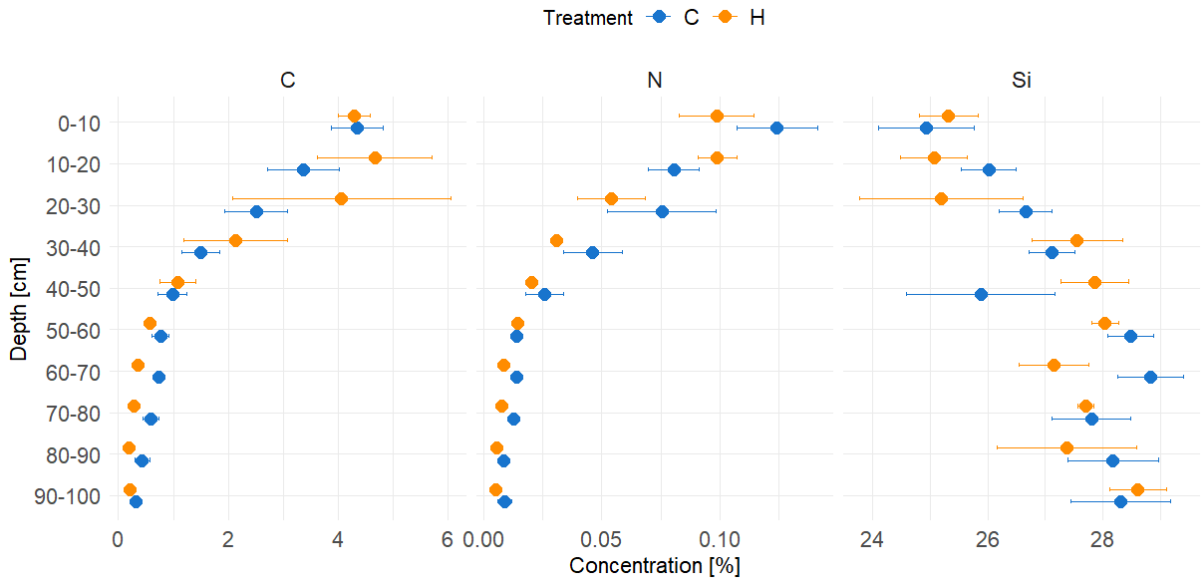

Figure 6: Total C and N content [%] and relative Si concentration [%] per depth for the control (blue) and warmed (orange) soil plots (mean ± SE, n = 3).

3.3 Oxalate-extracted Fe, Al and Mn

The oxalate-extracted Fe of the control plots showed a negative trend with depth, whereas in the warmed plots Fe_o concentrations increased from 50-60 cm depth downwards. Treatment alone showed no significant effect, but depth had a significant impact on Fe_o ($p < 0.001$). The interaction between depth and treatment was also significant ($p = 0.003$). At 70-80 cm the warmed plots showed a marginal increase in Fe_o concentrations (+104 %; $p = 0.086$), and at 90-100 cm depth the increase was significant (+269 %; $p = 0.015$). The relative change throughout the soil profile ranged from -4 % to +269 %.

Both, oxalate-extracted Al and Mn showed a negative trend with depth for both treatments, which was more pronounced in the upper half of the soil profile. For both elements, depth had a significant effect ($p < 0.001$). Al_o and Mn_o concentrations were lower with warming across almost all depths. However, treatment showed no significant effect on Al_o and Mn_o concentrations ($p = 0.384$ and $p = 0.467$, respectively). For Al the relative change was between – 41 % and +24 % and for Mn the relative change ranged from -61 % to +121 %.

3.4 Dithionite-extracted Fe, Al and Mn

The Fe_d concentration was significantly affected by depth ($p = 0.004$) and showed a very slight positive trend with depth in the control plots. The warmed plots followed an increase as well until 60-70 cm depth and decreased thereafter. The concentrations were similar between warmed and control plots until 30-40 cm depth, then the concentration was higher with warming until 70-80 cm, and in the subsoil the concentration was lower with warming. However, neither treatment alone nor the interaction between treatment and depth had a significant impact on Fe_d concentrations ($p = 0.833$ and $p = 0.196$, respectively). The relative change ranged between -9 % and +17 %.

The dithionite-extracted Al followed a clear negative trend with depth for both treatments, which was significant ($p < 0.001$). The concentration was lower with warming throughout the soil profile but was not significant ($p = 0.587$). The relative change ranged between -15 % to +4 %.

Depth had a significant impact on Mn_d ($p < 0.001$), which followed a clear negative trend with depth for both treatments until 40-50 cm, then the decrease slowed. Although treatment had no significant effect on Mn_d ($p = 0.430$), the concentration in the warmed plots was lower than in the control plots throughout the soil profile, with the relative change ranging from -58 % to +21 %.

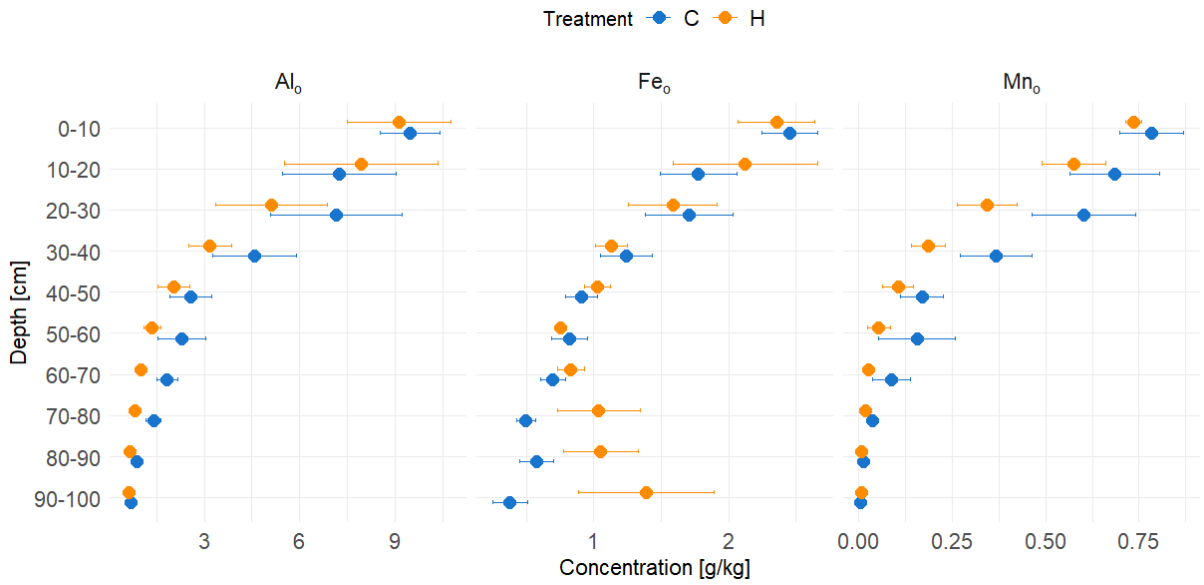

Figure 7: Concentration in g/kg of oxalate-extracted Al, Fe and Mn per depth for the control (blue) and warmed (orange) plots (mean ± SE, n = 3).

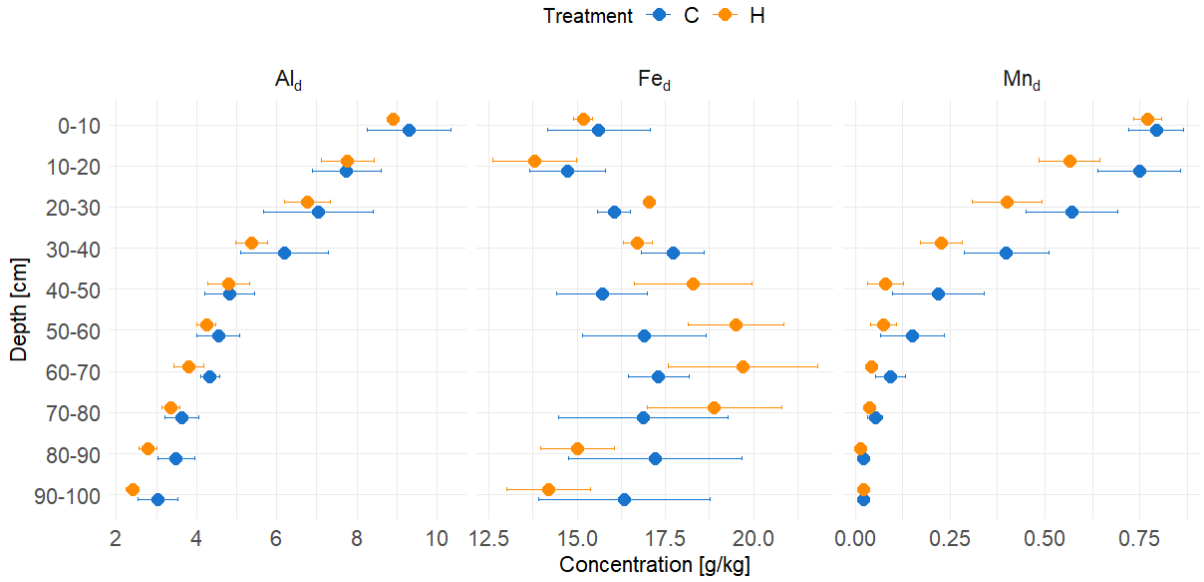

Figure 8: Concentration in g/kg of dithionite-extracted Al, Fe and Mn per depth for the control (blue) and warmed (orange) plots (mean ± SE, n = 3).

3.5 Soil organic matter composition

In general, in the topsoil aliphatic compounds dominated with 50 % at the surface, followed by aromatic compounds. Lignin, carboxylic and polysaccharide compounds were low at the top. With depth the aliphatic compounds declined rapidly, whereas the aromatics and lignin increased with depth. Carboxylic and polysaccharide compounds stayed within a similar concentration throughout the profile relative to all compounds.

The aliphatic functional group had a high concentration at the surface and showed a significant negative trend with depth for both treatments which stagnated at 60-70 cm depth ($p < 0.001$). The concentration was higher until 40-50 cm depth with warming, then the control plots had a higher aliphatic abundance downwards, which was not significant ($p = 0.943$). The relative change with warming lay between -23 % and +42 %.

Within the aromatic C-C group a positive trend with depth was seen for both treatments ($p < 0.001$). Treatment had no significant effect on the aromatic C-C functional group ($p = 0.517$), showing no clear patterns of difference with warming, and the relative change ranged between -10 % to +6 %.

The aromatic C-H group showed a clear positive trend with depth in both treatments, which was significant ($p < 0.001$). In surface horizons, the concentration for the warmed plots was slightly lower than for the control plots throughout most of the soil profile, however, treatment had no significant effect on aromatic C-H ($p = 0.603$). The relative change ranged from -23 % to +5 %.

The carboxylic group showed a weak positive trend with depth until 50-60 cm for the warmed and control plots, then downwards, the concentrations had a negative trend. The concentration with warming was lower in the top half and higher in the bottom half of the profile. In the control plots, there was an outlier which gives the profile a peak at 30-40 cm. Neither treatment, nor depth had a significant effect on the carboxylic group ($p = 0.854$; $p = 0.093$). The relative change with warming lay between -37 % to +72 %.

There was a significant positive trend with depth for lignin in both treatments until 50-60 cm depth, then stable concentrations downwards were observed ($p < 0.001$). In the upper half of the profile the concentrations were similar between warmed and control plots, in the lower half, the concentrations with warming were higher, but showed no significant difference ($p = 0.502$). The relative change ranged between -9 % to +53 %.

The polysaccharide group had no clear trend. The concentration was generally higher with warming and had similar values throughout the profile. Depth, treatment and their interaction showed no significance ($p = 0.266$; $p = 0.121$; $p = 0.497$, respectively). But at 40-50 cm depth polysaccharide abundance was marginally higher with warming ($p = 0.076$). The relative change ranged between +18 % to +469 %. However, the uncertainties shown by the standard error were high, showing variability between individual plots.

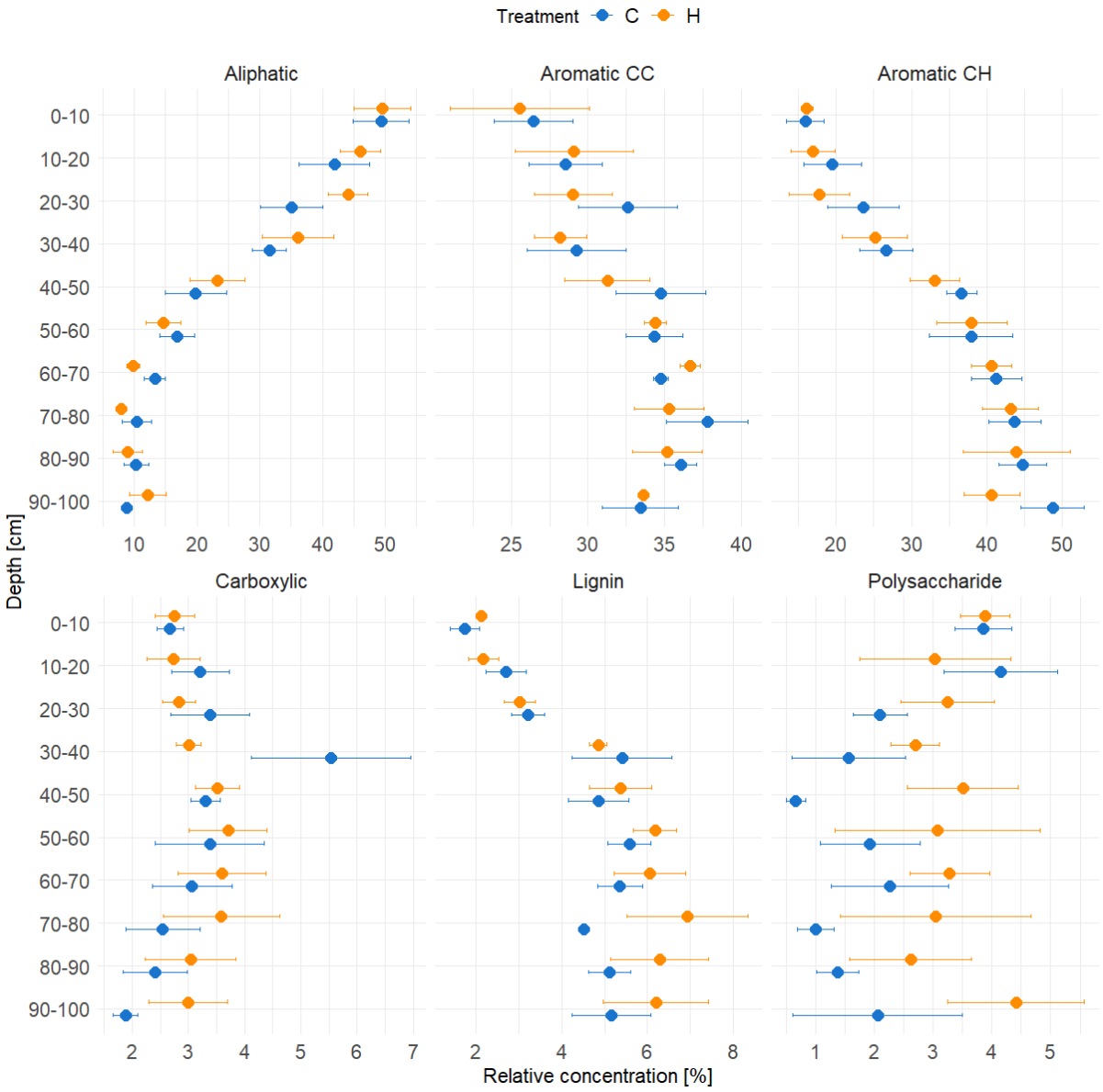

Figure 9: Relative concentration [%] per depth for aliphatic, aromatic C-C, aromatic C-H, carboxylic, lignin and polysaccharides for the control (blue) and warmed (orange) soil plots using the area under curve data (mean ± SE, n = 3).

3.6 Weathering indices: CIA & PIA

The results for the CIA of the 10-year warming experiment showed for both treatments advanced weathered soil throughout the soil profile. The control plots showed increased weathering with depth, whereas the warmed plots showed the highest weathering at 40-50 cm and the lowest weathering towards the bottom and the top of the profile. Depth had a significant effect on the CIA (p = 0.036). Additionally, although treatment and the interaction of treatment and depth were not significant (p = 0.120; p = 0.188), the control plots showed higher weathering compared to the warmed plots throughout the profile. The pairwise comparison from *emmeans* showed marginally lower CIA for the warmed plots at 60-70 cm depth (-4 %; p = 0.095), and at 90-100 cm depth (-4 %; p = 0.080), and significantly lower CIA at 80-90 cm depth (-6 %; p = 0.041). The relative change ranged between -6 % to 0 % with warming.

The PIA showed a negative trend with depth for both treatments ($p < 0.001$). The PIA was generally lower with warming, especially at deeper depths, but showed no significant difference ($p = 0.3943$). The relative change between warmed and control plots lay between -2 % and 0 %. Both the warmed and the control plots were highly weathered soils as expressed by the PIA.

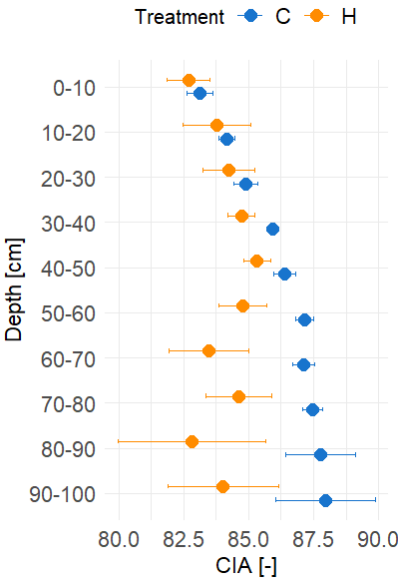

Figure 10: CIA per depth for the control (blue) and warmed (orange) soil plots (mean ± SE, n = 3).

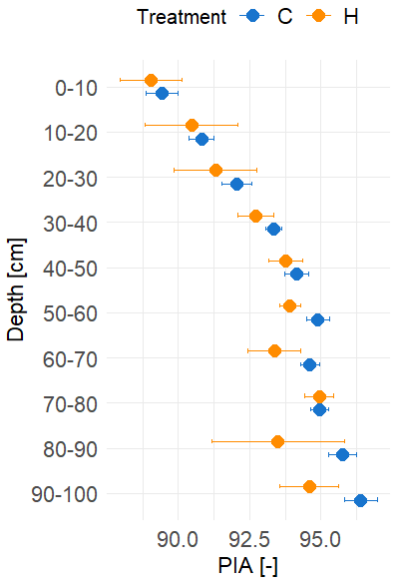

Figure 11: PIA per depth for the control (blue) and warmed (orange) soil plots (mean ± SE, n = 3).

3.7 Ratios

The Al_o/Al_d ratio showed a negative trend with depth for both treatments, which was significant ($p < 0.001$) and more pronounced until 40-50 cm depth, then the decrease was minor. Even though not significant ($p = 0.287$), the warmed plots generally had a lower ratio than the control plots. The relative change lay between -35 % and +20 %.

The Fe_o/Fe_d ratio showed a significant negative trend with depth ($p < 0.001$) for the control plots, and for the warmed plots it showed a curve, which decreased until 40-50 cm and then increased again. In the middle of the soil profile, the ratio for the control plots was higher, below 60 cm the ratio for the warmed plots was higher. Even though treatment alone had no significant effect on the ratio ($p = 0.210$), the interaction of treatment and depth was significant ($p = 0.009$), showing a marginal increase with warming at 80-90 cm depth (+112 %; $p = 0.093$), and a significantly higher ratio for the warmed plots at 90-100 cm depth (+383 %; $p = 0.013$). The relative change overall ranged from -16 % to +383 %.

The Mn_o/Mn_d ratio decreased with depth for both treatments, where the warmed plots were slightly lower than the control plots, apart from an outlier at 40-50 cm depth. Depth had a significant effect on the ratio ($p < 0.001$), whereas treatment alone and in interaction with depth did not ($p = 0.552$; $p = 0.102$, respectively). However, pairwise comparison showed that the ratio at 40-50 cm depth was significantly higher with warming (+63 %; $p = 0.039$). The relative change between the warmed and control plots ranged from -34 % to +79 %.

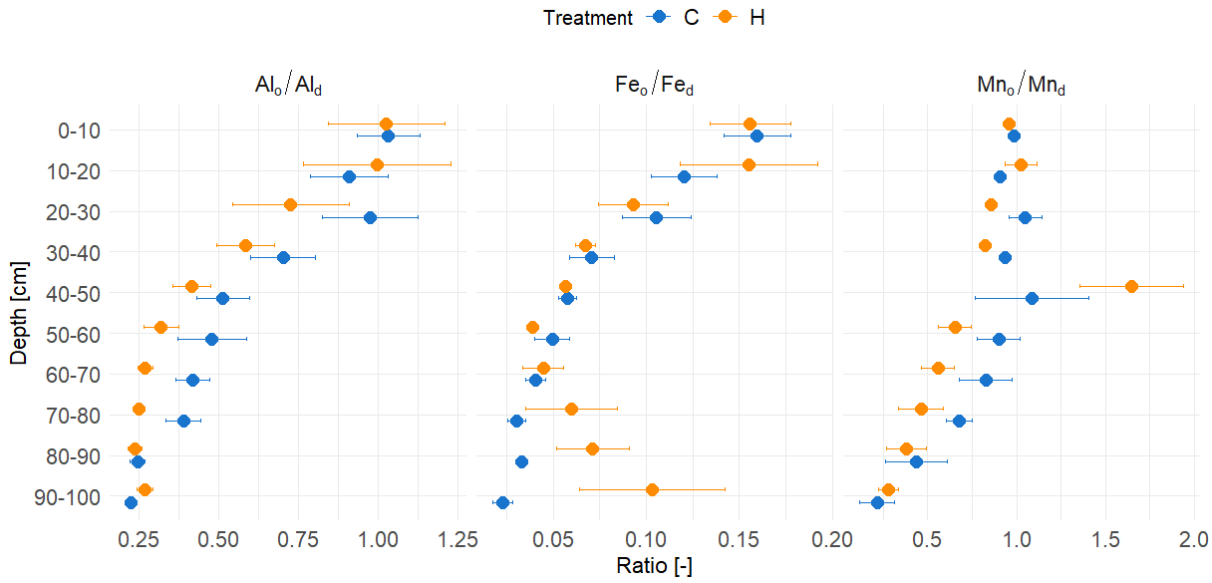

Figure 12: Al_o/Al_d, Fe_o/Fe_d and Mn_o/Mn_d ratios per depth for the control (blue) and warmed (orange) soil plots (mean ± SE, n = 3).

The Al_d/Al_t ratio followed a significant negative trend with depth for both treatments ($p < 0.001$). In the topsoil the ratio for the warmed plots was slightly higher, in the rest of the soil profile, the ratio for the control plots was higher, but treatment did not have a significant effect ($p = 0.823$). The relative change between treatments ranged from -9 % to +10 %.

The Fe_d/Fe_t ratio showed no clear trend with depth even though depth still had a significant effect ($p = 0.043$). The ratio for the warmed plots increased until 50-60 cm depth, then decreased again, whereas the ratio of the control plots increased until 30-40 cm depth and then stayed consistent downwards. Treatment and the interaction of treatment and depth were not significant ($p = 0.489$, $p = 0.114$) but showed a marginally lower ratio at 80-90 cm and 90-100 cm depth with warming (-20 %; $p = 0.072$ and -16 %; $p = 0.090$, respectively). The relative difference between warmed and control plots lay between -20 % and +12 %.

The Mn_d/Mn_t ratio decreased significantly with depth ($p < 0.001$), where the ratio was generally higher with warming but not significant ($p = 0.332$). The relative difference ranged from -47 % to +5 %.

Treatment and depth showed no significant effect for the C/N ratio ($p = 0.782$; $p = 0.935$). However, a trend in the upper half of the profile showed a higher C/N ratio, and in the bottom half of the soil profile, it showed a lower C/N ratio with warming. The relative difference lies between -23 % and + 90 %.

The DSI followed a negative trend for both treatments until 50-60 cm depth, then the ratio remained consistent downwards. There were no significant differences between treatment ($p = 0.809$), however, depth had a significant effect ($p < 0.001$). The relative difference between warmed and control plots lies between - 24 % and +54 %.

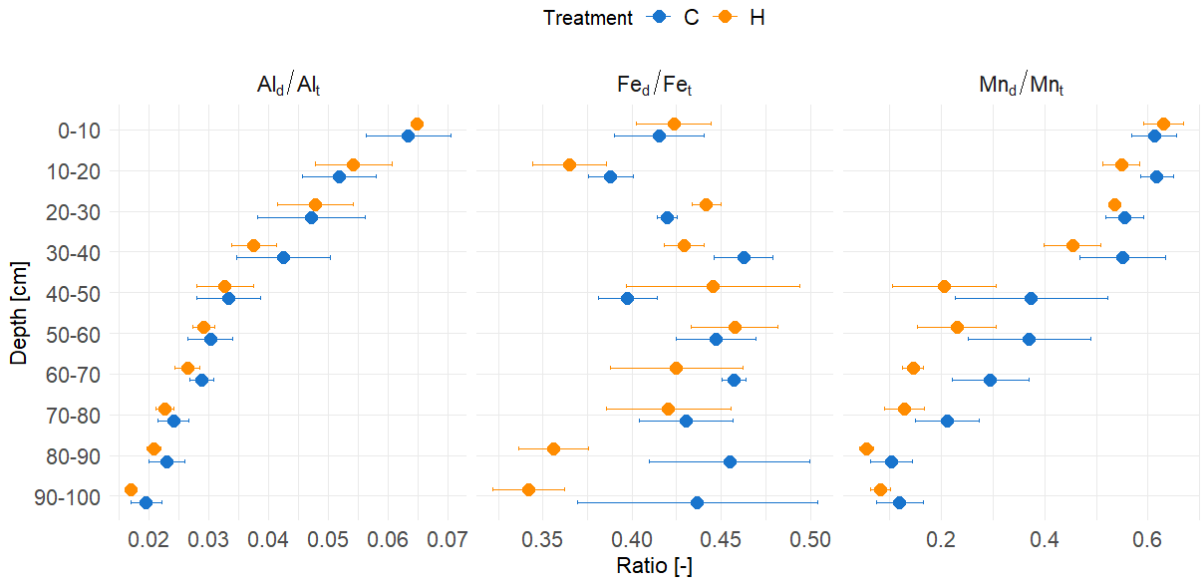

Figure 13: Al_d/Al_t, Fe_d/Fe_t and Mn_d/Mn_t ratios per depth for the control (blue) and warmed (orange) soil plots (mean ± SE, n = 3).

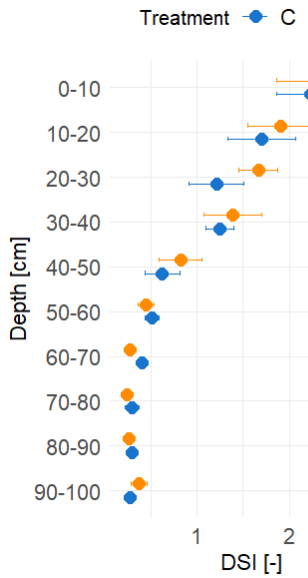

Figure 14: DSI per depth for the control (blue) and warmed (orange) soil plots (mean ± SE, n = 3).

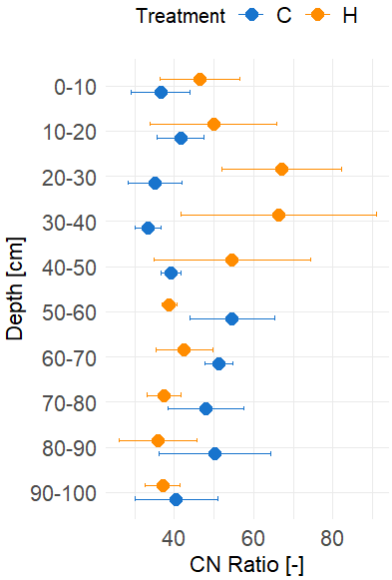

Figure 15: C/N ratio per depth for the control (blue) and warmed (orange) soil plots (mean ± SE, n = 3).

3.8 Correlation analysis

The correlation without depth adjustment showed moderate to strong significant positive relationships for all tested variable pairs (Table 1). The correlation between Fe_o and C, and Fe_o and the DSI showed significant differences between treatments, where the warmed plots had a weaker relationship than the control plots. After accounting for depth, the correlations generally weakened and ranged from no correlation to moderate correlation (Table 1). With depth adjustment, the correlation between Fe_o and C significantly differed between treatments, where no correlation with warming was found.

Table 1: Results for correlation analysis.

Correlations	Treatment	Estimate ρ	p-value	z-score fisher	p-value fisher	Depth-adjusted estimate ρ	Depth-adjusted p-value	z-score fisher	p-value fisher
Fe_o vs DSI	C	0.914	<0.001	2.9914	0.003	0.542	0.002	0.6611	0.509
Fe_o vs DSI	H	0.626	<0.001	2.9914	0.003	0.403	0.030	0.6611	0.509
Al_o vs DSI	C	0.890	<0.001	0.5666	0.571	0.388	0.037	0.9613	0.336
Al_o vs DSI	H	0.853	<0.001	0.5666	0.571	0.147	0.446	0.9613	0.336
Fe_o vs C	C	0.921	<0.001	4.0482	<0.001	0.541	0.002	2.6332	0.009
Fe_o vs C	H	0.459	0.012	4.0482	<0.001	-0.111	0.567	2.6332	0.009
Al_o vs C	C	0.960	0	-0.0209	0.983	0.754	<0.001	0.9753	0.329
Al_o vs C	H	0.960	0	-0.0209	0.983	0.614	<0.001	0.9753	0.329

3.9 Spatial heterogeneity

The t-test showed significant spatial differences between soil plots for several variables across all depths, with the strongest heterogeneity in the subsoil at 60-100 cm depth.

The most significant spatial variation was found in Al, Fe, K, Mg, S, Al_d, Fe_d, and the CIA. Furthermore, limited differences were found in Mn, P, aliphatic, lignin, polysaccharide, the DSI, the PIA and the ratio Al_o/Al_d. No significant spatial heterogeneity was observed for pH, Ca, Na, Si, C, N, C/N, Fe_o/Fe_d, Mn_o/Mn_d, Al_d/Al_t, Fe_d/Fe_t, Mn_d/Mn_t, aromatic C-C, aromatic C-H, carboxylic, Al_o, Fe_o, Mn_o and Mn_d. The results for all significant t-tests can be found in the appendix in Table 5. Certain plots showed consistent trends over multiple variables. Plot 6 often had higher concentrations, such as for Fe, Mg, Fe_d and the CIA, but showed a trend for the lowest pH. Plot 3 tended to have lower values, such as for Fe, P and Fe_d. Other plots like plots 4 and 5 varied with depth and by variable and sometimes had lower or higher concentrations compared to the other plots. Elemental concentrations showed more heterogeneity than soil organic matter functional groups. The results for the most important variables will be given in more detail.

More specifically, in the deep soil, Al concentrations were highest in plot 4, with plot 6 just slightly lower. A similar pattern could be seen for Fe, where plot 6 generally had the highest concentrations throughout the profile, while plots 2 and 3 consistently had the lowest, especially at 0-30 cm and 30-60 cm depth. K and Mg also showed spatial variations at all depths. Plot 4 had the highest K concentrations in the topsoil, whereas in the deep soil plot 5 reached the highest K concentrations. At 60-100 cm depth plot 6 had the lowest concentrations. Mg was consistently high in plot 3 in the topsoil, and plot 6 in the deep soil. At 30-60 cm depth, plot 4, on the other hand, showed the lowest concentrations. S had variability only in the deep soil, where plot 3 had the lowest concentration compared to higher concentration levels in plots 4, 5 and 6. Spatial differences were found for Al_d at 60-100 cm depth, where plot 5 had a lower concentration than plots 2, 4 and 6. For Fe_d, plot 6 again showed the highest concentration at 0-30 cm and 30-60 cm depth. Plots 2 and 3 exhibited the lowest values across all depths. In the deep soil plot 4 had the highest concentration. The CIA showed high spatial variation with the highest heterogeneity in the deep soil, where plot 6 consistently had the highest values across all depths. At 30-60 cm and 60-100 cm depth plot 5 showed the lowest values.

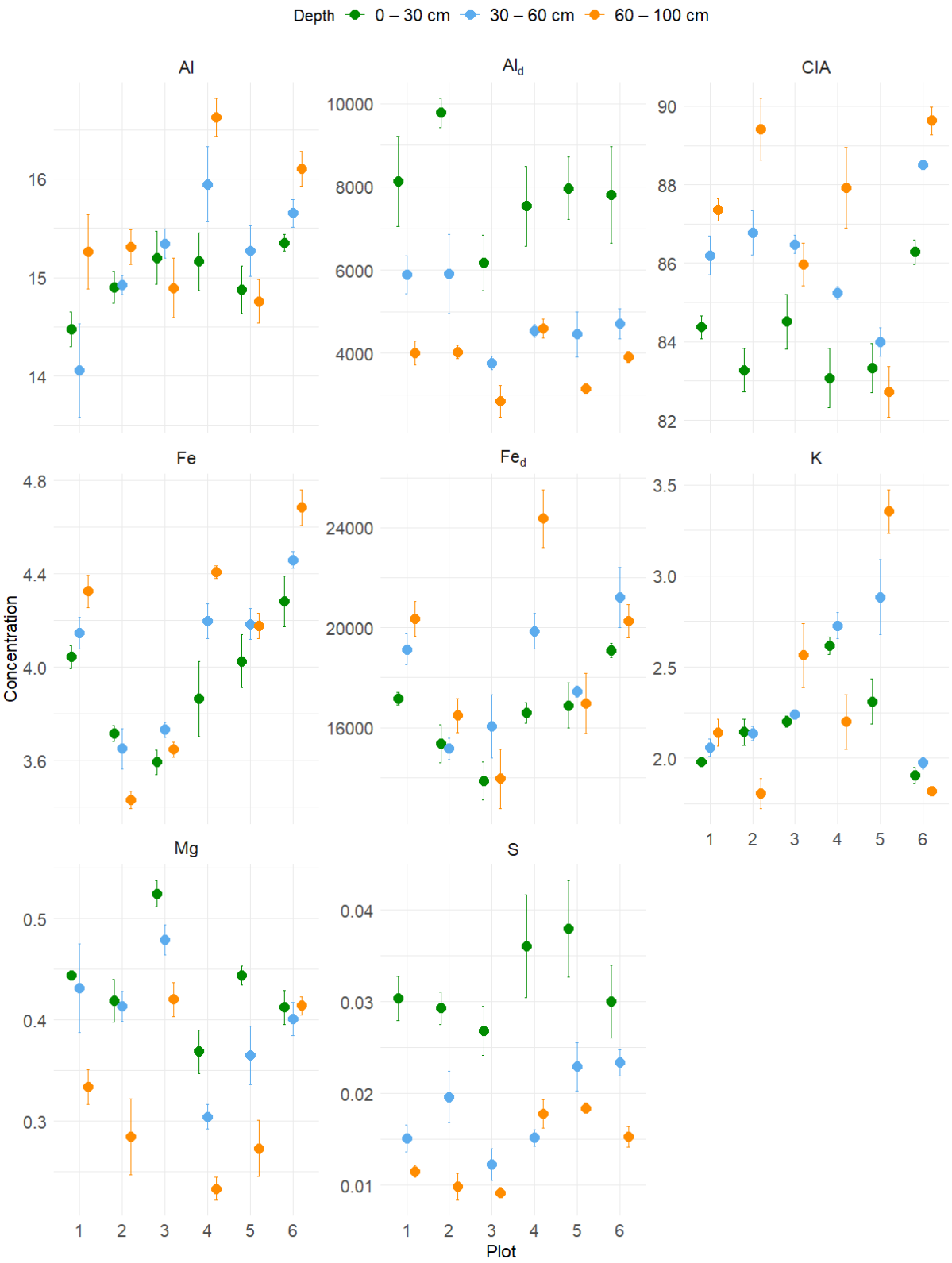

Figure 16: Relative Al, Fe, K, Mg and S concentration [%], Al_d and Fe_d concentration [g/kg] and the CIA ratio [-] for each individual soil plot at 0-30 cm depth (green), at 30-60 cm depth (blue) and at 60-100 cm depth (orange), (mean ± SE, for 0-30 and 30-60 cm depth n = 3, for 60-100 cm depth n = 4.

3.10 PCA analysis

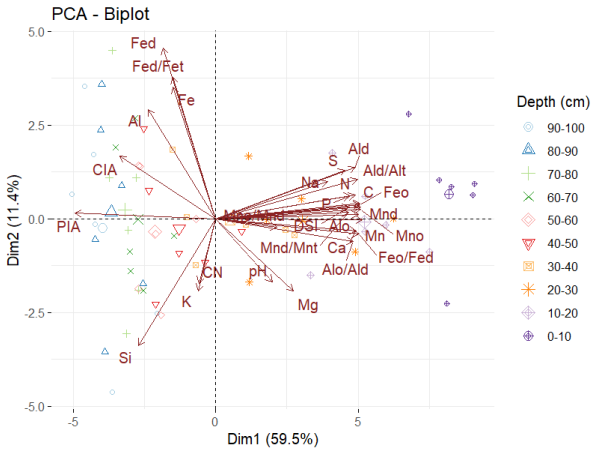

Figure 17: PCA biplot for PC1 (x-axis) and PC2 (y-axis), coloured by soil depth.

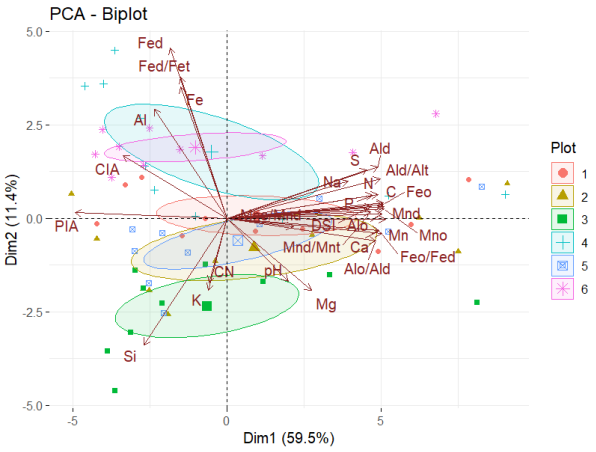

Figure 18: PCA biplot for PC1 (x-axis) and PC2 (y-axis), coloured by soil plot.

In PCA, PC1 explained 59.5 % of the variance and PC2 explained 11.4 %, together accounting for 70.9 % of the total variance in the data. PC3 explained 6.9 % and PC4 4.5 % of the total variance. All other PC contributions can be seen in a scree plot in Figure 20 in the appendix. As illustrated in Figures 17 and 18, the different soil plots are spread along the axis of PC2, whereas samples from different depths spread along the axis of PC1. Plots 4 and 6 are set highest on the PC2 axis, plot 3 is set lowest and plots 1, 2 and 5 lie at the centre. Shallow depth intervals are set to the right of the PC1 axis and deeper depths are set to the left, forming a gradient between shallow and deeper soil depths along the PC1 axis.

Many variables point to the right on PC1, showing a correlation to each other. These include Fe_o, Fe_o/Fe_d, Mn, Mn_o, Mn_d, Mn_o/Mn_d, Mn_d/Mn_t, Al_o, Ald, Al_d/Al_t, Al_o/Al_d, C, N, S, P, Ca, Na, Mg, DSI and pH, where pH and Mg point more diagonally to the bottom right. The PIA is the only variable pointing straight to the left. Pointing to the top left are Fe, Fe_d, Fe_d/Fe_t, Al and the CIA, and towards the bottom left point Si, K and the C/N ratio. In Table 7 in the appendix, the loadings of the variables for each PC can be seen.

4. Discussion

4.1 Soil weathering processes and the influence of temperature

Warming is expected to increase soil weathering, since chemical reactions increase with higher temperatures (Kronnäs et al., 2023). Soil moisture has a strong influence on weathering rates as well, since water is a main driver for the breakdown of minerals and the movement of elements throughout the soil profile as it acts as a medium for dissolution and transport (Kronnäs et al., 2023; Middelburg et al., 1988). In the Blodgett Forest soil warming experiment, soil warming was found to reduce soil moisture, influencing the weathering process and potentially inhibiting the expected weathering acceleration under warming with drier conditions (Kronnäs et al., 2023; Riley et al., 2025; Ofiti et al., 2021). After 4.5 years of soil warming the volumetric water content was found to be 2-5 % lower throughout the whole soil profile (Ofiti et al., 2021). Lower water filled pore space was specifically noted at 10 cm, 50 cm and 90 cm depth (Riley et al., 2025). Kronnäs et al. (2023) found that soil weathering rates were reduced by 78-96 % in drought years compared to non-drought years within a model. This suggests that without enough soil moisture, higher temperatures alone might not lead to accelerated weathering.

In temperate forest systems in granitic environments, acidic soil is inherent due to mineralogy consisting predominantly of feldspar, quartz and mica which are poor in base cations leading to lower buffer capacity (Kronnäs et al., 2023). In these ecosystems biological processes can lead to acidity and increased chemical weathering as well through plant root excretion and organic acids resulting from plant biodegradation (Kautz et al., 2013; Oliva et al., 2003; Williams et al., 2007). At an acidic pH between 4-4.4 the buffer system is based on the dissolution of Al-bearing minerals buffering soil acidity by consuming H^+ and releasing Al^{3+}, and Fe buffering could be present as well as it starts at pH 4 (Jiang et al., 2018). Temperature is a driver of acidification (Kronnäs et al., 2023), however, soil pH showed no differences with soil warming in the Blodgett Forest soil warming experiment. This could be due to lower soil moisture content, since humidity drives acidification through biological activity, suggesting pH could be more driven by humidity than warming (Kleber et al., 2015). Van den Enden et al. (2021), who did a warming experiment with N addition, also did not find any significant differences in soil pH after 10 years. This shows that 10 years of soil warming might not influence pH or is not enough time to show differences. The effect of 10 years of soil warming in the context of soil weathering, a process spanning long time periods, would be expected to be small and with a small number of replicates statistical significance is unlikely (Riley et al., 2025; Zhang et al., 2024). Spatial heterogeneity is a further important aspect which can explain differences with warming as it can distort the results, which will be discussed in chapter 4.5.

Soil surface horizons are usually more affected by weathering through the influence of climate with temperature and precipitation, and biological processes from roots and microbial activity (Ashida et al., 2021; Goebes et al., 2019). A thick soil profile can isolate the parent material from the effects of percolating precipitation, leading to lower weathering rates in the subsoil (Zhang et al., 2024; Guimarães et al., 2022; Oliva et al., 2003). This is why the CIA and PIA often decrease from the surface towards the bottom of the soil profile, as was reported by Zhang et al. (2024) and Guimarães et al. (2022). This was not the case for the warmed and control plots in our data. Both the CIA and the PIA showed very high values and increased with depth. This would indicate a high degree of weathering and more weathered soil with depth (Zhang et al., 2024; Guimarães et al., 2022). However, the high CIA and PIA values can be biased through the mineralogy. Granitic parent material is poor in nutrients which could result in the overestimation of the weathering index values, but the values are comparable between treatments (Kronnäs et al., 2023). The weathering indices of the warmed plots were lower than for the control plots throughout the soil profile, especially in the subsoil, which was significant for the CIA. This showed a lower weathering degree with warming in the subsoil suggesting that warming led to an elemental redistribution.

When looking at the elemental components of the CIA, K has the highest influence on the weathering index value, as it significantly increases with depth in the subsoil for the warmed plots compared to the control plots where K is more consistent throughout the soil profile. The PIA was calculated to account for the increase of K with depth, but the index still was lower with warming, especially in the lower part of the profile, however, not significantly. Na showed a trend of higher concentration in the subsoil with warming, influencing the PIA and still suggesting a trend of less weathered soil with warming. Additionally, the Al concentration had a trend to be lower in the warmed plots throughout the soil profile compared to the control plots, driving the lower weathering indices with warming as well.

The concentrations for Ca, Mg, Na, P and S were generally low, whereas K showed the highest concentration for both treatments. This is expected in acidic granitic soils in temperate forests, which are based on nutrient-poor mineralogy and further susceptible to leaching due to the low pH, leaving the soil more nutrient depleted (Kronnäs et al., 2023). The leaching process is strongly

influenced by water availability and soil moisture, since it is used to dissolve nutrients and needed for downward percolation, leading to the loss of nutrients from the soil profile (Heidari & Raheb, 2020). Ca, Na and K are very mobile elements and are leached from the soil quickly. Warming showed trends of depth redistributions for the elements K, Mg, P and S, where a lower concentration in the topsoil and a higher concentration in the subsoil could be seen with warming. This would suggest a higher weathering degree in the upper half of the soil profile with warming. In the lower half of the soil profile the higher K, Mg, Na, P and S concentrations suggest less weathered soil at this depth in the warmed plots as more nutrients and nutritious elements are present (Middelburg et al., 1988; Heidari & Raheb, 2020). The redistribution of the elements is less likely due to leaching, since warming reduced soil moisture which inhibits the leaching process (Abbaslou & Baghernejad, 2013; Lucas, 2001).

The elemental redistribution can be due to differences in plant nutrient cycling with warming (Lucas, 2001). Nutrients are kept from leaching through plant nutrient cycling, where nutrients are mobilized in the subsoil via microbial and root activity, and acidic exudates, which can result in local biopores and chemical weathering, releasing nutrients (Johnson & Turner, 2019). Through roots and long-term translocation into litter the nutrients are relocated to the topsoil. From the topsoil the nutrients can be remobilized and deposited into the subsoil (Kautz et al., 2013). Through plant nutrient cycling the macronutrients can be held and brought back into the topsoil and the leaching process can be delayed (Lucas, 2001; Kautz et al., 2013). This process might have led to consistent concentrations of K throughout the soil profile and higher Mg and Na concentrations in the topsoil within the control plots. However, in the warmed plots soil moisture is reduced which influences the production of plant biomass, such as roots, which impacts the amount of root exudates in the soil. Ofiti et al. (2021) found a reduction in root biomass in the warmed plots of the soil warming experiment in the Blodgett Forest. Soil moisture is needed to support the root exudates and serves as transport medium to transport dissolved nutrients to the roots for plant uptake (Kleber et al., 2015). Additionally, wet conditions help the release of K from expandable clay minerals by plants (Kautz et al., 2013). Thus, the drier conditions with warming could have led to reduced release and accessibility of nutrients to plants and to less plant cycling leading to lower redistribution to the topsoil and leaving the nutrients in the subsoil. On the other hand, the accumulation of K can also be due to the weathering of K-feldspar in the subsoil, which shows a more advanced stage of primary weathering than in the control plots, since K-feldspar has a higher resistance to weathering than plagioclase or mica (Middelburg et al., 1988). S concentrations were very low in the soil, since sulphur in its oxidized form is very soluble and thus lost during initial weathering stages (Middelburg et al., 1988). Higher S concentration in the deep soil of the warmed plots could also be due to less leaching through reduced soil moisture. P is also considered a very mobile element in granitic environments and with chemical weathering is lost through leaching and plant uptake (Middelburg et al., 1988; Kautz et al., 2013). Overall, warming seemed to reduce nutrient cycling and enhance subsoil nutrient retention, while control plots show stronger topsoil enrichment through biological redistribution.

Warming led to an accumulation of Fe in the subsoil, which suggests increased weathering compared to the control plots (Zhang et al., 2024). Iron is considered immobile during initial and moderate stages of weathering meaning it remains in the soil while other elements are removed. Fe is also strongly influenced by redox conditions in the soil (Middelburg et al., 1988). In acidic conditions iron oxidation becomes an important process, where ferrous iron (Fe^{2+}), which is mobilized through mineral weathering or organic matter decomposition, is oxidized to ferric iron (Fe^{3+}), which is insoluble and precipitates in the soil. This Fe enrichment through oxidation was found to be highest in more arid regions, where reduced leaching allows Fe to accumulate (Heidari

& Raheb, 2020; Middelburg et al., 1988). Warming can further influence Fe dynamics by increasing microbial activity, leading to higher decomposition rates (Ren et al., 2024; van den Enden et al., 2021), which can locally create reductive conditions in the rhizosphere. These reductive microsites can mobilize Fe^{2+} in the topsoil (Lucas, 2001), allowing it to be translocated downward. In the drier warmed plots, enhanced mineral weathering, altered redox conditions and reduced leaching could have promoted the precipitation and accumulation of this mobilized Fe in the subsoil, explaining the observed enrichment with warming.

A further weathering process which is influenced by temperature is the crystallization of amorphous and poorly crystalline Al, Fe and Mn (hydr)oxides. Warming can accelerate the crystallization of amorphous and poorly crystalline Al, Fe and Mn (hydr)oxides into more stable forms (Ren et al., 2024). The presence of poorly crystalline Al, Fe and Mn (hydr)oxides indicates active weathering of primary minerals, and their formation is promoted by the availability of primary minerals and sufficient soil moisture (Slessarev et al., 2022). The presence of primary minerals in the Blodgett Forest warming experiment was found in the subsoil at around 70-80 cm depth and downwards (Riley et al., 2024).

Fe (hydr)oxides responded differently to warming than Al and Mn (hydr)oxides and showed significant differences in the subsoil. Warming showed active primary weathering of Fe minerals in the subsoil. This is supported by the significant increase in poorly crystalline Fe_o (hydr)oxides in the subsoil at 80-90 and 90-100 cm depth, suggesting active primary weathering (Ren et al., 2024). The Fe_o/Fe_d ratio increases at the same depths in the subsoil with warming, indicating less crystalline phases and more active weathering compared to the control plots (Ren et al., 2024). However, the results of the Fe_o/Fe_d ratio, showed very low values (<0.2), which after Guimarães et al. (2022) points to the presence of a high number of crystalline forms like goethite and hematite. Since the ratio tends to decrease with soil age, this suggests quite well weathered conditions for all soil profiles. An increase in the ratio indicates that there is a greater activity of primary weathering compared to a lower degree of Fe (hydr)oxide crystallization (Jaworska et al., 2016). The Fe_d/Fe_t ratio represents the formation of pedogenic iron (hydr)oxides where a higher ratio shows progressive weathering of minerals containing Fe and their release of Fe (Jaworska et al., 2016; Huang et al., 2021). In the deep soil the ratio is marginally lower for the warmed plots, suggesting that soil warming showed a lower content of free Fe in relation to total Fe, which would suggest a lower weathering degree of Fe bearing minerals. However, for the plots of both treatments the ratio suggests a moderate weathering degree as the values are between 0.3 and 0.5, which is higher compared to the values Jaworska et al. (2016) found in low weathered Haplic Luvisols in temperate climate where most values ranged from 0.11- 0.4. Fe_d concentrations showed no significant differences. However, in the middle of the soil profile the concentration tended to be higher which could indicate an increased crystallization process with warming. In the lowest depths the Fe_d concentrations tended to be lower with warming, which would show lower crystallization of Fe (hydr)oxides with warming (Jaworska et al., 2016). Thus, warming could have accelerated active primary mineral weathering with the release of poorly crystalline Fe (hydr)oxides in the subsoil from parent material. This process was accelerated to the extent that it accumulated poorly crystalline Fe (hydr)oxides faster than the crystallization process to become visible (Jaworska et al., 2016).

This pattern was not seen for Al and Mn (hydr)oxides, as there were no significant differences with soil warming. However, tendencies for lower concentrations in oxalate extracted Al and Mn throughout the soil profile with soil warming were observed, indicating less poorly crystalline Al and Mn phases (Ren et al., 2024). Lower Al and Mn (hydr)oxides concentrations could either reflect more advanced crystallization, and thus a higher weathering degree, or lower poorly

crystalline (hydr)oxide formation due to lower soil moisture and thus a lower weathering degree. Ren et al. (2024) found that the higher the humidity in the soil, the higher were the concentrations of (hydr)oxides. Thus, the trends of lower concentration of Al and Mn (hydr)oxides with soil warming can also result from lower soil moisture, inhibiting the formation of new poorly crystalline phases.

Although Al_d and Mn_d concentrations tended to be consistently lower in the warmed plots, indicating reduced (hydr)oxide contents, the lower Al_o/Al_d and Mn_o/Mn_d ratios under warming suggest more advanced crystallization. This reflects a higher proportion of crystalline relative to poorly crystalline phases throughout the soil profiles (Jaworska et al., 2016). Conversely, the lower Ald/Alt and Mnd/Mnt ratios under warming suggest a smaller pedogenic proportion of Al and Mn relative to their total concentrations, indicating reduced soil weathering throughout the profile (Huang et al., 2021). Overall, Al and Mn (hydr)oxides exhibited ambiguous trends with warming, in contrast to Fe (hydr)oxides.

Comparisons with other studies further support the interpretation of well weathered soils in the Blodgett Forest. Zhang et al. (2024) analysed granitic soil and reported higher Fe_d, Al_d, and Mn_d values in subtropical compared to temperate granitic soils (subtropic: Fe_d = 17.8 g/kg, Al_d = 4.4 g/kg, Mn_d = 0.5 g/kg; temperate: Fe_d = 10.9 g/kg, Al_d = 2.1 g/kg, Mn_d = 0.3 g/kg), indicating higher crystalline phase concentrations and stronger weathering in warmer climates. Even though the Blodgett Forest lies within a mediterranean climate region, the dithionite extracted Fe, Al and Mn were closer to the concentrations of the subtropical soils in Zhang et al. (2024), implying weathered soils. The values can also be compared to the results of Rasmussen et al. (2005), who also analysed Fe and Al (hydr)oxides in granitic soil in the Blodgett Experimental Forest Research Station in California. The values (Fe_o = 1.42 g/kg, Fe_d = 23.82 g/kg, Al_o = 10.35 g/kg and Al_d = 4.11 g/kg, recalculated from stocks to g/kg) were generally comparable to those in this study. The Fe_o and Al_d concentrations were similar to the concentrations in this study, and the Fe_d and Al_o values were higher in Rasmussen et al. (2005). The dithionite-extracted Fe and Al also occur in high concentrations, similar to those reported for subtropical regions by Zhang et al. (2024), reflecting the weathered nature of the soils in the Blodgett Forest.

Warming influenced soil and weathering processes altering the soil weathering degree. Warming reduced soil moisture which influenced the elemental distribution, leaching and plant cycling leading to a trend of lower nutrient concentrations in the topsoil and accumulation in the subsoil. Primary mineral weathering of K-feldspar may have released additional K in the subsoil, so that despite lower CIA and PIA values in the subsoil, higher K concentrations reflect accelerated weathering of not easily weatherable K-feldspar (Middelburg et al., 1988). Enhanced primary weathering and redox activity contributed to the redistribution and accumulation of Fe in the subsoil (Slessarev et al., 2022; Heidari & Raheb, 2020). Warming also promoted the formation of poorly crystalline Fe (hydr)oxides through increased primary mineral weathering in the subsoil. This shows that soil weathering is impacted by warming even over short time scales and that these effects vary with depth and within different variables depending on which processes are active at certain depths.

4.2 Soil weathering and soil organic matter

Soil organic matter actively influences chemical soil weathering through processes that can either accelerate or delay mineral transformations. On the one hand, microbial decomposition of soil organic matter can contribute to reduction zones, leading to the dissolution and oxidative precipitation of Fe and Mn phases, enhancing soil weathering (Ren et al., 2024; Lucas, 2001). On the other hand, SOM can stabilize poorly crystalline Fe and Al (hydr)oxides by forming organo-

mineral associations through sorption and coprecipitation (Huang et al., 2021). This stabilization delays their transformation into crystalline phases, delaying soil weathering (Guimarães et al., 2022). Furthermore, the SOM derived from plant litter contains leachable elements that are retained through long-term plant recycling from different soil depths in the topsoil, reducing leaching losses and thus, delaying soil weathering (Lucas, 2001).

Poorly crystalline Fe and Al (hydr)oxides play an important role in the long-term soil organic carbon (SOC) storage. The reactive Fe and Al (hydr)oxides provide large surface areas for the adsorption of organic compounds, forming stable mineral-associated organic matter (MAOM) complexes, which are inaccessible for microbial decomposition due to physical encapsulation and chemical bonding by mineral particles (Ren et al., 2024; Song et al., 2022). Ashida et al. (2021) found that oxalate-extracted active Fe and Al are essential predictors of SOC in acidic soils.

Temperature influences the crystallization of Al_o and Fe_o, since with cooler temperatures organic matter decomposition is slower, leading to an increased adsorption of organic compounds to mineral surfaces, inhibiting the transformation of these reactive minerals into crystalline forms (Ren et al., 2024). Thus, with rising temperatures a decrease in Fe_o and Al_o is expected, potentially reducing MAOM formation and leading to less stable carbon in the soil. Our data only showed non-significant trends for a reduction of Al_o with warming and Fe_o showed a higher concentration in the subsoil, which did not confirm the expectation. Soil organic matter can inhibit the Fe crystallization process, leading to more amorphous and poorly crystalline Fe (hydr)oxides when the organic matter content is higher, like in the topsoil (Jaworska et al., 2016; Guimarães et al., 2022). This could be observed in our data, as the Fe_o and Al_o concentrations were highest in the topsoil as was the carbon content. Additionally, the Fe_d concentration was low in the topsoil compared to the whole soil profile, indicating a lower degree of Fe (hydr)oxide crystallization. The Fe_o/Fe_d ratio was highest at the top of the soil profile (Guimarães et al., 2022; Huang et al., 2021).

The C/N ratio tended to be higher in the topsoil and lower in the subsoil under warming. A trend of higher carbon concentration in the topsoil could be seen, and, in the subsoil, carbon was marginally lower with warming. Nitrogen did not show any trends with warming. The results show no clear changes in SOM input however hint at higher inputs of fresh and unprocessed material in the topsoil, and more highly processed and easily decomposable SOM in the subsoil compared to the control plots (Rumpel & Kögel-Knabner, 2009). Higher processed SOM material and increased decomposition in the subsoil with warming can lead to higher concentration of organic acids, which could accelerate the dissolution of minerals and thereby weathering (Soong et al., 2021; Kleber et al., 2015). Changing redox conditions due to increased microbial activity could accelerate weathering rates in the subsoil as well (Kleber et al., 2015). This would support the observed increased primary weathering in the subsoil.

The composition of soil organic matter functional groups gives more detailed insights into the stability and origin of soil organic matter, as well as its interactions with minerals. However, in this study the functional group composition did not show significant differences under warming. Nevertheless, some non-significant trends could be identified. In the topsoil a pattern of relatively larger abundance in aliphatic compounds and a relatively lower abundance in carboxylic compounds could be seen, which showed an inverse pattern in the subsoil, where carboxylic compounds were higher and aliphatic compounds lower in the warmed plots compared to the control plots. Aliphatic compounds are derived from plant materials (Angst et al., 2021), whereas carboxylic compounds include oxidized plant and microbial products, which have undergone more transformation (Kleber et al., 2015). The trend in higher abundance of aliphatics at the surface could therefore hint to higher plant inputs, and the higher abundance of carboxylic

compounds in the subsoil hint to less fresh and more oxidized organic matter. This points at increased decomposition and microbial respiration with soil warming in the subsoil, as was also reflected in the trend of the C/N ratio (Hicks Pries et al., 2017). Higher microbial activity and decomposition can be due to the higher SOM quality coming from lower C/N ratio, as microbes can use higher quality SOM more efficiently. This leads to an increase in microbial biomass and with that to a loss of carbon (Angst et al., 2021). Thus, a trend of increased biological activity in the subsoil could be a reason for the increased subsoil soil weathering with warming.

The DSI (drifts stability index), including the ratio between aliphatic compounds and aromatic C-C compounds from the higher absorption bands, showed not significant difference with warming, suggesting warming had no influence on the stability of SOM composition. The depth gradient in our data showed that the topsoil contained SOM with lower stability and the subsoil had SOM with higher stability, indicating more processed SOM in the subsoil (Zheng et al., 2021). The DSI was positively correlated with Fe_o and Al_o for both treatments but warming led to a significantly lower positive correlation between the DSI and Fe_o, however, not when adjusted for depth. But the correlation between C and Fe_o showed a significantly weaker relationship with warming even after depth adjustment. This suggests that there must be another process driving the carbon and poorly crystalline Fe (hydr)oxide concentration with warming.

Warming reduced carbon in the subsoil but did not have a significant effect on SOM composition and stability. However, trends in aliphatic and carboxylic compounds, as well as the C/N ratio across the soil profile, were observed which hint towards more microbially transformed organic matter and increased decomposition in the subsoil with warming (Hicks Pries et al., 2017). Higher biological activity and decomposition lead to increased organic acid production which could increase soil weathering in the subsoil and increase carbon loss with warming (Kleber et al., 2015). Even though Fe_o increased in the subsoil and thereby increased the potential for MAOM formation, carbon was lost from the subsoil. This suggests that the effect of accelerated soil weathering through warming could not buffer carbon loss through microbial decomposition by forming MAOM to the extent that it would prevent carbon loss from the subsoil.

4.4 Influence of depth on weathering

Depth was a significant factor for the distribution within almost all analysed soil variables. This indicates that throughout the soil profile the soil variables change, forming a concentration gradient. It is evident that for both treatments many soil variables show a change in concentration trend within the soil profile and with warming at soil depths of 40-50 cm, 50-60 cm or 60-70 cm. All significant differences related to warming were found in the subsoil. The topsoil showed no significant differences with warming throughout all variables. This highlights that depth is a crucial factor for how soils respond to warming and that processes differ strongly with depth. It also highlights the importance of including subsoil data into soil studies which has often been neglected in the past (Fang et al., 2023; Kautz et al., 2013). The results suggest that warming influences subsoil processes and revealed differences in soil weathering, especially in the subsoil.

Soil variables usually follow a gradient along soil depth (Rasmussen et al., 2005; Heidari & Raheb, 2020). These depth gradients are influenced by biogenic, geogenic and pedogenic processes, with different processes active at different soil depths (Goebes et al., 2019). The topsoil is more influenced by biogenic surface processes like increased biological activity, litter inputs and higher root density, which impacts soil structure, porosity and acidity. Deeper horizons are more influenced by geogenic and abiotic weathering processes, where biological activity and root

density are reduced (Lucas, 2001; Goebes et al., 2019). But biotic processes such as plant cycling through deeper roots are still present (Kautz et al., 2013).

It seems that plant inputs influenced the soil until a depth of 40-50 cm. This can be seen in the depth gradients of the DSI, individual aliphatics, aromatic C-C, as well as for carbon and the C/N ratio. They all showed a change at this depth, where afterwards the concentration did not change anymore. This gradient and the change at that specific depth are also seen for oxalate-extracted Al, Fe and Mn which are highest in the topsoil, as they form MAOM with organic matter there (Guimarães et al., 2022). Significant differences with soil weathering did not occur above this depth interval, where the soil is influenced by plant inputs and is biologically more active (Kautz et al., 2013). The differences occurred where biological inputs and activity are lower.

In the subsoil, increased primary mineral weathering was observed, with the increase in Fe_o, total Fe, K and Mg. A reason for the greater response to warming of the subsoil compared to the topsoil could originate from the distribution of primary minerals which were reactive to warming, as no primary minerals were found in the topsoil, but in the subsoil (Riley et al., 2024). It is also possible that changes in soil weathering were not observed due to the more dynamic and fast cycling processes in the topsoil, where plants compensate for the increases in weathering (Kautz et al., 2013). Warming could have shifted processes that were present at higher horizons, like biological activity, downwards into more isolated parts of the soil, influencing otherwise stable conditions there (Soong et al., 2021). Further research is required to understand what drives the differences in weathering response to warming at different depths.

4.5 Spatial heterogeneity

Various factors influence the spatial heterogeneity of soils. Parent material and mineralogy determine the distribution of elements during initial stages of development and lead to variation in weathering processes and thus, to differences in chemical and mineralogical composition (Abbaslou & Baghernejad, 2013; Jaworska et al., 2016). Climate influences temperature and precipitation which drive weathering and soil development creating heterogeneities (Zhang et al., 2024). However, this research focuses on local spatial heterogeneity which develops from the same parent material and under the same climate and looks at soils in closer proximity to each other as seen on the schematic map of the soil plot distribution of the soil warming experiment in the Blodgett Forest (Figure 19).

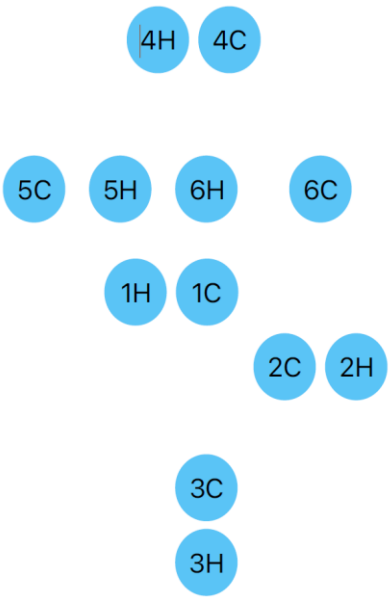

Figure 19: Schematic location map showing the spatial arrangement of the soil plots in the Blodgett Forest soil warming experiment (Created by Steve Kwatcho Kengdo).

On a local scale spatial heterogeneity can develop through differences in vegetation species and density, which controls litterfall which influences soil organic matter distribution and content (Johnson & Turner, 2019). Microclimates and topography play a role in the development of local heterogeneities (Pan et al., 2024; Štursová et al., 2016). Furthermore, heterogeneity originates from downward transport and biopore formation by earthworms, which create pathways for water and roots leading to different soil structures and locally increased chemical weathering (Kautz et al., 2013). This process can be especially important in the subsoil, where the macropore formation is not disrupted by surface activities, which can homogenise the soil (Kautz et al., 2013).

Fine-scale heterogeneity can include nutrient-rich hotspots, which are microsites with high nutrient availability and influence nutrient cycling in forest soil systems, as roots access these sites for enhanced nutrient uptake (Johnson & Turner, 2019). These spatial variations in the soil can influence the outcome of in-situ experiments, where local differences may be overlooked and therefore underestimated, or overestimated. Thus, spatial heterogeneity is a limiting factor in the evaluation of in-situ experiments (Riley et al., 2025).

The t-test and PCA results have found spatial heterogeneity between the six different control plots, which shows that spatial heterogeneity plays a role at a local scale within a temperate forest. Additionally, patterns emerged indicating which plots were more similar or different to each other. Not all variables showed significant spatial differences between plots. However, some plots more often showed similar trends to each other than other plot pairs. It is evident that with increasing depth there was increased spatial heterogeneity. The most heterogeneity was found at 60-100 cm depth. Overall, based on the pairwise t-tests, plot 1 differed the least from the other plots, whereas plots 3 and 6 differed the most from all other plots, as can also be seen in the PCA biplot in Figure 17. This is interesting because plot 1 is geographically closest to the centre of all plots, whereas plot 3 is located farther to the others. Another striking result is that plot 3 and plot 4 differed from each other the most often out of all pairs, especially in the subsoil and deep soil. Plot 3 and 4 are the most distant plot pair. These findings show that indeed the plots which were geographically farthest apart also showed the most differences between each other. And the plots closer to each other showed more similar results. But it also points out that spatial heterogeneity only was found for some variables, whereas others did not differ from each other between plots. Garten et al. (2007) who analysed spatial heterogeneity of texture, C and N in a deciduous forest with acidic soils has found several parameters which do not differ across distances of 1-500 m, whereas only 3 variables are found to increase spatial heterogeneity with increasing distance. Other variables show spatial heterogeneity however not in the pattern of increased heterogeneity with increased distance. This shows that the hypothesis of increased heterogeneity with increased distance depends on the soil variable.

Spatial heterogeneity regarding carbon has been found (Ofiti et al., 2021). Especially in the subsoil carbon shows heterogeneity (Kautz et al., 2013). Physical parameters like soil moisture, porosity, texture and bulk density have been analysed often regarding spatial heterogeneity (Pan et al., 2024; Saleh, 2018; Stoyan et al., 2000). Chemical parameters not centring on carbon dynamics and biological activity, such as soil weathering parameters, have not been thoroughly analysed for spatial heterogeneity. The main drivers of the found heterogeneities were differences in elemental concentrations for certain elements, differences in ratios and pH between the soil plots. These differences hint at differences in weathering between plots. In plot 4 and 6 lower pH corresponds to higher Al and Fe values, a higher degree of crystallization of Fe (hydr)oxides, a higher pedogenic Fe proportion and higher CIA. These indicators point to a higher weathering degree in plot 4 and 6 compared to plot 3, as plot 3 had a higher pH and higher concentration of elements from primary minerals. The t-tests as well as the PCA showed that these differences were particularly seen in the subsoil. The reason for this difference is not clear; however, the vegetation cover differed slightly between soil plots and there was a small slope of around 3-5°. Additionally, there could be differences in microclimate causing differences in local temperature and soil moisture which influence biological processes and nutrient cycling (Haesen et al., 2021).

The pronounced spatial heterogeneity in the subsoil emphasizes the necessity of carefully interpreting significant findings from the warming experiment. Natural spatial heterogeneity may lead to the overestimation of the warming effect. It is important to note that some of the variables

which were most influenced by warming in the subsoil were also the variables which showed the most spatial heterogeneity in the subsoil. These included the CIA, K, Mg, S and Fe.

Therefore, spatial heterogeneity plays a critical role in in-situ deep mineral soil profiles regarding weathering indicators since the elemental concentration in particular exhibits spatial heterogeneity. The results showed that spatial heterogeneity is variable-specific and depth-dependent and suggest that even within a small forest area there are spatial differences in the soil within weathering parameters. This can distort treatment effects in in-situ experiments. Thus, recognizing and accounting for spatial heterogeneity is essential for the interpretation of soil warming effects in the Blodgett Forest.

5. Conclusion

In this study, the effect of soil warming on the weathering degree in a 10-year long in-situ soil warming experiment in 1 m deep mineral soil profiles was analysed. To our knowledge, this is the first study linking soil warming to soil weathering responses with in-situ field data, which expands the scope of previous warming studies. Furthermore, the role of spatial heterogeneity within deep mineral soil profiles based on soil weathering indicators was evaluated.

It was found that 10 years of warming influenced the soil weathering degree, especially in the subsoil. Accelerated weathering with warming could be seen by the increased Fe, K, Mg and Fe_o concentrations in the subsoil, which showed increased primary mineral dissolution and transformation (Heidari & Raheb, 2020; Middelburg et al., 1988). This could be due to higher temperature increasing mineral dissolution and due to increased microbial activity and SOM decomposition with warming, which increases organic acid production and thereby accelerates mineral dissolution (Soong et al., 2021; Huang et al., 2014). The topsoil indicated no changes in the weathering degree with soil warming. This could be due to reduced soil moisture with warming which slows soil processes like mineral dissolution, leaching, acidification and plant nutrient cycling and has been observed particularly in the topsoil (Riley et al., 2025).

Spatial heterogeneity in the soil played a significant role and was found especially in the subsoil. Since the strongest differences with warming were also found in the subsoil caution is required when interpreting the impact of soil warming on soil weathering in the subsoil. It was also found that spatial heterogeneity increased with geographical distance between the sampling sites. However, it depends on the soil variable and spatial variation was not found for all analysed variables.

These findings highlight the sensitivity of subsoil processes and the need for including the subsoil when analysing the effect of soil warming on soil weathering or spatial heterogeneity. The soil warming experiment in the Blodgett Forest has been running for 10 years, which is a very short period to analyse soil weathering which runs over geological time scales and controls elemental cycling and dynamics over decades to millennia (Zhang et al., 2024; Doetterl et al., 2018). Finding significant differences and trends in soil weathering with warming within 10 years demonstrates that warming might influence soil mineralogy and geochemical processes over short timescales, and potentially more strongly over longer periods. It shows the need for even longer-term in-situ warming experiments. Furthermore, there is the need for more comparable whole-soil studies regarding the impact of warming on the weathering degree to build more robust findings for soils in similar conditions and across different climates and soil types. The strength of the Blodgett Forest whole-soil warming experiment is its long-term data including the depth dimension, though the limited number of replicates constrains the statistical robustness.

Understanding changes in soil weathering in increasing temperatures is essential in the context of climate warming. Soil weathering provides nutrients and non-nutrient elements to the soil system for plants and microbial communities to take up (Doetterl et al., 2018). In this way weathering influences soil fertility and changing weathering patterns could change soil fertility which has an impact on sustainable land and resource management (Doetterl et al., 2018; Abbaslou & Baghernejad, 2013).

References

Abbaslou, H., & Baghernejad, M. (2013): Effect of weathering and mineralogy on the distribution of major and trace elements (Hormozgan province, Southern Iran*). International Journal of Forest, Soil and Erosion (IJFSE), 3*(1), 15-25.

Akselsson, C., Olsson, J., Belyazid, S., & Capell, R. (2016): Can increased weathering rates due to future warming compensate for base cation losses following whole-tree harvesting in spruce forests? *Biogeochemistry*, *128*(1–2), 89–105. https://doi.org/10.1007/s10533-016-0196-6.

Alsalam, O., Şeker, C., & Dedeoğlu, M. (2020): Quantifying the role of chemical weathering rates on soil developed along an altitudinal transect in the mountainous environments, Turkey. *Eurasian Journal of Soil Science (EJSS)*, *9*(2), 140–150. https://doi.org/10.18393/ejss.689428.

Amorim, H. C. S., Araujo, M. A., Lal, R., & Zinn, Y. L. (2023): What C:N ratios in soil particle-size fractions really say: N is preferentially sorbed by clays over organic C. *CATENA*, *230*, 107230. https://doi.org/10.1016/j.catena.2023.107230.

Angst, G., Mueller, K. E., Nierop, K. G. J., & Simpson, M. J. (2021): Plant- or microbial-derived? A review on the molecular composition of stabilized soil organic matter. *Soil Biology and Biochemistry*, *156*, 108189. https://doi.org/10.1016/j.soilbio.2021.108189.

Ashida, K., Watanabe, T., Urayama, S., Hartono, A., Kilasara, M., Mvondo Ze, A. D., Nakao, A., Sugihara, S., & Funakawa, S. (2021): Quantitative relationship between organic carbon and geochemical properties in tropical surface and subsurface soils. *Biogeochemistry*, *155*(1), 77–95. https://doi.org/10.1007/s10533-021-00813-8.

Belyazid, S., Akselsson, C., & Zanchi, G. (2022): Water limitation in forest soils regulates the increase in weathering rates under climate change. *Forests*, *13*(2), 310. https://doi.org/10.3390/f13020310.

Cheng, L., Zhang, N., Yuan, M., Xiao, J., Qin, Y., Deng, Y., Tu, Q., Xue, K., Van Nostrand, J. D., Wu, L., He, Z., Zhou, X., Leigh, M. B., Konstantinidis, K. T., Schuur, E. A. G., Luo, Y., Tiedje, J. M., & Zhou, J. (2017): Warming enhances old organic carbon decomposition through altering functional microbial communities, *The ISME Journal*, *11*(8), 1825–1835. https://doi.org/10.1038/ismej.2017.48.

Dahms, D., Favilli, F., Krebs, R., & Egli, M. (2012): Soil weathering and accumulation rates of oxalate-extractable phases derived from alpine chronosequences of up to 1 Ma in age. Geomorphology, 151-152, 99-113. https://doi.org/10.1016/j.geomorph.2012.01.021.

De Winter, J. C. F., Gosling, S. D., & Potter, J. (2016): Comparing the Pearson and Spearman correlation coefficients across distributions and sample sizes: A tutorial using simulations and empirical data. *Psychological Methods, 21*, 273–290. https://doi.org/10.1037/met0000079.

Diedenhofen, B. & Musch, J. (2015): cocor: A comprehensive solution for the statistical comparison of correlations. PLoS ONE, 10(4): e0121945. http://dx.doi.org/10.1371/journal.pone.0121945.

Doetterl, S., Berhe, A. A., Arnold, C., Bodé, S., Fiener, P., Finke, P., Fuchslueger, L., Griepentrog, M., Harden, J. W., Nadeu, E., Schnecker, J., Six, J., Trumbore, S., Van Oost, K., Vogel, C., & Boeckx, P. (2018): Links among warming, carbon and microbial dynamics mediated by soil mineral weathering. *Nature Geoscience*, *11*(8), 589–593. https://doi.org/10.1038/s41561-018-0168-7.

Durán, J., Delgado-Baquerizo, M., Dougill, A. J., Guuroh, R. T., Linstädter, A., Thomas, A. D., & Maestre, F. T. (2018): Temperature and aridity regulate spatial variability of soil multifunctionality in drylands across the globe. *Ecology*, *99*(5), 1184–1193. https://doi.org/10.1002/ecy.2199.

Egli, M., Mirabella, A., & Sartori, G. (2008): The role of climate and vegetation in weathering and clay mineral formation in late Quaternary soils of the Swiss and Italian Alps. *Geomorphology*, *102*(3–4), 307–324. https://doi.org/10.1016/j.geomorph.2008.04.001.

Fang, Q., Lu, A., Hong, H., Kuzyakov, Y., Algeo, T. J., Zhao, L., Olshansky, Y., Moravec, B., Barrientes, D. M., & Chorover, J. (2023): Mineral weathering is linked to microbial priming in the critical zone. *Nature Communications*, *14*(1), 345. https://doi.org/10.1038/s41467-022-35671-x.

Fay, M. P. & Proschan, M. A. (2010): Wilcoxon-Mann-Whitney or t-test? On assumptions for hypothesis tests and multiple interpretations of decision rules. *Stat Surv*, *4*, 1-39. https://doi.org/10.1214/09-SS051. PMID: 20414472; PMCID: PMC2857732.

Fedo, C. M., Nesbitt, H. W., & Young, G. M. (1995): Unraveling the effects of potassium metasomatism in sedimentary rocks and paleosols, with implications for paleoweathering conditions and provenance. *Geology, 23*(10), 921-924. https://doi.org/10.1130/0091-7613(1995)023<0921:UTEOPM>2.3.CO;2.

Garten, C. T., Kang, S., Brice, D. J., Schadt, C. W., & Zhou, J. (2007): Variability in soil properties at different spatial scales (1m–1km) in a deciduous forest ecosystem. *Soil Biology and Biochemistry*, *39*(10), 2621–2627. https://doi.org/10.1016/j.soilbio.2007.04.033.

Gewirtzman, J., Tang, J., Melillo, J. M., Werner, W. J., Kurtz, A. C., Fulweiler, R. W., & Carey, J. C. (2019): Soil warming accelerates biogeochemical silica cycling in a temperate forest. *Frontiers in Plant Science*, *10*, 1097. https://doi.org/10.3389/fpls.2019.01097.

Goddéris, Y., Brantley, S. L., François, L. M., Schott, J., Pollard, D., Déqué, M., & Dury, M. (2013): Rates of consumption of atmospheric CO_2 through the weathering of loess during the next 100 yr of climate change. *Biogeosciences*, *10*(1), 135–148. https://doi.org/10.5194/bg-10-135-2013.

Goebes, P., Schmidt, K., Seitz, S., Both, S., Bruelheide, H., Erfmeier, A., Scholten, T., & Kühn, P. (2019): The strength of soil-plant interactions under forest is related to a critical coil depth. *Scientific Reports*, *9*(1), 8635. https://doi.org/10.1038/s41598-019-45156-5.

Greenacre, M., Groenen, P. J. F., Hastie, T., D'Enza, A. I., Markos, A., & Tuzhilina, E. (2022): Principal component analysis. *Nature Reviews Methods Primers*, *2*(1), 100. https://doi.org/10.1038/s43586-022-00184-w.

Guimarães, C. C. B., Demattê, J. A. M., Azevedo, A. C. D., Sayão, V. M., Silva, R. C. D., Poppiel, R. R., Marques, K. P. P., Nanni, M. R., Curi, N., Silva, S. H. G., Rosas, J. T. F., & Teixeira, A. F. D. S. (2022): Assessing soil mineralogy and weathering degree by a multi-range sensor synergistic approach: From parent rock to topsoil. *Journal of South American Earth Sciences*, *116*, 103855. https://doi.org/10.1016/j.jsames.2022.103855.

Haesen, S., Lembrechts, J. J., De Frenne, P., Lenoir, J., Aalto, J., Ashcroft, M. B., Kopecký, M., Luoto, M., Maclean, I., Nijs, I., Niittynen, P., Van Den Hoogen, J., Arriga, N., Brůna, J., Buchmann, N., Čiliak, M., Collalti, A., De Lombaerde, E., Descombes, P., … Van Meerbeek, K. (2021): ForestTemp – Sub-canopy microclimate temperatures of European forests. *Global Change Biology*, *27*(23), 6307–6319. https://doi.org/10.1111/gcb.15892.

Hanson, P. J., Childs, K. W., Wullschleger, S. D., Riggs, J. S., Thomas, W. K., Todd, D. E., & Warren, J. M. (2011): A method for experimental heating of intact soil profiles for application to

climate change experiments. *Global Change Biology, 17*, 1083-1096. https://doi.org/10.1111/j.1365-2486.2010.02221.x.

Hanson, P. J., Griffiths, N. A., Iversen, C. M., Norby, R. J., Sebestyen, S. D., Phillips, J. R., Chanton, J. P., Kolka, R. K., Malhotra, A., Oleheiser, K. C., Warren, J. M., Shi, X., Yang, X., Mao, J., & Ricciuto, D. M. (2020): Rapid net carbon loss from a whole-ecosystem warmed Peatland. *AGU Advances*, 1, e2020AV000163. https://doi.org/10.1029/2020AV000163.

Heidari, A., & Raheb, A. (2020): Geochemical indices of soil development on basalt rocks in arid to sub-humid climosequence of Central Iran. *Journal of Mountain Science*, *17*(7), 1652–1669. https://doi.org/10.1007/s11629-019-5862-4.

Hicks Pries, C. E., Castanha, C., Porras, R. C., & Torn, M. S. (2017): The whole-soil carbon flux in response to warming. *Science*, *355*(6332), 1420–1423. https://doi.org/10.1126/science.aal1319.

Huang, C., Meng, S., Tan, W., Wen, S., Li, D., Wang, B., & Koopal, L. K. (2021): Regional differences in mineral weathering characteristics of zonal soils under intensive agriculture. *Applied Clay Science*, *215*, 106336. https://doi.org/10.1016/j.clay.2021.106336.

Huang, J., Sheng, X., Xi, J., He, L., Huang, Z., Wang, Q., & Zhang, Z. (2014): Depth-related changes in community structure of culturable mineral weathering bacteria and in weathering patterns caused by them along two contrasting soil profiles. *Applied and Environmental Microbiology, 80*(1), 29-42. https://doi.org/10.1128/aem.02335-13.

Jaworska, H., Dąbkowska-Naskręt, H., & Kobierski, M. (2016): Iron oxides as weathering indicator and the origin of Luvisols from the Vistula glaciation region in Poland. *Journal of Soils and Sediments*, *16*(2), 396–404. https://doi.org/10.1007/s11368-015-1201-8.

Jiang, J., Wang, Y.-P., Yu, M., Cao, N., & Yan, J. (2018): Soil organic matter is important for acid buffering and reducing aluminum leaching from acidic forest soils. *Chemical Geology*, *501*, 86–94. https://doi.org/10.1016/j.chemgeo.2018.10.009.

Johnson, D. W., & Turner, J. (2019): Tamm Review: Nutrient cycling in forests: A historical look and newer developments. *Forest Ecology and Management*, *444*, 344–373. https://doi.org/10.1016/j.foreco.2019.04.052.

Jones, E., & Singh, B. (2014): Organo-mineral interactions in contrasting soils under natural vegetation. *Frontiers in Environmental Science*, *2*. https://doi.org/10.3389/fenvs.2014.00002.

Kassambara, A., Mundt, F. (2020): _factoextra: Extract and visualize the results of multivariate data analyses_. R package version 1.0.7, https://CRAN.R-project.org/package=factoextra.

Kautz, T., Amelung, W., Ewert, F., Gaiser, T., Horn, R., Jahn, R., Javaux, M., Kemna, A., Kuzyakov, Y., Munch, J.-C., Pätzold, S., Peth, S., Scherer, H. W., Schloter, M., Schneider, H., Vanderborght, J., Vetterlein, D., Walter, A., Wiesenberg, G. L. B., & Köpke, U. (2013): Nutrient acquisition from arable subsoils in temperate climates: A review. *Soil Biology and Biochemistry*, *57*, 1003–1022. https://doi.org/10.1016/j.soilbio.2012.09.014.

Kim, S. (2015): _ppcor: Partial and semi-partial (part) correlation_. R package version 1.1, https://CRAN.R-project.org/package=ppcor.

Kleber, M., Eusterhues, K., Keiluweit, M., Mikutta, C., Mikutta, R., & Nico, P. S. (2015): Mineral–organic associations: Formation, properties, and relevance in soil environments. *Advances in Agronomy*, 130, 1–140. https://doi.org/10.1016/bs.agron.2014.10.005.

Kronnäs, V., Lucander, K., Zanchi, G., Stadlinger, N., Belyazid, S., & Akselsson, C. (2023): Effect of droughts and climate change on future soil weathering rates in Sweden.

Biogeosciences, *20*(10), 1879–1899. https://doi.org/10.5194/bg-20-1879-2023.

Laub, M., Demyan, M. S., Nkwain, Y. F., Blagodatsky, S., Kätterer, T., Piepho, H.-P., & Cadisch, G. (2020): DRIFTS band areas as measured pool size proxy to reduce parameter uncertainty in soil organic matter models. *Biogeosciences*, *17*(6), 1393–1413. https://doi.org/10.5194/bg-17-1393-2020.

Lenth, R. (2025): _emmeans: Estimated marginal means, aka least-squares means_. R package version 1.11.1, https://CRAN.R-project.org/package=emmeans.

Lucas, Y. (2001): The role of plants in controlling rates and products of weathering: Importance of biological pumping. *Annual Review of Earth and Planetary Sciences*, *29*(1), 135–163. https://doi.org/10.1146/annurev.earth.29.1.135.

Margenot, A. J., Calderón, F. J., Bowles, T. M., Parikh, S. J., & Jackson, L. E. (2015): Soil organic matter functional group composition in relation to organic carbon, nitrogen, and phosphorus fractions in organically managed tomato fields. *Soil Science Society of America Journal, 79*, 772-782. https://doi.org/10.2136/sssaj2015.02.0070.

Middelburg, J. J., Van Der Weijden, C. H., & Woittiez, J. R. W. (1988): Chemical processes affecting the mobility of major, minor and trace elements during weathering of granitic rocks. *Chemical Geology*, *68*(3–4), 253–273. https://doi.org/10.1016/0009-2541(88)90025-3.

Neuwirth, E. (2022): _RColorBrewer: ColorBrewer Palettes_. R package version 1.1-3, https://CRAN.R-project.org/package=RColorBrewer.

Oberg, A. L., & Mahoney, D. W. (2007): Linear mixed effects models. In Ambrosius, W. T. (Ed.), *Topics in biostatistics*, 213–235. Humana Press.

Ofiti, N. O. E., Zosso, C. U., Soong, J. L., Solly, E. F., Torn, M. S., Wiesenberg, G. L. B., & Schmidt, M. W. I. (2021): Warming promotes loss of subsoil carbon through accelerated degradation of plant-derived organic matter. *Soil Biology and Biochemistry*, *156*, 108185. https://doi.org/10.1016/j.soilbio.2021.108185.

Oliva, P., Viers, J., & Dupré, B. (2003): Chemical weathering in granitic environments. *Chemical Geology*, *202*(3–4), 225–256. https://doi.org/10.1016/j.chemgeo.2002.08.001.

Pan, Z., Dong, Y., He, G., Guo, T., & Zhu, N. (2024): Spatial heterogeneity of soil properties in planted mixed forests in the rocky desertification areas of the Wuling Mountain. *PeerJ*, *12*, e18724. https://doi.org/10.7717/peerj.18724.

Pansu, M., & Gautheyrou, J., (2006): Handbook of soil analysis. Mineralogical, organic and inorganic methods. Springer Berlin / Heidelberg.

Pareek, N. (2017): Climate change impact on soils: Adaptation and mitigation. *MOJ Ecology & Environmental Sciences*, *2*(3). https://doi.org/10.15406/mojes.2017.02.00026.

Pinheiro, J., Bates, D., R Core Team (2025): _nlme: Linear and nonlinear mixed effects models_. R package version 3.1-168, https://CRAN.R-project.org/package=nlme.

Price, J. R., & Velbel, M. A. (2003): Chemical weathering indices applied to weathering profiles developed on heterogeneous felsic metamorphic parent rocks. *Chemical Geology*, *202*(3–4), 397–416. https://doi.org/10.1016/j.chemgeo.2002.11.001.

Rasmussen, C., Torn, M. S., & Southard, R. J. (2005): Mineral assemblage and aggregates control carbon dynamics in a California conifer forest. *Soil Science Society of America Journal*, *69*(6), 1711–1721. https://doi.org/10.2136/sssaj2005.0040.

R Core Team (2023): _R: A language and environment for statistical computing_. R Foundation for Statistical Computing, Vienna, Austria. https://www.R-project.org/.

Ren, S., Wang, C., & Zhou, Z. (2024): Global distributions of reactive iron and aluminum influence the spatial variation of soil organic carbon. *Global Change Biology*, *30*(11), e17576.

https://doi.org/10.1111/gcb.17576.

Riley, W., Tao, J., Pegoraro, E. (2024): Experimental soil warming impacts soil moisture and plant water stress and thereby ecosystem carbon dynamics (Blodgett, CA). Belowground Biogeochemistry Scientific Focus Area, *ESS-DIVE*. Dataset. https://doi.org/10.15485/2480291.

Riley, W. J., Tao, J., Mekonnen, Z. A., Grant, R. F., Brodie, E. L., Pegoraro, E., & Torn, M. S. (2025): Experimental soil warming impacts soil moisture and plant water stress and thereby ecosystem carbon dynamics. *Journal of Advances in Modeling Earth Systems*, *17*(2), e2024MS004714. https://doi.org/10.1029/2024MS004714.

Rumpel, C., & Kögel-Knabner, I. (2011): Deep soil organic matter—A key but poorly understood component of terrestrial C cycle. *Plant and Soil*, *338*(1–2), 143–158. https://doi.org/10.1007/s11104-010-0391-5.

Saleh, A. M. (2018): Spatial variability mapping of some soil properties in Jadwal Al_Amir Project/Babylon/Iraq. *Journal of the Indian Society of Remote Sensing*, *46*(9), 1481–1495. https://doi.org/10.1007/s12524-018-0795-x.

Slessarev, E. W., Chadwick, O. A., Sokol, N. W., Nuccio, E. E., & Pett-Ridge, J. (2022): Rock weathering controls the potential for soil carbon storage at a continental scale. *Biogeochemistry*, *157*(1), 1–13. https://doi.org/10.1007/s10533-021-00859-8.

Song, X., Wang, P., Van Zwieten, L., Bolan, N., Wang, H., Li, X., Cheng, K., Yang, Y., Wang, M., Liu, T., & Li, F. (2022): Towards a better understanding of the role of Fe cycling in soil for carbon stabilization and degradation. *Carbon Research*, *1*(1), 5. https://doi.org/10.1007/s44246-022-00008-2.

Soong, J. L., Castanha, C., Hicks Pries, C. E., Ofiti, N., Porras, R. C., Riley, W. J., Schmidt, M. W. I., & Torn, M. S. (2021): Five years of whole-soil warming led to loss of subsoil carbon stocks and increased CO_2 efflux. *Science Advances, 7*, eabd1343. https://doi.org/10.1126/sciadv.abd1343.

Stevens, A., & Ramirez-Lopez, L. (2024): An introduction to the prospectr package. R package Vignette R package version 0.2.7.

Stoyan, H., De-Polli, H., Böhm, S., Robertson, G. P., & Paul, E. A. (2000): Spatial heterogeneity of soil respiration and related properties at the plant scale. *Plant and Soil, 222970*(1), 203-214. https://doi.org/10.1023/A:1004757405147.

Štursová, M., Bárta, J., Šantrůčková, H., & Baldrian, P. (2016): Small-scale spatial heterogeneity of ecosystem properties, microbial community composition and microbial activities in a temperate mountain forest soil. *FEMS Microbiology Ecology*, *92*(12), fiw185. https://doi.org/10.1093/femsec/fiw185.

van den Enden, L., Anthony, M. A., Frey, S. D., & Simpson, M. J. (2021): Biogeochemical evolution of soil organic matter composition after a decade of warming and nitrogen addition. *Biogeochemistry*, *156*(2), 161–175. https://doi.org/10.1007/s10533-021-00837-0.

Wani, S. A., Najar, G. R., Wani, J. A., Ramzan, M., & Hakeem, K. R. (2016): Weathering and approaches to evaluation of weathering indices for soil profile studies – An overview. In Hakeem, K. R., Akhtar, J., & Sabir, M. (Eds), *Soil Science: Agricultural and Environmental Prospectives*, 183–198. Springer International Publishing. https://doi.org/10.1007/978-3-319-34451-5_8.

Wei, Y., Wu, X., Xia, J., Shen, X., & Cai, C. (2016): Variation of soil aggregation along the weathering gradient: Comparison of grain size distribution under different disruptive forces. *PLoS one, 11*(8), e0160960. https://doi.org/10.1371/journal.pone.0160960.

Williams, E. L., Walter, L. M., Ku, T. C. W., Baptist, K. K., Budai, J. M., & Kling, G. W. (2007): Silicate weathering in temperate forest soils: Insights from a field experiment. *Biogeochemistry*, *82*(2), 111–126. https://doi.org/10.1007/s10533-006-9057-z.

Zhang, S., Zhang, Y., Huang, G., Zhang, B., Li, Y., Chen, X., Xu, J., & Wei, Y. (2024): Linkage between granite weathering and gully erosion in subtropical region. *Water*, *16*(5), 751. https://doi.org/10.3390/w16050751.

Zheng, S., Zhang, J., Chi, F., Zhou, B., Wei, D., Kuang, E., Jiang, Y., Mi, G., & Chen, Y. P. (2021): Response of the chemical structure of soil organic carbon to modes of maize straw return. *Scientific Reports*, *11*(1), 6574. https://doi.org/10.1038/s41598-021-84697-6.

Appendix

Linear mixed effect model

Table 2: Linear mixed effects model structure for each variable. The model structure was selected based on AIC and significance.

Variable	Model
pH	pH ~ Treatment + Depth, random = ~ 1 | ID, correlation = corAR1(form = ~ mid_depth | ID), data = df
Fe_o	log_Feo ~ Treatment * Depth, random = ~ 1 | ID, correlation = corAR1(form = ~ mid_depth | ID), data = df
Al_o	log_Alo ~ Treatment + Depth, random = ~ 1 | ID, correlation = corAR1(form = ~ mid_depth | ID), data = df
Mn_o	log_Mno ~ Treatment + Depth, random = ~ 1 | ID, correlation = corAR1(form = ~ mid_depth | ID), data = df
Fe_d	log_Fed ~ Treatment * Depth, random = ~ 1 | ID, correlation = corAR1(form = ~ mid_depth | ID), data = df
Al_d	log_Ald ~ Treatment + Depth, random = ~ 1 | ID, correlation = corAR1(form = ~ mid_depth | ID), data = df
Mn_d	log_Mnd ~ Treatment + Depth, random = ~ 1 | ID, correlation = corAR1(form = ~ mid_depth | ID), data = df
Al	Al ~ Treatment * Depth, random = ~ 1 | ID, correlation = corAR1(form = ~ mid_depth | ID), data = df
Fe	log_Fe ~ Treatment * Depth, random = ~ 1 | ID, correlation = corAR1(form = ~ mid_depth | ID), data = df
Mn	log_Mn ~ Treatment + Depth, random = ~ 1 | ID, correlation = corAR1(form = ~ mid_depth | ID), data = df
Si	Si ~ Treatment * Depth, random = ~ 1 | ID, correlation = corAR1(form = ~ mid_depth | ID), data = df
Ca	log_Ca ~ Treatment + Depth, random = ~ 1 | ID, correlation = corAR1(form = ~ mid_depth | ID), data = df
K	log_K ~ Treatment * Depth, random = ~ 1 | ID, correlation = corAR1(form = ~ mid_depth | ID), data = df
Mg	Mg ~ Treatment * Depth, random = ~ 1 | ID, correlation = corAR1(form = ~ mid_depth | ID), data = df
Na	Na ~ Treatment + Depth, random = ~ 1 | ID, correlation = corAR1(form = ~ mid_depth | ID), data = df
S	log_S ~ Treatment * Depth, random = ~ 1 | ID, correlation = corAR1(form = ~ mid_depth | ID), data = df
P	log_P ~ Treatment + Depth, random = ~ 1 | ID, correlation = corAR1(form = ~ mid_depth | ID), data = df
C	log_C ~ Treatment * Depth, random = ~ 1 | ID, correlation = corAR1(form = ~ mid_depth | ID), data = df
N	log_N ~ Treatment + Depth, random = ~ 1 | ID, correlation = corAR1(form = ~ mid_depth | ID), data = df
Aliphatic	log_Aliphatic ~ Treatment + Depth, random = ~ 1 | ID, correlation = corAR1(form = ~ mid_depth | ID), data = df
Aromatic C-C	log_AromaticCC ~ Treatment + Depth, random = ~ 1 | ID, correlation = corAR1(form = ~ mid_depth | ID), data = df
Aromatic C-H	log_AromaticCH ~ Treatment + Depth, random = ~ 1 | ID, correlation = corAR1(form = ~ mid_depth | ID), data = df
Carboxylic	log_Carboxylic ~ Treatment + Depth, random = ~ 1 | ID, correlation = corAR1(form = ~ mid_depth | ID), data = df
Lignin	log_Lignin ~ Treatment + Depth, random = ~ 1 | ID, correlation = corAR1(form = ~ mid_depth | ID), data = df
Polysaccharide	log_Polysaccharide ~ Treatment * Depth, random = ~ 1 | ID, correlation = corAR1(form = ~ mid_depth | ID), data = df
CIA	log_CIA ~ Treatment * Depth, random = ~ 1 | ID, correlation = corAR1(form = ~ mid_depth | ID), data = df
PIA	log_PIA ~ Treatment + Depth, random = ~ 1 | ID, correlation = corAR1(form = ~ mid_depth | ID), data = df
Al_o/Al_d Ratio	log_AloAld ~ Treatment + Depth, random = ~ 1 | ID, correlation = corAR1(form = ~ mid_depth | ID), data = df
Fe_o/Fe_d Ratio	log_FeoFed ~ Treatment * Depth, random = ~ 1 | ID, correlation = corAR1(form = ~ mid_depth | ID), data = df
Mn_o/Mn_d Ratio	MnoMnd ~ Treatment * Depth, random = ~ 1 | ID, correlation = corAR1(form = ~ mid_depth | ID), data = df
Fe_d/Fe_t	log_Fed_Fet_ratio ~ Treatment * Depth, random = ~ 1 | ID, correlation = corAR1(form = ~ mid_depth | ID), data = df
Al_d/Al_t	log_Ald_Alt_ratio ~ Treatment + Depth, random = ~ 1 | ID, correlation = corAR1(form = ~ mid_depth | ID), data = df
Mn_d/Mn_t	Mnd_Mnt_ratio ~ Treatment + Depth, random = ~ 1 | ID, correlation = corAR1(form = ~ mid_depth | ID), data = df
C/N	log_CN ~ Treatment + Depth, random = ~ 1 | ID, correlation = corAR1(form = ~ mid_depth | ID), data = df
DSI	log_DSI ~ Treatment + Depth, random = ~ 1 | ID, correlation = corAR1(form = ~ mid_depth | ID), data = df

Table 3: ANOVA results for the fixed effects of the linear mixed effects model.

Variable	Effect	NumDF	DenDF	F value	p-value
pH	Treatment	1	4	0.841	0.4109
	Depth	9	45	1.264	0.2824
Fe_o	Treatment	1	4	1.697	0.2626
	Depth	9	36	16.886	< 0.0001
	Treatment:Depth	9	36	3.507	0.0033
Al_o	Treatment	1	4	0.954	0.3839
	Depth	9	45	91.562	< 0.0001

Mn_o	Treatment	1	4	0.64499	0.4669
	Depth	9	45	85.55836	< 0.0001
Fe_d	Treatment	1	4	0.05	0.8325
	Depth	9	36	3.44	0.0038
	Treatment:Depth	9	36	1.47	0.1955
Al_d	Treatment	1	4	0.348	0.5872
	Depth	9	45	90.609	< 0.0001
Mn_d	Treatment	1	4	0.7687	0.4301
	Depth	9	45	87.686	< 0.0001
Al	Treatment	1	4	4.985	0.0893
	Depth	9	36	0.55	0.8277
	Treatment:Depth	9	36	0.826	0.5967
Fe	Treatment	1	4	2.0698	0.2236
	Depth	9	36	4.1267	0.001
	Treatment:Depth	9	36	3.6338	0.0026
Mn	Treatment	1	4	0.1372	0.7298
	Depth	9	45	51.4471	< 0.0001
Si	Treatment	1	4	5076.883	0.7738
	Depth	9	36	9.691	< 0.0001
	Treatment:Depth	9	36	2.013	0.0664
Ca	Treatment	1	4	0.78255	0.4263
	Depth	9	45	145.25829	< 0.0001
K	Treatment	1	4	4.0954	0.1130
	Depth	9	36	3.5939	0.0028
	Treatment:Depth	9	36	2.8728	0.0116
Mg	Treatment	1	4	1.1320	0.3473
	Depth	9	36	0.4465	0.9000
	Treatment:Depth	9	36	4.2811	0.0008
Na	Treatment	1	4	1.2606	0.3244
	Depth	9	45	6.1702	< 0.0001
S	Treatment	1	4	6.411	0.0645
	Depth	9	36	43.726	< 0.0001
	Treatment:Depth	9	36	3.182	0.0063
P	Treatment	1	4	0.8418	0.4108
	Depth	9	45	22.6269	< 0.0001
C	Treatment	1	4	0.58534	0.4869
	Depth	9	36	80.01796	< 0.0001
	Treatment:Depth	9	36	3.80104	0.0019
N	Treatment	1	4	2.7720	0.1713
	Depth	9	45	72.3971	< 0.0001
Aliphatic	Treatment	1	4	0.0058	0.9428
	Depth	9	45	47.3871	< 0.0001
Aromatic C-C	Treatment	1	4	0.505	0.5167
	Depth	9	45	5.078	0.0001
Aromatic C-H	Treatment	1	4	0.3184	0.6027
	Depth	9	45	39.2963	< 0.0001
Carboxylic	Treatment	1	4	0.03861	0.8538
	Depth	9	45	1.80635	0.0934
Lignin	Treatment	1	4	0.5437	0.5018
	Depth	9	45	22.8752	< 0.0001
Polysaccharide	Treatment	1	4	3.857610	0.1210
	Depth	9	36	1.311152	0.2654
	Treatment:Depth	9	36	0.948501	0.4969
CIA	Treatment	1	4	3.9	0.1202
	Depth	9	36	2.3	0.0362
	Treatment:Depth	9	36	1.5	0.1875
PIA	Treatment	1	4	0.9	0.3943
	Depth	9	45	20.5	< 0.0001
Alo/Ald Ratio	Treatment	1	4	1.50416	0.2873
	Depth	9	45	37.46413	< 0.0001
Feo/Fet Ratio	Treatment	1	4	2.2232	0.2102

	Depth	9	36	13.5869	< 0.0001
	Treatment:Depth	9	36	2.9751	0.0094
Mno/Mnd Ratio	Treatment	1	4	0.4205	0.5520
	Depth	9	36	12.1215	< 0.0001
	Treatment:Depth	9	36	1.7997	0.1024
Fed/Fet	Treatment	1	4	0.8110	0.4188
	Depth	9	36	2.2227	0.0433
	Treatment:Depth	9	36	1.7474	0.1137
Ald/Alt	Treatment	1	4	0.0568	0.8234
	Depth	9	45	98.8583	< 0.0001
Mnd/Mnt	Treatment	1	4	1.21757	0.3318
	Depth	9	45	46.66985	< 0.0001
C/N	Treatment	1	4	0.0879	0.7816
	Depth	9	45	0.3875	0.9350
DSI	Treatment	1	4	0.06702	0.8085
	Depth	9	45	40.81852	< 0.0001

Table 4: Results for the emmeans post hoc test showing only marginal and significant Treatment:Depth interactions.

Variable	Depth	Contrast	Estimate	SE	df	t-ratio	p-value
Fe_o	70-80	C – H	-0.6750159	0.2973717	4	-2.270	0.0857
	90-100	C – H	-1.2167434	0.2973717	4	-4.092	0.0150
Al	80-90	C – H	1.820000	0.6560285	4	2.774	0.0501
Fe	60-70	C – H	-0.19934251	0.06287745	4	-3.170	0.0338
	70-80	C – H	-0.1475413	0.06287745	4	-2.346	0.0788
K	60-70	C – H	-0.2953313	0.1070482	4	-2.759	0.0509
	70-80	C – H	-0.3327592	0.1070482	4	-3.108	0.0359
	80-90	C – H	-0.2764867	0.1070482	4	-2.583	0.0611
	90-100	C – H	-0.2414609	0.1070482	4	-2.256	0.0871
Mg	80-90	C – H	-0.14066667	0.06297865	4	-2.234	0.0893
	90-100	C – H	-0.23520000	0.06297865	4	-3.735	0.0202
S	60-70	C – H	-0.5279253	0.1462227	4	-3.610	0.0225
	80-90	C – H	-0.3517201	0.1462227	4	-2.405	0.0739
	90-100	C – H	-0.6281850	0.1462227	4	-4.296	0.0127
C	60-70	C – H	0.7437557	0.3660362	4	2.142	0.0989
	80-90	C – H	0.8311190	0.3660362	4	2.271	0.0857
Polysaccharide	40-50	C – H	-1.6266476	0.6823862	4	-2.384	0.0757
CIA	60-70	C – H	0.04311258	0.01977794	4	2.180	0.0948
	80-90	C – H	0.05896701	0.01977794	4	2.981	0.0407
	90-100	C – H	0.04608539	0.01977794	4	2.330	0.0802
Fe_o/Fe_d Ratio	80-90	C – H	-0.6842584	0.3114398	4	-2.197	0.0930
	90-100	C – H	-1.3393866	0.3114398	4	-4.301	0.0126
Mn_o/Mn_d Ratio	40-50	C – H	-0.5601904	0.1845863	4	-3.035	0.0386
Fe_d/Fe_t	80-90	C – H	0.23729661	0.09754844	4	2.433	0.0718
	90-100	C – H	0.22201394	0.09754844	4	2.276	0.0852

Spatial heterogeneity t-tests

Table 5: Spatial heterogeneity normality, variance and marginal and significant t-test results at 0-30 cm (depth1), 30-60 cm (depth2) and 60-100 cm (depth3) depth.

Variable	Plot 1	Plot 2	Normality1 p-value	Normality2 p-value	Equal Variance p-value	Test	p-value	Depth	Adjusted p-value
Al	1	6	0.411044732	0.391384367	0.380064121	t-test equal var	0.010764211	Depth1	0.084641604
Al	2	6	0.11799156	0.198557026	0.622626582	t-test equal var	0.012103079	Depth2	0.084641604
Al	1	4	0.73615953	0.232378865	0.300188902	t-test equal var	0.018268114	Depth3	0.097819016
Al	2	4	0.985800867	0.232378865	0.888347926	t-test equal var	0.002420622	Depth3	0.034966997
Al	2	6	0.985800867	0.185888233	0.989438687	t-test equal var	0.019563803	Depth3	0.097819016

Al	3	4	0.522547968	0.232378865	0.494874191	t-test equal var	0.002812102	Depth3	0.034966997
Al	3	6	0.522547968	0.185888233	0.421496101	t-test equal var	0.013166472	Depth3	0.084641604
Al	4	5	0.232378865	0.651382941	0.842272897	t-test equal var	0.000692533	Depth3	0.031163969
Al	5	6	0.651382941	0.185888233	0.744849907	t-test equal var	0.003108178	Depth3	0.034966997
Fe	1	2	0.323022398	0.113932703	0.665079927	t-test equal var	0.005149394	Depth1	0.024474141
Fe	1	3	0.323022398	0.993974568	0.90483769	t-test equal var	0.003202858	Depth1	0.024474141
Fe	2	6	0.113932703	0.856191786	0.17763384	t-test equal var	0.007662581	Depth1	0.030577578
Fe	3	6	0.993974568	0.856191786	0.382921958	t-test equal var	0.004636841	Depth1	0.024474141
Fe	1	2	0.882843154	0.482423742	0.749558288	t-test equal var	0.011146566	Depth2	0.033439699
Fe	1	3	0.882843154	0.35219587	0.382673306	t-test equal var	0.005438698	Depth2	0.024474141
Fe	2	4	0.482423742	0.103735595	0.836614025	t-test equal var	0.008936222	Depth2	0.0307754
Fe	2	5	0.482423742	0.570310335	0.718648389	t-test equal var	0.008154021	Depth2	0.030577578
Fe	3	4	0.35219587	0.103735595	0.329475994	t-test equal var	0.004643661	Depth2	0.024474141
Fe	3	5	0.35219587	0.570310335	0.403685161	t-test equal var	0.003523808	Depth2	0.024474141
Fe	1	2	0.014272821	0.006570923	0.348184331	Wilcoxon	0.028571429	Depth3	0.055900621
Fe	1	3	0.014272821	0.3825079	0.227687131	Wilcoxon	0.028571429	Depth3	0.055900621
Fe	1	6	0.014272821	0.780341613	0.874000019	Wilcoxon	0.042066412	Depth3	0.078874523
Fe	2	3	0.006570923	0.3825079	0.767884182	Wilcoxon	0.028571429	Depth3	0.055900621
Fe	2	4	0.006570923	0.056457989	0.638088878	Wilcoxon	0.028571429	Depth3	0.055900621
Fe	2	5	0.006570923	0.299688929	0.555305187	Wilcoxon	0.028571429	Depth3	0.055900621
Fe	2	6	0.006570923	0.780341613	0.278575802	Wilcoxon	0.028571429	Depth3	0.055900621
Fe	3	4	0.3825079	0.056457989	0.859201525	t-test equal var	1.86556E-06	Depth3	8.39502E-05
Fe	3	5	0.3825079	0.299688929	0.383147401	t-test equal var	0.000158546	Depth3	0.002378186
Fe	3	6	0.3825079	0.780341613	0.178664495	t-test equal var	1.56157E-05	Depth3	0.000351354
Fe	4	5	0.056457989	0.299688929	0.300067729	t-test equal var	0.009574569	Depth3	0.0307754
Fe	4	6	0.056457989	0.780341613	0.134832081	t-test equal var	0.014591452	Depth3	0.04103846
Fe	5	6	0.299688929	0.780341613	0.602204146	t-test equal var	0.001675524	Depth3	0.018849645
Mn	3	4	0.507423284	0.863806472	0.05951413	t-test equal var	0.00041276	Depth3	0.00928709
Mn	4	6	0.863806472	0.060276524	0.530875594	t-test equal var	8.07867E-06	Depth3	0.00036354
K	1	3	0.065695402	0.739097607	0.807670535	t-test equal var	0.004957461	Depth1	0.01859048
K	1	4	0.065695402	0.909261223	0.416098575	t-test equal var	0.000323538	Depth1	0.005811803
K	2	4	0.335972636	0.909261223	0.648467933	t-test equal var	0.005377709	Depth1	0.018615147
K	2	6	0.335972636	0.144693471	0.518374292	t-test equal var	0.044829492	Depth1	0.084384135
K	3	4	0.739097607	0.909261223	0.558890842	t-test equal var	0.002021344	Depth1	0.01010672
K	3	6	0.739097607	0.144693471	0.694387208	t-test equal var	0.0046232	Depth1	0.01859048
K	4	6	0.909261223	0.144693471	0.843391455	t-test equal var	0.000387454	Depth1	0.005811803
K	5	6	0.690281178	0.144693471	0.202767395	t-test equal var	0.036974268	Depth1	0.075629185
K	1	3	0.463262875	0.872957965	0.186795048	t-test equal var	0.021646929	Depth2	0.057300694
K	1	4	0.463262875	0.109106686	0.609675629	t-test equal var	0.001396639	Depth2	0.008978396
K	1	5	0.463262875	0.157673535	0.097961307	t-test equal var	0.017563147	Depth2	0.049396351
K	3	4	0.872957965	0.109106686	0.086445425	t-test equal var	0.002488261	Depth2	0.011197176
K	3	6	0.872957965	0.155528377	0.36316634	t-test equal var	0.001718186	Depth2	0.009664794
K	4	6	0.109106686	0.155528377	0.338332842	t-test equal var	0.000631996	Depth2	0.005980202
K	5	6	0.157673535	0.155528377	0.046710998	t-test unequal var	0.045004872	Depth2	0.084384135
K	1	2	0.023353785	0.729247887	0.823550408	Wilcoxon	0.028571429	Depth3	0.06122449
K	1	5	0.023353785	0.961945947	0.429712086	Wilcoxon	0.028571429	Depth3	0.06122449
K	1	6	0.023353785	0.617439601	0.141226319	Wilcoxon	0.028571429	Depth3	0.06122449

K	2	3	0.729247887	0.098633244	0.245572815	t-test equal var	0.008157576	Depth3	0.026220779
K	2	5	0.729247887	0.961945947	0.565052095	t-test equal var	4.01924E-05	Depth3	0.001808656
K	3	5	0.098633244	0.961945947	0.535475278	t-test equal var	0.009965607	Depth3	0.02989682
K	3	6	0.098633244	0.617439601	0.011636704	t-test unequal var	0.022955823	Depth3	0.057389559
K	4	5	0.822699488	0.961945947	0.70881934	t-test equal var	0.000959743	Depth3	0.007198069
K	5	6	0.961945947	0.617439601	0.036021402	t-test unequal var	0.000664467	Depth3	0.005980202
Mg	1	3	0.636886845	0.719949343	0.085135135	t-test equal var	0.003262652	Depth1	0.020974191
Mg	2	3	0.954693797	0.719949343	0.523264402	t-test equal var	0.012571373	Depth1	0.03771412
Mg	3	4	0.719949343	0.799437882	0.515033003	t-test equal var	0.003217185	Depth1	0.020974191
Mg	3	5	0.719949343	0.862406323	0.705344906	t-test equal var	0.006544037	Depth1	0.024540138
Mg	3	6	0.719949343	0.574020333	0.728534704	t-test equal var	0.005679903	Depth1	0.024540138
Mg	4	5	0.799437882	0.862406323	0.317855055	t-test equal var	0.031853423	Depth1	0.075442318
Mg	2	3	0.524880742	0.872957965	0.989833871	t-test equal var	0.036148366	Depth2	0.080411638
Mg	2	4	0.524880742	0.921476522	0.768079939	t-test equal var	0.004556626	Depth2	0.022783128
Mg	3	4	0.872957965	0.921476522	0.758483241	t-test equal var	0.000793321	Depth2	0.011899809
Mg	3	5	0.872957965	0.666659824	0.431165406	t-test equal var	0.024509516	Depth2	0.062421757
Mg	3	6	0.872957965	0.403137775	0.905886931	t-test equal var	0.024968703	Depth2	0.062421757
Mg	4	6	0.921476522	0.403137775	0.67182945	t-test equal var	0.008940113	Depth2	0.030946544
Mg	1	3	0.46275743	0.45333131	0.997830624	t-test equal var	0.01133894	Depth3	0.036446592
Mg	1	4	0.46275743	0.999469578	0.503174731	t-test equal var	0.002544321	Depth3	0.020974191
Mg	1	6	0.46275743	0.462396052	0.350657504	t-test equal var	0.006037787	Depth3	0.024540138
Mg	2	3	0.608663819	0.45333131	0.223925281	t-test equal var	0.016737823	Depth3	0.047075127
Mg	2	6	0.608663819	0.462396052	0.046127325	t-test unequal var	0.037525431	Depth3	0.080411638
Mg	3	4	0.45333131	0.999469578	0.501509279	t-test equal var	9.18769E-05	Depth3	0.002067231
Mg	3	5	0.45333131	0.937206332	0.443989406	t-test equal var	0.003957207	Depth3	0.02225929
Mg	4	6	0.999469578	0.462396052	0.780683428	t-test equal var	1.61162E-05	Depth3	0.000725228
Mg	5	6	0.937206332	0.462396052	0.106547329	t-test equal var	0.002914736	Depth3	0.020974191
Na	5	6	0.91523587	0.080634332	0.906350915	t-test equal var	0.001280127	Depth2	0.05760573
P	3	4	0.866927463	0.891404446	0.186496138	t-test equal var	0.002007097	Depth2	0.045159686
P	3	5	0.866927463	0.973285364	0.077596269	t-test equal var	0.001321657	Depth2	0.045159686
S	1	4	0.254219491	0.716089639	0.168804555	t-test equal var	0.009184009	Depth3	0.082656083
S	1	5	0.254219491	0.864867106	0.889826028	t-test equal var	0.00017839	Depth3	0.004013772
S	3	4	0.770930918	0.716089639	0.128408941	t-test equal var	0.001882642	Depth3	0.028239637
S	3	5	0.770930918	0.864867106	0.973830733	t-test equal var	2.4429E-05	Depth3	0.001099304
S	3	6	0.770930918	0.368503254	0.280500259	t-test equal var	0.002668262	Depth3	0.030017944
Al_d	2	3	0.491313103	0.767405888	0.432015809	t-test equal var	0.008553509	Depth1	0.076981584
Al_d	1	3	0.06867118	0.109622647	0.217559262	t-test equal var	0.011429393	Depth2	0.085720447
Al_d	2	5	0.930750155	0.509323407	0.161900459	t-test equal var	0.002596717	Depth3	0.038950755
Al_d	3	4	0.66085228	0.94314323	0.431023649	t-test equal var	0.007381749	Depth3	0.076981584
Al_d	4	5	0.94314323	0.509323407	0.069411256	t-test equal var	0.00090456	Depth3	0.038950755
Al_d	5	6	0.509323407	0.70006302	0.285313902	t-test equal var	0.0020527	Depth3	0.038950755
Fe_d	1	3	0.185488085	0.463262875	0.219454823	t-test equal var	0.015125019	Depth1	0.045375056
Fe_d	1	6	0.185488085	0.58096191	0.957751177	t-test equal var	0.00757147	Depth1	0.030799629
Fe_d	2	6	0.345560486	0.58096191	0.241632478	t-test equal var	0.009804549	Depth1	0.031514622
Fe_d	3	4	0.463262875	0.203423114	0.443383655	t-test equal var	0.034448332	Depth1	0.086120831
Fe_d	3	6	0.463262875	0.58096191	0.236526493	t-test equal var	0.003003322	Depth1	0.030799629
Fe_d	4	6	0.203423114	0.58096191	0.640272292	t-test equal var	0.007159063	Depth1	0.030799629

Fe_d	1	2	0.552207751	0.450519083	0.618400164	t-test equal var	0.006222455	Depth2	0.030799629
Fe_d	2	5	0.450519083	0.18713119	0.412094422	t-test equal var	0.008213234	Depth2	0.030799629
Fe_d	2	6	0.450519083	0.281098412	0.21483652	t-test equal var	0.009099824	Depth2	0.031499392
Fe_d	3	6	0.832060498	0.281098412	0.958388435	t-test equal var	0.041746561	Depth2	0.093929763
Fe_d	1	2	0.243746342	0.839729415	0.986292581	t-test equal var	0.007500258	Depth3	0.030799629
Fe_d	1	3	0.243746342	0.787521289	0.403630496	t-test equal var	0.003526067	Depth3	0.030799629
Fe_d	1	4	0.243746342	0.602512423	0.427270625	t-test equal var	0.025530954	Depth3	0.067581936
Fe_d	2	4	0.839729415	0.602512423	0.417871846	t-test equal var	0.001111602	Depth3	0.025011036
Fe_d	2	6	0.839729415	0.594402576	0.937858913	t-test equal var	0.007415097	Depth3	0.030799629
Fe_d	3	4	0.787521289	0.602512423	0.965122478	t-test equal var	0.000770085	Depth3	0.025011036
Fe_d	3	6	0.787521289	0.594402576	0.355404123	t-test equal var	0.003552147	Depth3	0.030799629
Fe_d	4	5	0.602512423	0.118982915	0.949460505	t-test equal var	0.004474247	Depth3	0.030799629
Fe_d	4	6	0.602512423	0.594402576	0.377019415	t-test equal var	0.021814757	Depth3	0.061354005
Aliphatic	5	6	0.973257181	0.887451275	0.26644987	t-test equal var	0.000602761	Depth3	0.027124245
Lignin	1	5	0.757506685	0.098674402	0.182902144	t-test equal var	0.002038143	Depth3	0.030572146
Lignin	2	5	0.100448545	0.098674402	0.22858786	t-test equal var	0.001182289	Depth3	0.030572146
Lignin	5	6	0.098674402	0.282046512	0.10648568	t-test equal var	0.001570022	Depth3	0.030572146
Polysaccharide	1	6	0.136987994	0.386085436	0.512835227	t-test equal var	0.00057944	Depth1	0.015286822
Polysaccharide	3	4	0.840028417	0.451469336	0.263052859	t-test equal var	0.000679414	Depth2	0.015286822
CIA	1	6	0.718424277	0.913238816	0.929934123	t-test equal var	0.010430797	Depth1	0.034803961
CIA	2	6	0.533148201	0.913238816	0.470042178	t-test equal var	0.009009742	Depth1	0.034803961
CIA	4	6	0.850744803	0.913238816	0.284289727	t-test equal var	0.01700373	Depth1	0.042509325
CIA	5	6	0.664896206	0.913238816	0.393736206	t-test equal var	0.012995754	Depth1	0.036550557
CIA	2	5	0.943726287	0.79407468	0.576198314	t-test equal var	0.014614144	Depth2	0.038684498
CIA	3	4	0.744058441	0.641364218	0.645260304	t-test equal var	0.011069934	Depth2	0.034803961
CIA	3	5	0.744058441	0.79407468	0.564425879	t-test equal var	0.004371499	Depth2	0.028102495
CIA	3	6	0.744058441	0.655796768	0.032361408	t-test unequal var	0.011239433	Depth2	0.034803961
CIA	4	6	0.641364218	0.655796768	0.066755904	t-test equal var	3.34677E-05	Depth2	0.001506046
CIA	5	6	0.79407468	0.655796768	0.012849733	t-test unequal var	0.00610598	Depth2	0.0305299
CIA	1	5	0.991614551	0.654697284	0.203391863	t-test equal var	0.000630869	Depth3	0.00709728
CIA	1	6	0.991614551	0.285235182	0.731836359	t-test equal var	0.002350114	Depth3	0.017625858
CIA	2	3	0.367763878	0.655468088	0.560982231	t-test equal var	0.01160132	Depth3	0.034803961
CIA	2	5	0.367763878	0.654697284	0.76037159	t-test equal var	0.000621354	Depth3	0.00709728
CIA	3	5	0.655468088	0.654697284	0.778918396	t-test equal var	0.008943209	Depth3	0.034803961
CIA	3	6	0.655468088	0.285235182	0.485288265	t-test equal var	0.001342693	Depth3	0.012084241
PIA	3	6	0.894361034	0.317687516	0.065668346	t-test equal var	0.001582333	Depth2	0.036393649
PIA	4	6	0.646099464	0.317687516	0.117133921	t-test equal var	0.00047656	Depth2	0.021921771
Al_o/Al_d	2	6	0.129876005	0.470082951	0.37873423	t-test equal var	0.000845521	Depth1	0.038048424
C/N	1	6	0.698288629	0.97294562	0.442022258	t-test equal var	0.001314919	Depth1	0.059171349
DSI	5	6	0.277615083	0.407383366	0.864316253	t-test equal var	0.000865939	Depth3	0.038967244

PCA analysis

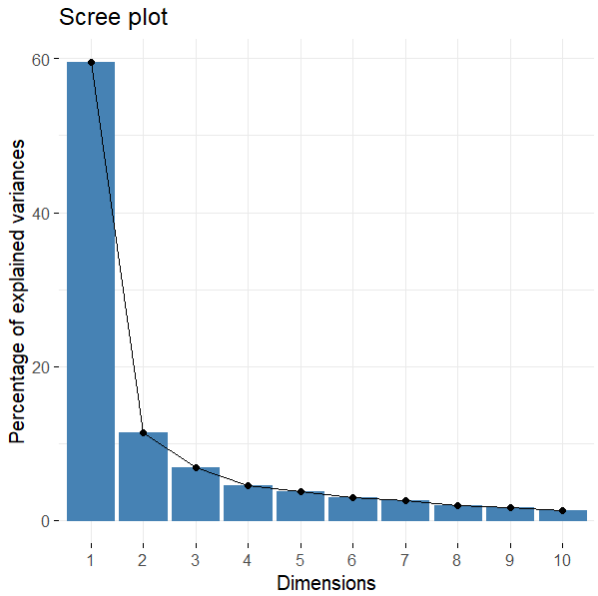

Figure 20: Scree plot of PCA analysis, showing the percentage of explained variation for the first 10 PCs.

Table 6: Importance of components in the PCA including the standard deviation, the proportion of variance and their cumulative proportion for each component.

Component	Standard deviation	Proportion of Variance	Cumulative Proportion
PC1	4.1193347	0.5950527	0.5950527
PC2	1.8010136	0.1137458	0.7087984
PC3	1.39940360	0.06867319	0.77747161
PC4	1.13358728	0.04506207	0.82253369
PC5	1.03259067	0.03739019	0.85992387
PC6	0.91315224	0.02924069	0.88916456
PC7	0.86375816	0.02616288	0.91532745
PC8	0.74831845	0.01963696	0.93496440
PC9	0.69820604	0.01709497	0.95205938
PC10	0.60687580	0.01291519	0.96497457
PC11	0.500957822	0.008800423	0.973774991
PC12	0.448940898	0.007067724	0.980842715
PC13	0.380106315	0.005066539	0.985909254
PC14	0.308579098	0.003339137	0.989248391
PC15	0.283915965	0.002826707	0.992075099
PC16	0.256406247	0.002305465	0.994380563
PC17	0.220286514	0.001701677	0.996082240
PC18	0.195171368	0.001335775	0.997418015
PC19	0.1670627761	0.0009787249	0.9983967403
PC20	0.1473710908	0.0007615981	0.9991583384
PC21	0.090708323	0.000288533	0.999446871
PC22	0.0754004920	0.0001993653	0.9996462367
PC23	0.0619041449	0.0001343819	0.9997806186
PC24	4.763383e-02	7.956685e-05	9.998602e-01
PC25	4.491647e-02	7.074771e-05	9.999309e-01
PC26	3.618813e-02	4.592336e-05	9.999769e-01
PC27	2.066629e-02	1.497705e-05	9.999918e-01
PC28	1.176050e-02	4.850125e-06	9.999967e-01
PC29	9.724733e-03	3.316321e-06	1.000000e+00

Table 7: PCA loadings for the first four principal components including all variables.

Variable	Component 1	Component 2	Component 3	Component 4
Feo	0.23224353	0.038277393	0.07445217	0.039964860
Alo	0.22965069	0.012151134	0.10740257	0.013078805

Mno	0.23353771	0.025652597	0.06877023	0.010677413
Fed	-0.08515302	0.476794266	-0.03547575	0.135797473
Ald	0.22455027	0.143019587	0.08492310	0.055008870
Mnd	0.23356223	0.031910638	0.06681661	0.012460347
Ca	0.22623816	-0.033387986	-0.03450792	0.010951785
Na	0.17991984	0.104331898	-0.24121435	0.069143068
K	-0.02754537	-0.201885025	-0.62455282	0.080380908
Al	-0.10849738	0.305743704	-0.01827015	-0.110930214
Fe	-0.06872962	0.367891673	-0.22325187	-0.255549019
Mn	0.23595092	-0.002324558	0.03767035	-0.039935860
DSI	0.21450437	0.032735034	-0.04066675	0.103780599
Mg	0.12529952	-0.202989558	0.20119317	-0.450928909
Si	-0.12409689	-0.355483588	0.16086708	0.067736751
P	0.21661148	0.064055355	-0.20684446	-0.078974089
S	0.20832004	0.136129195	-0.13954750	-0.054673495
C	0.23247068	0.042160022	0.03707219	0.066231053
N	0.22434421	0.065970042	0.02940902	-0.064970182
C/N	-0.02664628	-0.180791962	0.07624886	0.678467756
CIA	-0.15455947	0.174796179	0.47722522	-0.094468387
PIA	-0.22614872	0.014898867	0.16645773	-0.058698369
Alo/Ald	0.22130683	-0.064146028	0.16201691	-0.007324599
Feo/Fed	0.23035852	-0.043623700	0.07959729	0.002425575
Mno/Mnd	0.09871857	-0.023312846	-0.04431358	-0.020047302
Fed/Fet	-0.06943267	0.394994288	0.12327985	0.393859909
Ald/Alt	0.22813534	0.109956283	0.08626924	0.068488403
Mnd/Mnt	0.21353134	0.017141023	0.10419903	0.064965572
pH	0.09100804	-0.177485474	0.04899972	0.110508946

R code

```
library(readxl)
library(dplyr)
library(tidyr)
library(ggplot2)
library(writexl)
library(lmerTest)
library(Matrix)
library(lme4)
library(e1071)
library(nlme)
library(emmeans)
library(RColorBrewer)
library(ggcorrplot)
library(corrr)
library(FactoMineR)
library(factoextra)
library(purrr)
library(cocor)
library(stringr)

######################
#### Calculations ####
######################

df <- read_excel("All_data_Rversion.xlsx")

df$Depth <- factor(df$Depth, levels = rev(sort(unique(df$Depth))))

# Convert elemental oxides
df <- df %>%
  mutate(
    Na2O = Na * 1.3477599,
    K2O = K * 1.20448616,
    CaO = Ca * 1.3989521,
    Al2O3 = Al * 1.88899185
  )

# Molar masses [g/mol]
molar_mass <- list(
```

```
  Al2O3 = 101.96,
  CaO   = 56.0774,
  Na2O  = 61.9789,
  K2O   = 94.20
)

#CIA
df <- df %>%
  mutate(
    mol_Al2O3 = Al2O3 / molar_mass$Al2O3,
    mol_CaO   = CaO   / molar_mass$CaO,
    mol_Na2O  = Na2O  / molar_mass$Na2O,
    mol_K2O   = K2O   / molar_mass$K2O,

    CIA = (mol_Al2O3 / (mol_Al2O3 + mol_CaO + mol_Na2O + mol_K2O)) * 100
  )

#PIA
df$PIA <- ((df$mol_Al2O3 - df$mol_K2O) /
             (df$mol_Al2O3 + df$mol_CaO + df$mol_Na2O - df$mol_K2O)) * 100

# oxalate / dithionite ratio
df_ratios <- df %>%
  mutate(
    AloAld = Alo_avg / Ald_avg,
    FeoFed = Feo_avg / Fed_avg,
    MnoMnd = Mno_avg / Mnd_avg
  )

# Convert Fe, Al, Mn [%] to mg/kg
df$Fe_total <- df$Fe * 10000
df$Al_total <- df$Al * 10000
df$Mn_total <- df$Mn * 10000

# dithionite / total ratio
df$Fed_Fet_ratio <- df$Fed_avg / df$Fe_total
df$Ald_Alt_ratio <- df$Ald_avg / df$Al_total
df$Mnd_Mnt_ratio <- df$Mnd_avg / df$Mn_total

# DSI
df <- df %>%
  mutate(
      DSI = (RP_Aliphatic / RP_Aromatic_CC_2)
        )
##################################
#### Relative difference [%] ####
##################################

df <- read_excel("All_data_Rversion.xlsx ")

df$Depth <- factor(df$Depth, levels = rev(sort(unique(df$Depth))))

# wide format one row per plot and depth
df_wide <- df %>%
  select(
    Plot, Depth, Treatment,
    # Ratios
    Fed_Fet_ratio, Ald_Alt_ratio, Mnd_Mnt_ratio,
    AloAld, FeoFed, MnoMnd,
    # Indices
    PIA, CIA, CN, DSI,
    # Extractions
    Feo_avg, Alo_avg, Mno_avg,   # oxalate
    Fed_avg, Ald_avg, Mnd_avg,   # dithionite
    # pH
    pH,
    # XRF elements
    Fe, Al, Mn, Mg, Ca, K, Na, Si, P, S,
    # C & N
    C, N,
    # DRIFT
    RP_Aliphatic, RP_Carboxylic, RP_Polysaccharide, RP_Lignin, RP_Aromatic_CC_total,
RP_Aromatic_CH_total
  ) %>%
  pivot_wider(
```

```
    names_from = Treatment,
    values_from = c(
      Fed_Fet_ratio, Ald_Alt_ratio, Mnd_Mnt_ratio,
      AloAld, FeoFed, MnoMnd,
      PIA, CIA, CN, DSI,
      Feo_avg, Alo_avg, Mno_avg,
      Fed_avg, Ald_avg, Mnd_avg,
      pH,
      Fe, Al, Mn, Mg, Ca, K, Na, Si, P, S,
      C, N,
      RP_Aliphatic, RP_Carboxylic, RP_Polysaccharide, RP_Lignin, RP_Aromatic_CC_total,
RP_Aromatic_CH_total
    ),
    names_sep = "_"
  )

# relative change per plot and depth
df_change <- df_wide %>%
  mutate(
    # Ratios
    FedFet_change = (Fed_Fet_ratio_H - Fed_Fet_ratio_C) / Fed_Fet_ratio_C * 100,
    AldAlt_change = (Ald_Alt_ratio_H - Ald_Alt_ratio_C) / Ald_Alt_ratio_C * 100,
    MndMnt_change = (Mnd_Mnt_ratio_H - Mnd_Mnt_ratio_C) / Mnd_Mnt_ratio_C * 100,

    FeoFed_change = (FeoFed_H - FeoFed_C) / FeoFed_C * 100,
    AloAld_change = (AloAld_H - AloAld_C) / AloAld_C * 100,
    MnoMnd_change = (MnoMnd_H - MnoMnd_C) / MnoMnd_C * 100,

    # Indices
    PIA_change = (PIA_H - PIA_C) / PIA_C * 100,
    CIA_change = (CIA_H - CIA_C) / CIA_C * 100,
    CN_change  = (CN_H  - CN_C)  / CN_C  * 100,
    DSI_change = (DSI_H - DSI_C) / DSI_C * 100,

    # Extractions
    Feo_change = (Feo_avg_H - Feo_avg_C) / Feo_avg_C * 100,
    Alo_change = (Alo_avg_H - Alo_avg_C) / Alo_avg_C * 100,
    Mno_change = (Mno_avg_H - Mno_avg_C) / Mno_avg_C * 100,

    Fed_change = (Fed_avg_H - Fed_avg_C) / Fed_avg_C * 100,
    Ald_change = (Ald_avg_H - Ald_avg_C) / Ald_avg_C * 100,
    Mnd_change = (Mnd_avg_H - Mnd_avg_C) / Mnd_avg_C * 100,

    # pH
    pH_change = (pH_H - pH_C) / pH_C * 100,

    # XRF elements
    Fe_change = (Fe_H - Fe_C) / Fe_C * 100,
    Al_change = (Al_H - Al_C) / Al_C * 100,
    Mn_change = (Mn_H - Mn_C) / Mn_C * 100,
    Mg_change = (Mg_H - Mg_C) / Mg_C * 100,
    Ca_change = (Ca_H - Ca_C) / Ca_C * 100,
    K_change  = (K_H  - K_C)  / K_C  * 100,
    Na_change = (Na_H - Na_C) / Na_C * 100,
    Si_change = (Si_H - Si_C) / Si_C * 100,
    P_change  = (P_H  - P_C)  / P_C  * 100,
    S_change  = (S_H  - S_C)  / S_C  * 100,

    # C & N
    C_change = (C_H - C_C) / C_C * 100,
    N_change = (N_H - N_C) / N_C * 100,

    # DRIFT
    Aliphatic_change      = (RP_Aliphatic_H      - RP_Aliphatic_C)      / RP_Aliphatic_C * 100,
    Carboxylic_change     = (RP_Carboxylic_H     - RP_Carboxylic_C)     / RP_Carboxylic_C * 100,
    Polysaccharide_change = (RP_Polysaccharide_H - RP_Polysaccharide_C) / RP_Polysaccharide_C * 100,
    Lignin_change         = (RP_Lignin_H         - RP_Lignin_C)         / RP_Lignin_C * 100,
    Aromatic_CC_change    = (RP_Aromatic_CC_total_H    - RP_Aromatic_CC_total_C)    /
RP_Aromatic_CC_total_C * 100,
    Aromatic_CH_change    = (RP_Aromatic_CH_total_H    - RP_Aromatic_CH_total_C)    /
RP_Aromatic_CH_total_C * 100
  )

# mean and standard error per depth
df_change_summary <- df_change %>%
```

```
  group_by(Depth) %>%
  summarise(
    across(
      ends_with("_change"),
      list(
        mean = ~mean(.x, na.rm = TRUE),
        se   = ~sd(.x, na.rm = TRUE) / sqrt(n())
      ),
      .names = "{.col}_{.fn}"
    ),
    .groups = "drop"
  )

print(df_change_summary)


###############
#### Plots ####
###############

df <- read_excel("All_data_Rversion.xlsx ")

df$Depth <- factor(df$Depth, levels = rev(sort(unique(df$Depth))))

df <- df %>%
  mutate(Experiment = case_when(
    Plot %in% c(1, 2, 3) ~ "10y",
    Plot %in% c(4, 5, 6) ~ "2y"
  )
  ) %>%
  filter(Experiment == "10y")

# Plots displaying only one variable were created with the following code, including the variables pH,
CIA, PIA, CN and DSI. The variables were substituted in the code written in bold and the x-axis label
was adjusted accordingly as in the example for the CIA.

# CIA: mean + SE per depth and treatment
df_summary <- df %>%
  group_by(Depth, Treatment) %>%
  summarise(
    CIA_mean = mean(CIA, na.rm = TRUE),
    CIA_se   = sd(CIA, na.rm = TRUE) / sqrt(n()),
    .groups = "drop"
  )

# Plot
ggplot(df_summary, aes(x = CIA_mean, y = Depth, color = Treatment)) +
  geom_point(position = position_dodge(width = 0.6), size = 3) +
  geom_errorbarh(aes(xmin = CIA_mean - CIA_se, xmax = CIA_mean + CIA_se), position =
position_dodge(width = 0.6), height = 0.2) +
  scale_color_manual(values = c("H" = "darkorange", "C" = "dodgerblue3")) +
  labs(
    x = expression("CIA [-]"),
    y = "Depth [cm]",
    color = "Treatment"
  ) +
  theme_minimal() +
  theme(
    axis.title = element_text(size = 12),
    axis.text = element_text(size = 12),
    legend.position = "top",
    legend.text = element_text(size = 12),
    strip.text = element_text(size = 12)
  )

# Plots displaying more than one variable were created with the following code using facets. Facets were
created for (Al, Fe, Mn), (C, N, Si), (Ca, K, Mg, Na, P, S), (Alo_avg, Feo_avg, Mno_avg), (Ald_avg,
Fed_avg, Mnd_avg), (AloAld, FeoFed, MnoMnd), (Ald_Alt_ratio, Fed_Fet_ratio, Mnd_Mnt_ratio),
(RP_Aliphatic, RP_Carboxylic, RP_Polysaccharide, RP_Lignin, RP_Aromatic_CC_total, RP_Aromatic_CH_total)
The variables were substituted in the code written in bold and the x-axis label was adjusted accordingly.
Furthermore, for some variables the names were adjusted for the plots.

### facets for Al, Fe, Mn
df_long <- df %>%
  pivot_longer(
```

```
    cols = c(Al, Fe, Mn),
    names_to = "Elements",
    values_to = "Value"
  )

# rename variable names for plots
df_long$Elements <- recode(df_long$Elements,
                           Feo_avg = "Fe[o]",
                           Alo_avg = "Al[o]",
                           Mno_avg = "Mn[o]"
)

df_long$Elements <- recode(df_long$Elements,
                           Fed_avg = "Fe[d]",
                           Ald_avg = "Al[d]",
                           Mnd_avg = "Mn[d]"
)

df_long$Elements <- recode(df_long$Elements,
                           "AloAld" = "Al[o]/Al[d]",
                           "FeoFed" = "Fe[o]/Fe[d]",
                           "MnoMnd" = "Mn[o]/Mn[d]"
)

df_long$Elements <- recode(df_long$Elements,
                           "Ald_Alt_ratio" = "Al[d]/Al[t]",
                           "Fed_Fet_ratio" = "Fe[d]/Fe[t]",
                           "Mnd_Mnt_ratio" = "Mn[d]/Mn[t]"
)


df_long$Elements <- recode(df_long$Elements,
                            RP_Aliphatic = "Aliphatic",
                            RP_Carboxylic = "Carboxylic",
                            RP_Polysaccharide = "Polysaccharide",
                            RP_Lignin = "Lignin",
                            RP_Aromatic_CC_total  = "Aromatic CC",
                            RP_Aromatic_CH_total = "Aromatic CH"
)

# Calculate mean & SE
df_summary <- df_long %>%
  group_by(Depth, Treatment, Elements) %>%
  summarise(
    mean = mean(Value, na.rm = TRUE),
    se = sd(Value, na.rm = TRUE) / sqrt(n()),
    .groups = "drop"
  )

ggplot(df_summary, aes(x = mean, y = Depth, color = Treatment)) +
  geom_point(position = position_dodge(width = 0.6), size = 3) +
  geom_errorbarh(aes(xmin = mean - se, xmax = mean + se),
                 position = position_dodge(width = 0.6), height = 0.2) +
  facet_wrap(~ Elements, labeller = label_parsed, scales = "free_x") +
  labs(
    x = "Relative concentration [%]",
    y = "Depth [cm]",
    color = "Treatment"
  ) +
  scale_color_manual(values = c("C" = "dodgerblue3", "H" = "darkorange")) +
  theme_minimal() +
  theme(
    axis.title = element_text(size = 12),
    axis.text = element_text(size = 12),
    legend.position = "top",
    legend.text = element_text(size = 12),
    strip.text = element_text(size = 12)
  )

#### Spatial heterogeneity plot ####
df <- read_excel("All_data_Rversion.xlsx ")

df$Depth <- factor(df$Depth, levels = rev(sort(unique(df$Depth))))

# grouping depths together for pseudo-replicates
```

```
depth_group_1 <- c("0-10", "10-20", "20-30")
depth_group_2 <- c("30-40", "40-50", "50-60")
depth_group_3 <- c("60-70", "70-80", "80-90", "90-100")


df <- df  %>%
  mutate(
    Depth_Group = case_when(
      Depth %in% depth_group_1 ~ "Depth1",
      Depth %in% depth_group_2 ~ "Depth2",
      Depth %in% depth_group_3 ~ "Depth3",
      TRUE ~ NA_character_
    )
  )

df <- df %>%
  pivot_longer(cols = c(Al, Fe, K, Mg, S, Ald_avg, Fed_avg, CIA),
               names_to = "Elements",
               values_to = "Value")

# Calculate mean & SE
df_summary <- df %>%
  group_by(Plot, Depth_Group, Elements) %>%
  summarise(
    mean_value = mean(Value, na.rm = TRUE),
    se = sd(Value, na.rm = TRUE) / sqrt(n()),
    .groups = "drop"
  )

df_summary <- df_summary %>%
  mutate(Plot = factor(Plot, levels = unique(df_summary$Plot))) %>%
  mutate(Elements = case_when(
  Elements == "Ald_avg" ~ "Al[d]",
  Elements == "Fed_avg" ~ "Fe[d]",
  TRUE ~ Elements
))
# Plot
ggplot(df_summary, aes(x = Plot, y = mean_value, color = as.factor(Depth_Group), group = Depth_Group))+
  geom_point(position = position_dodge(width = 0.6), size = 3) +
  geom_errorbar(aes(ymin = mean_value - se, ymax = mean_value + se),position = position_dodge(width =
0.6), width = 0.2, ) +
  facet_wrap(~ Elements, scales = "free_y", labeller = label_parsed) +
  scale_color_manual(
    values = c("Depth1" = "green4", "Depth2" = "steelblue2", "Depth3" = "darkorange"),
    labels = c("Depth1" = "0 – 30 cm", "Depth2" = "30 – 60 cm", "Depth3" = "60 – 100 cm") ) +
  #scale_y_continuous(limits = c(0, NA))+
  labs(
    x = "Plot",
    y = "Concentration",
    color = "Depth" ) +
  theme_minimal() +
  theme(
    axis.title = element_text(size = 12),
    axis.text = element_text(size = 12),
    legend.position = "top",
    legend.text = element_text(size = 12),
    strip.text = element_text(size = 12)
  )

#####################################
#### Linear mixed effects models ####
#####################################

# The following R code was used as a template for all analysed variables. The example for Fe was used,
and any variable can be substituted into the code written in bold letters. The code was used for the
following variables (variable names for R): Fe, Al, Mn, Si, Ca, K, Mg, Na, P, S, C, N, pH, Fe_o (Feo_avg),
Al_o (Alo_avg), Mn_o (Mno_avg), Fe_d (Fed_avg), Al_d (Ald_avg), Mn_d (Mnd_avg), Fe_o/Fe_d (FeoFed), Al_o/Al_d (AloAld),
Mn_o/Mn_d (MnoMnd), Al_d/Al_t (Ald_Alt_ratio), Fe_d/Fe_t (Fed_Fet_ratio), Mn_d/Mn_t (Mnd_Mnt_ratio), Aliphatic
(RP_Aliphatic), Aromatic CC (RP_Aromatic_CC_total), Aromatic CH (RP_Aromatic_CH_total), Carboxylic
(RP_Carboxylic), Lignin (RP_Lignin), Polysaccharide (RP_Polysaccharide), CIA, PIA, DSI and C/N (CN).

df <- read_excel("All_data_Rversion.xlsx ")

df$mid_depth <- as.numeric(sub(".*-", "", df$Depth)) - 5
df$mid_depth
```

```
df[, c(1, 2)] <- lapply(df[, c(1, 2)], factor)
df$ID <- interaction(df$Plot, df$Treatment)

# Code workflow for Fe, substitutable for all other variables (bold)
# How is the data distributed? is log-transform needed?
skewness(df$Fe)
hist(df$Fe)

# lmem model
Fe_model <- lme(
  Fe ~ Treatment * Depth,
  random = ~ 1 | ID,
  correlation = corAR1(form = ~ mid_depth | ID),
  data = df
)
summary(Fe_model)

# check the model
anova(Fe_model)
plot(resid(Fe_model)~(fitted(Fe_model)))
qqnorm(resid(Fe_model))
shapiro.test(Fe_model$residuals)

# log transformed model
df$log_Fe <- log(df$Fe)

Fe_model2 <- lme(
  log_Fe ~ Treatment * Depth,
  random = ~ 1 | ID,
  correlation = corAR1(form = ~ mid_depth | ID),
  data = df
)
summary(Fe_model2)

anova(Fe_model2)
plot(resid(Fe_model2) ~ fitted(Fe_model2))
qqnorm(resid(Fe_model2))
shapiro.test(Fe_model2$residuals)

AIC(Fe_model)
AIC(Fe_model2)

Fe_model3 <- lme(
  log_Fe ~ Treatment + Depth,
  random = ~ 1 | ID,
  correlation = corAR1(form = ~ mid_depth | ID),
  data = df
)
summary(Fe_model3)
anova(Fe_model3)

AIC(Fe_model2)
AIC(Fe_model3)

# post hoc emmeans when significance was found & log back-transformation
# choose model, model2 or model3 based on AIC and significance

Fe_emm <- emmeans(Fe_model2, ~ Treatment | Depth)

Fe_emm_bt <- regrid(Fe_emm, transform = "response") # log back-transform only if needed!

pairs_res<- pairs(Fe_emm_bt, adjust = "tukey")  # adjusted p-values

pairs_df <- as.data.frame(pairs_res)
print(pairs_df)

########################################
#### t-tests spatial heterogeneity ####
########################################
```

The following R code was used as a template for all analysed variables. The example for Fe was used, and any variable can be substituted into the code written in bold letters. The code was used for the following variables (variable names for R): Fe, Al, Mn, Si, Ca, K, Mg, Na, P, S, C, N, pH, Fe_o (Feo_avg), Al_o (Alo_avg), Mn_o (Mno_avg), Fe_d (Fed_avg), Al_d (Ald_avg), Mn_d (Mnd_avg), Fe_o/Fe_d (FeoFed), Al_o/Al_d (AloAld), Mn_o/Mn_d (MnoMnd), Al_d/Al_t (Ald_Alt_ratio), Fe_d/Fe_t (Fed_Fet_ratio), Mn_d/Mn_t (Mnd_Mnt_ratio), Aliphatic

(RP_Aliphatic), Aromatic CC (RP_Aromatic_CC_total), Aromatic CH (RP_Aromatic_CH_total), Carboxylic (RP_Carboxylic), Lignin (RP_Lignin), Polysaccharide (RP_Polysaccharide), CIA, PIA, DSI and C/N (CN).

```
df <- read_excel("All_data_Rversion.xlsx ")
df$Depth <- factor(df$Depth, levels = rev(sort(unique(df$Depth))))

# grouping depths together for pseudo-replicates
depth_group_1 <- c("0-10", "10-20", "20-30")
depth_group_2 <- c("30-40", "40-50", "50-60")
depth_group_3 <- c("60-70", "70-80", "80-90", "90-100")

df <- df %>%
  mutate(
    Depth_Group = case_when(
      Depth %in% depth_group_1 ~ "Depth1",
      Depth %in% depth_group_2 ~ "Depth2",
      Depth %in% depth_group_3 ~ "Depth3",
      TRUE ~ NA_character_
    )
  )

################
# depth 1 Fe #

depth1 <- df %>% filter(Depth_Group == "Depth1")
plot_pairs <- combn(unique(depth1$Plot), 2, simplify = FALSE)

# Empty data frame to store results
results_Fe <- data.frame(
  Plot1 = character(),
  Plot2 = character(),
  Normality1_p = numeric(),
  Normality2_p = numeric(),
  VarEqual_p = numeric(),
  TestUsed = character(),
  p_value = numeric(),
  stringsAsFactors = FALSE
)

for (pair in plot_pairs) {
  # Filter data for these two plots
  data_pair <- depth1 %>% filter(Plot %in% pair)

  # Shapiro-Wilk normality test for each plot
  p_norm1 <- shapiro.test(data_pair$Fe[data_pair$Plot == pair[1]])$p.value
  p_norm2 <- shapiro.test(data_pair$Fe[data_pair$Plot == pair[2]])$p.value

  # Variance test
  p_var <- var.test(Fe ~ Plot, data = data_pair)$p.value

  # Decide which test to run
  if (p_norm1 > 0.05 & p_norm2 > 0.05) {  # Both normal
    if (p_var > 0.05) {                    # Variances equal
      test_name <- "t-test equal var"
      p_test <- t.test(Fe ~ Plot, data = data_pair, var.equal = TRUE)$p.value
    } else {                               # Variances unequal
      test_name <- "t-test unequal var"
      p_test <- t.test(Fe ~ Plot, data = data_pair, var.equal = FALSE)$p.value
    }
  } else {                                 # Non-normal, use Wilcoxon
    test_name <- "Wilcoxon"
    p_test <- wilcox.test(Fe ~ Plot, data = data_pair)$p.value
  }

  # Append results to the dataframe
  results_Fe <- rbind(results_Fe, data.frame(
    Plot1 = pair[1],
    Plot2 = pair[2],
    Normality1_p = p_norm1,
    Normality2_p = p_norm2,
    VarEqual_p = p_var,
    TestUsed = test_name,
    p_value = p_test,
    stringsAsFactors = FALSE
  ))
```

```
}

print(results_Fe)

###############
# depth 2 Fe #

depth2 <- df %>% filter(Depth_Group == "Depth2")
plot_pairs <- combn(unique(depth2$Plot), 2, simplify = FALSE)

# Empty data frame to store results
results_Fe2 <- data.frame(
  Plot1 = character(),
  Plot2 = character(),
  Normality1_p = numeric(),
  Normality2_p = numeric(),
  VarEqual_p = numeric(),
  TestUsed = character(),
  p_value = numeric(),
  stringsAsFactors = FALSE
)

for (pair in plot_pairs) {
  # Filter data for these two plots
  data_pair <- depth2 %>% filter(Plot %in% pair)

  # Shapiro-Wilk normality test for each plot
  p_norm1 <- shapiro.test(data_pair$Fe[data_pair$Plot == pair[1]])$p.value
  p_norm2 <- shapiro.test(data_pair$Fe[data_pair$Plot == pair[2]])$p.value

  # Variance test
  p_var <- var.test(Fe ~ Plot, data = data_pair)$p.value

  # Decide which test to run
  if (p_norm1 > 0.05 & p_norm2 > 0.05) {  # Both normal
    if (p_var > 0.05) {                    # Variances equal
      test_name <- "t-test equal var"
      p_test <- t.test(Fe ~ Plot, data = data_pair, var.equal = TRUE)$p.value
    } else {                               # Variances unequal
      test_name <- "t-test unequal var"
      p_test <- t.test(Fe ~ Plot, data = data_pair, var.equal = FALSE)$p.value
    }
  } else {                                 # Non-normal, use Wilcoxon
    test_name <- "Wilcoxon"
    p_test <- wilcox.test(Fe ~ Plot, data = data_pair)$p.value
  }

  # Append results to the dataframe
  results_Fe2 <- rbind(results_Fe2, data.frame(
    Plot1 = pair[1],
    Plot2 = pair[2],
    Normality1_p = p_norm1,
    Normality2_p = p_norm2,
    VarEqual_p = p_var,
    TestUsed = test_name,
    p_value = p_test,
    stringsAsFactors = FALSE
  ))
}

print(results_Fe2)

###############
# depth 3 Fe #

depth3 <- df %>% filter(Depth_Group == "Depth3")
plot_pairs <- combn(unique(depth3$Plot), 2, simplify = FALSE)

# Empty data frame to store results
results_Fe3 <- data.frame(
  Plot1 = character(),
  Plot2 = character(),
  Normality1_p = numeric(),
  Normality2_p = numeric(),
  VarEqual_p = numeric(),
```

```
  TestUsed = character(),
  p_value = numeric(),
  stringsAsFactors = FALSE
)

for (pair in plot_pairs) {
  # Filter data for these two plots
  data_pair <- depth3 %>% filter(Plot %in% pair)

  # Shapiro-Wilk normality test for each plot
  p_norm1 <- shapiro.test(data_pair$Fe[data_pair$Plot == pair[1]])$p.value
  p_norm2 <- shapiro.test(data_pair$Fe[data_pair$Plot == pair[2]])$p.value

  # Variance test
  p_var <- var.test(Fe ~ Plot, data = data_pair)$p.value

  # Decide which test to run
  if (p_norm1 > 0.05 & p_norm2 > 0.05) {  # Both normal
    if (p_var > 0.05) {                    # Variances equal
      test_name <- "t-test equal var"
      p_test <- t.test(Fe ~ Plot, data = data_pair, var.equal = TRUE)$p.value
    } else {                               # Variances unequal
      test_name <- "t-test unequal var"
      p_test <- t.test(Fe ~ Plot, data = data_pair, var.equal = FALSE)$p.value
    }
  } else {                                 # Non-normal, use Wilcoxon
    test_name <- "Wilcoxon"
    p_test <- wilcox.test(Fe ~ Plot, data = data_pair)$p.value
  }

  # Append results to the dataframe
  results_Fe3 <- rbind(results_Fe3, data.frame(
    Plot1 = pair[1],
    Plot2 = pair[2],
    Normality1_p = p_norm1,
    Normality2_p = p_norm2,
    VarEqual_p = p_var,
    TestUsed = test_name,
    p_value = p_test,
    stringsAsFactors = FALSE
  ))
}

print(results_Fe3)

##############
#### PCA ####
##############

df <- read_excel("All_data_Rversion.xlsx")

df <- df %>%
  mutate(Experiment = case_when(
    Plot %in% c(1, 2, 3) ~ "10y",
    Plot %in% c(4, 5, 6) ~ "2y"
  )
  ) %>%
  filter(Treatment == "C")

df$Depth <- factor(df$Depth, levels = rev(sort(unique(df$Depth))))

### Checking data ###
df_vars <- df[,5:(ncol(df)-11)]  # all numerical
colSums(is.na(df_vars))         # check null values

colnames(df_vars) <- c("Feo", "Alo", "Mno", "Fed", "Ald",
                       "Mnd", "Ca", "Na", "K", "Al",
                       "Fe", "Mn", "DSI", "Mg", "Si",
                       "P", "S", "C", "N", "CN",
                       "CIA", "PIA", "Alo/Ald", "Feo/Fed", "Mno/Mnd",
                       "Fed/Fet", "Ald/Alt", "Mnd/Mnt", "pH")
df_scaled <- scale(df_vars)     # scale variables
head(df_scaled)
### PCA ###
data.pca <- princomp(df_scaled)
```

```
summary(data.pca)

data.pca$loadings[, 1:4]

# scree plot
fviz_eig(data.pca, addlabels = TRUE)
# Graph of the variables
fviz_pca_var(data.pca, col.var = "black")
fviz_cos2(data.pca, choice = "var", axes = 1:2)

fviz_pca_var(data.pca, col.var = "cos2",
             gradient.cols = c("black", "orange", "blue"),
             repel = TRUE)

plot_colors <- brewer.pal(n = 10, name = "Dark2")

fviz_pca_biplot(data.pca,
                geom.ind = "point",
                col.ind = df$Plot,                  # color points by Plot
                palette = plot_colors,              # colors for plots
                addEllipses = TRUE,
                ellipse.type = "confidence",        # 95% confidence ellipse
                habillage = df$Plot,                # group ellipses by Plot
                repel = TRUE,                       # avoid overlapping labels
                col.var = "brown4",
                legend.title = "Plot")

depth_colors <- brewer.pal(n = 10, name = "Paired")

fviz_pca_biplot(data.pca,
                geom.ind = "point",
                col.ind = df$Depth,                  # color points by depth
                palette = depth_colors,
                addEllipses = FALSE,
                repel = TRUE,                        # avoid overlapping labels
                col.var = "brown4",
                legend.title = "Depth (cm)")

summary(data.pca)
fviz_eig(data.pca)

##############################
#### Correlation Analysis ####
##############################

df <- read_excel("C:/Users/Julia/Documents/Julia synch/Julia
alles/1_UNI/Masterarbeit/Data/All_data/All_data.xlsx")

df <- df %>%
  mutate(Experiment = case_when(
    Plot %in% c(1, 2, 3) ~ "10y",
    Plot %in% c(4, 5, 6) ~ "2y"
  )
  ) %>%
  filter(Experiment == "10y")

### Checking assumptions: normality and linearity ###
df %>% group_by(Treatment) %>% summarise(
  p_DSI = shapiro.test(DSI)$p.value,
  p_Alo = shapiro.test(Alo_avg)$p.value,
  p_Feo = shapiro.test(Feo_avg)$p.value,
  p_C = shapiro.test(C)$p.value
)

### Correlation test: Spearman correlation ###
## DSI
ggplot(df, aes(x = Feo_avg, y = DSI, color = Treatment)) +
  geom_point() +
  geom_smooth(method = "lm", se = FALSE) +
  geom_smooth(method = "loess", se = FALSE)

ggplot(df, aes(x = Alo_avg, y = DSI, color = Treatment)) +
  geom_point() +
  geom_smooth(method = "lm", se = FALSE) +
  geom_smooth(method = "loess", se = FALSE)
```

```
## Carbon
ggplot(df, aes(x = Feo_avg, y = C, color = Treatment)) +
  geom_point() +
  geom_smooth(method = "lm", se = FALSE) +
  geom_smooth(method = "loess", se = FALSE)

ggplot(df, aes(x = Alo_avg, y = C, color = Treatment)) +
  geom_point() +
  geom_smooth(method = "lm", se = FALSE) +
  geom_smooth(method = "loess", se = FALSE)

df %>%
  group_by(Treatment) %>%
  summarise(
    cor = cor(Feo_avg, DSI, method = "spearman"),
    p   = cor.test(Feo_avg, DSI, method = "spearman")$p.value
  )

df %>%
  group_by(Treatment) %>%
  summarise(
    cor = cor(Alo_avg, DSI, method = "spearman"),
    p   = cor.test(Alo_avg, DSI, method = "spearman")$p.value
  )

df %>%
  group_by(Treatment) %>%
  summarise(
    cor = cor(Feo_avg, C, method = "spearman"),
    p   = cor.test(Feo_avg, C, method = "spearman")$p.value
  )


df %>%
  group_by(Treatment) %>%
  summarise(
    cor = cor(Alo_avg, C, method = "spearman"),
    p   = cor.test(Alo_avg, C, method = "spearman")$p.value
  )
### Check significance of correlation difference ###
# --- DSI vs Feo ---
# Control
cor_control <- cor.test(df$Feo_avg[df$Treatment=="C"],
                        df$DSI[df$Treatment=="C"], method="spearman")
n_control <- sum(df$Treatment=="C")
cat("Control: Spearman rho =", cor_control$estimate, ", p =", cor_control$p.value, "\n")

# Heated
cor_heated <- cor.test(df$Feo_avg[df$Treatment=="H"],
                       df$DSI[df$Treatment=="H"], method="spearman")
n_heated <- sum(df$Treatment=="H")
cat("Heated: Spearman rho =", cor_heated$estimate, ", p =", cor_heated$p.value, "\n")

# Fisher's z test
cocor.indep.groups(r1.jk = cor_control$estimate,
                   r2.hm = cor_heated$estimate,
                   n1 = n_control,
                   n2 = n_heated,
                   alternative = "two.sided",
                   test = "fisher1925")

# --- DSI vs Alo ---
cor_control <- cor.test(df$Alo_avg[df$Treatment=="C"],
                        df$DSI[df$Treatment=="C"], method="spearman")
n_control <- sum(df$Treatment=="C")
cat("Control: Spearman rho =", cor_control$estimate, ", p =", cor_control$p.value, "\n")

cor_heated <- cor.test(df$Alo_avg[df$Treatment=="H"],
                       df$DSI[df$Treatment=="H"], method="spearman")
n_heated <- sum(df$Treatment=="H")
cat("Heated: Spearman rho =", cor_heated$estimate, ", p =", cor_heated$p.value, "\n")

cocor.indep.groups(r1.jk = cor_control$estimate,
                   r2.hm = cor_heated$estimate,
```

```
                  n1 = n_control,
                  n2 = n_heated,
                  alternative = "two.sided",
                  test = "fisher1925")

# --- C vs Alo ---
cor_control <- cor.test(df$Alo_avg[df$Treatment=="C"],
                        df$C[df$Treatment=="C"], method="spearman")
n_control <- sum(df$Treatment=="C")
cat("Control: Spearman rho =", cor_control$estimate, ", p =", cor_control$p.value, "\n")

cor_heated <- cor.test(df$Alo_avg[df$Treatment=="H"],
                       df$C[df$Treatment=="H"], method="spearman")
n_heated <- sum(df$Treatment=="H")
cat("Heated: Spearman rho =", cor_heated$estimate, ", p =", cor_heated$p.value, "\n")

cocor.indep.groups(r1.jk = cor_control$estimate,
                  r2.hm = cor_heated$estimate,
                  n1 = n_control,
                  n2 = n_heated,
                  alternative = "two.sided",
                  test = "fisher1925")

# --- C vs Feo ---
cor_control <- cor.test(df$Feo_avg[df$Treatment=="C"],
                        df$C[df$Treatment=="C"], method="spearman")
n_control <- sum(df$Treatment=="C")
cat("Control: Spearman rho =", cor_control$estimate, ", p =", cor_control$p.value, "\n")

cor_heated <- cor.test(df$Feo_avg[df$Treatment=="H"],
                       df$C[df$Treatment=="H"], method="spearman")
n_heated <- sum(df$Treatment=="H")
cat("Heated: Spearman rho =", cor_heated$estimate, ", p =", cor_heated$p.value, "\n")

cocor.indep.groups(r1.jk = cor_control$estimate,
                  r2.hm = cor_heated$estimate,
                  n1 = n_control,
                  n2 = n_heated,
                  alternative = "two.sided",
                  test = "fisher1925")

# correlation in control
r_control <- cor(df$Feo_avg[df$Treatment=="C"],
                 df$DSI[df$Treatment=="C"], method="spearman")
n_control <- sum(df$Treatment=="C")

# correlation in heated
r_heated <- cor(df$Feo_avg[df$Treatment=="H"],
                df$DSI[df$Treatment=="H"], method="spearman")
n_heated <- sum(df$Treatment=="H")

# Fisher's z test
cocor.indep.groups(r1.jk = r_control,
                  r2.hm = r_heated,
                  n1 = n_control,
                  n2 = n_heated,
                  alternative = "two.sided",
                  test = "fisher1925")

# correlation in control
r_control <- cor(df$Alo_avg[df$Treatment=="C"],
                 df$DSI[df$Treatment=="C"], method="spearman")
n_control <- sum(df$Treatment=="C")

# correlation in heated
r_heated <- cor(df$Alo_avg[df$Treatment=="H"],
                df$DSI[df$Treatment=="H"], method="spearman")
n_heated <- sum(df$Treatment=="H")

# Fisher's z test
cocor.indep.groups(r1.jk = r_control,
                  r2.hm = r_heated,
                  n1 = n_control,
                  n2 = n_heated,
                  alternative = "two.sided",
```

```
                  test = "fisher1925")

# correlation in control
r_control <- cor(df$Alo_avg[df$Treatment=="C"],
                 df$C[df$Treatment=="C"], method="spearman")
n_control <- sum(df$Treatment=="C")

# correlation in heated
r_heated <- cor(df$Alo_avg[df$Treatment=="H"],
                df$C[df$Treatment=="H"], method="spearman")
n_heated <- sum(df$Treatment=="H")

# Fisher's z test
cocor.indep.groups(r1.jk = r_control,
                   r2.hm = r_heated,
                   n1 = n_control,
                   n2 = n_heated,
                   alternative = "two.sided",
                   test = "fisher1925")
# correlation in control
r_control <- cor(df$Feo_avg[df$Treatment=="C"],
                 df$C[df$Treatment=="C"], method="spearman")
n_control <- sum(df$Treatment=="C")

# correlation in heated
r_heated <- cor(df$Feo_avg[df$Treatment=="H"],
                df$C[df$Treatment=="H"], method="spearman")
n_heated <- sum(df$Treatment=="H")

# Fisher's z test
cocor.indep.groups(r1.jk = r_control,
                   r2.hm = r_heated,
                   n1 = n_control,
                   n2 = n_heated,
                   alternative = "two.sided",
                   test = "fisher1925")

### Account for depth ###
# install if not already installed

#install.packages("ppcor")
library(ppcor)
citation("ppcor")
library(stringr)


df <- df %>%
  mutate(
    Depth_mid = str_extract(Depth, "^[0-9]+") |>   # extract first number
      as.numeric() + 5                  # add 5 to get midpoint
  )

##### Feo vs C ####
# Control
df_control <- df %>% filter(Treatment == "C")
pcor_control <- pcor.test(df_control$Feo_avg, df_control$C, df_control$Depth_mid, method = "spearman")
r_control <- pcor_control$estimate
n_control <- nrow(df_control)

# Heated
df_heated <- df %>% filter(Treatment == "H")
pcor_heated <- pcor.test(df_heated$Feo_avg, df_heated$C, df_heated$Depth_mid, method = "spearman")
r_heated <- pcor_heated$estimate
n_heated <- nrow(df_heated)

# --- Compare correlations using Fisher's z ---
cocor_result <- cocor.indep.groups(
  r1.jk = r_control,
  r2.hm = r_heated,
  n1 = n_control,
  n2 = n_heated,
  alternative = "two.sided",
  test = "fisher1925"
)
```

```
# Print results
pcor_control
pcor_heated
cocor_result

##### Feo vs DSI ####
# Control
df_control <- df %>% filter(Treatment == "C")
pcor_control <- pcor.test(df_control$Feo_avg, df_control$DSI, df_control$Depth_mid, method =
"spearman")
r_control <- pcor_control$estimate
n_control <- nrow(df_control)

# Heated
df_heated <- df %>% filter(Treatment == "H")
pcor_heated <- pcor.test(df_heated$Feo_avg, df_heated$DSI, df_heated$Depth_mid, method = "spearman")
r_heated <- pcor_heated$estimate
n_heated <- nrow(df_heated)

# --- Compare correlations using Fisher's z ---
cocor_result <- cocor.indep.groups(
  r1.jk = r_control,
  r2.hm = r_heated,
  n1 = n_control,
  n2 = n_heated,
  alternative = "two.sided",
  test = "fisher1925"
)

# Print results
pcor_control
pcor_heated
cocor_result

##### Feo vs DSI ####
# Control
df_control <- df %>% filter(Treatment == "C")
pcor_control <- pcor.test(df_control$Alo_avg, df_control$DSI, df_control$Depth_mid, method =
"spearman")
r_control <- pcor_control$estimate
n_control <- nrow(df_control)

# Heated
df_heated <- df %>% filter(Treatment == "H")
pcor_heated <- pcor.test(df_heated$Alo_avg, df_heated$DSI, df_heated$Depth_mid, method = "spearman")
r_heated <- pcor_heated$estimate
n_heated <- nrow(df_heated)

# --- Compare correlations using Fisher's z ---
cocor_result <- cocor.indep.groups(
  r1.jk = r_control,
  r2.hm = r_heated,
  n1 = n_control,
  n2 = n_heated,
  alternative = "two.sided",
  test = "fisher1925"
)

# Print results
pcor_control
pcor_heated
cocor_result

##### Alo vs C ####
# Control
df_control <- df %>% filter(Treatment == "C")
pcor_control <- pcor.test(df_control$Alo_avg, df_control$C, df_control$Depth_mid, method = "spearman")
r_control <- pcor_control$estimate
n_control <- nrow(df_control)

# Heated
df_heated <- df %>% filter(Treatment == "H")
pcor_heated <- pcor.test(df_heated$Alo_avg, df_heated$C, df_heated$Depth_mid, method = "spearman")
r_heated <- pcor_heated$estimate
n_heated <- nrow(df_heated)
```

```
# --- Compare correlations using Fisher's z ---
cocor_result <- cocor.indep.groups(
  r1.jk = r_control,
  r2.hm = r_heated,
  n1 = n_control,
  n2 = n_heated,
  alternative = "two.sided",
  test = "fisher1925"
)

# Print results
pcor_control
pcor_heated
cocor_result
```

Personal Declaration

Personal declaration: I hereby declare that the submitted thesis is the result of my own, independent work. All external sources are explicitly acknowledged in this Thesis.

I further acknowledge that ChatGPT (OpenAI) was used to assist with grammar, syntax and content refinement.

Zurich, September 30, 2025

Julia van Leeuwen